



UNIVERSITÀ  
DEGLI STUDI  
DI PADOVA

Università degli Studi di Padova

Dipartimento di Scienze Chimiche

CORSO DI DOTTORATO DI RICERCA IN: SCIENZE MOLECOLARI

CURRICULUM: CHIMICA

XXX CICLO

# **Atmospheric plasma chemistry for environmental and biological applications**

**Coordinatore:** Ch.mo Prof. Leonard Prins

**Supervisore:** Ch.ma Prof.ssa Cristina Paradisi

**Dottorando :** Agata Giardina

# Preface

Plasma chemistry is a new area of scientific interest, rapidly growing during the last years and expanding to develop into different technological applications. Plasma is currently employed on a large industrial scale for diverse uses, including ozone generation, pollution control, surface treatment, high power CO<sub>2</sub> lasers, ultraviolet excimer lamps, excimer based mercury-free fluorescent lamps, and flat large-area plasma displays. Even the popular *Star Wars* guns are nothing more than plasma guns. Furthermore, the wide spectrum of possible treatments of materials and a tremendous variety of applications, from manufacturing to medicine, can explain the increasing amount of publications and scientific endeavor in plasma research.

The motivation for this thesis was to contribute to the understanding of the chemical phenomena associated to non thermal plasma. In particular, my research work investigated some fundamental aspects of non thermal plasma applications for the environment, notably in water treatment processes, and in the biological field, by applying four different dielectric barrier discharge (DBD) and jet systems. Specifically, my research activity developed along five lines: four of them focused on the use of plasma for water remediation, the fifth one concerned the sterilization properties of atmospheric pressure plasma. The results regarding this last project were obtained during a four-month stay in the laboratories of Prof. Julia Bandow and Jan Benedikt at Ruhr University of Bochum, in Germany.

The thesis consists of seven chapters. The first is an introduction which summarizes the fundamental aspects of discharges in a gas at ambient pressure, the ensuing plasma chemistry and its specific applications in environmental and biological areas. The following five chapters describe and discuss the results obtained in air plasma treatment of water contaminated by different organic pollutants, chosen among common compounds and emerging organic contaminants (EOCs). In each chapter, one or more critical aspects of the application of plasma for water remediation are dealt with and discussed. They range from the assessment of the toxicity of plasma treated water (chapter 2), to the implementation of the system by addition of a photocatalyst (chapter 3) or by changing the discharge and the plasma reactor features (chapter 6), to the investigation of possible reciprocal effects of two pollutants treated together (chapter 4), to the extended study of plasma effects on different classes of environmentally adverse compounds (chapter 5).

The final chapter, based on the research activity carried out during my stay at Ruhr University of Bochum, reports on studies in one of the hot topic related to applications of plasma, i.e. the relevance of ionic components of plasma and its sterilization properties.

*To my family*

# CONTENTS

Summary.....	vii
Riassunto.....	ix
Personal contribution statement.....	xi

## **Chapter 1 - Introduction**

1.1 Non thermal plasma.....	1
1.3 Atmospheric pressure plasma discharges.....	1
1.3 Plasma chemistry.....	3
1.4 Plasma and liquid: reactions induced by air NTP in water.....	5
1.5 Applications of non thermal plasmas.....	9
1.5.1 Water remediation by non thermal plasma.....	9
1.5.1.1 Water pollution emergency.....	9
1.5.1.2 Emerging organic contaminants (EOCs).....	10
1.5.1.3 Advanced Oxidation Processes (AOPs).....	10
1.5.1.4 Non thermal plasma for water remediation: state of the art.....	11
1.5.2 Biological applications of plasma: sterilization.....	9

## **Chapter 2 - Non-thermal plasma oxidation: degradation, kinetics, intermediate products and toxicity studies of sulfamethoxazole in aqueous solution**

2.1 Introduction.....	19
2.2 Materials ad methods.....	21
2.2.1 Materials.....	21
2.2.2 Experimental apparatus.....	21
2.2.3 Sulfamethoxazole treatment experiments.....	22
2.2.4 Toxicity assessment.....	23
2.2.4.1 Toxicity assessment on <i>Daphnia Magna</i> .....	23

2.2.4.2 Toxicity assessment on <i>R. subcapitata</i> .....	23
2.2.4.3 Toxicity assessment on <i>Vibrio Fischeri</i> .....	23
<b>2.3. Results and discussion.....</b>	<b>24</b>
2.3.1 Effect of Sulfamethoxazole initial concentration .....	24
2.3.2 Effect of pH.....	25
2.3.3 Transformation products characterization .....	26
2.3.4 Toxicity assessment .....	32

### **Chapter 3 - Air non-thermal plasma treatment of Irgarol deposited on TiO<sub>2</sub>**

<b>3.1 Introduction .....</b>	<b>38</b>
<b>3.2 Experimental section .....</b>	<b>40</b>
3.2.1 Materials .....	40
3.2.2 Preparation of Irgarol on TiO <sub>2</sub> .....	40
3.2.3 Plasma degradation procedure .....	40
3.2.4 Analytical procedures .....	40
<b>3.3 Results and discussion .....</b>	<b>41</b>
3.3.1 Kinetic experiments .....	41
3.3.2 Product analysis .....	45
<b>3.4 Conclusions .....</b>	<b>51</b>

### **Chapter 4 - Atmospheric plasma treatment of mesotrione and metolachlor in water**

<b>4.1 Introduction .....</b>	<b>54</b>
<b>4.2 Experimental section.....</b>	<b>56</b>
4.2.1 Chemicals .....	56
4.2.2 Dielectric Barrier Discharge (DBD) reactor .....	56
<b>4.3 Results and discussion.....</b>	<b>58</b>
4.3.1 Degradation kinetics .....	58

4.3.2 Transformation products (TPs) of metolachlor and mesotrione.....	60
4.4 Conclusions .....	67

**Chapter 5 - Plasma treatment of other persistent organic contaminants:  
Triclosan and PFOA**

5.1 Triclosan .....	72
5.1.1 Introduction.....	72
5.1.2 Experimental section.....	73
5.1.2.1 Materials .....	73
5.1.2.2 Plasma reactor .....	73
5.1.2.3 Analysis of Triclosan and its degradation products .....	73
5.1.3 Results and discussion .....	74
5.1.3.1 The effect of initial concentration and pH.....	74
5.1.3.2 Determination of Triclosan degradation products .....	77
5.2 Perfluorooctanoic acid (PFOA) .....	80
5.2.1 Introduction.....	80
5.2.2 Experimental setup .....	81
5.2.2.1 Materials and methods .....	81
5.2.3 PFOA treatment by DBD discharge.....	81
5.2.4 Conclusions .....	84

**Chapter 6 - Removal of persistent organic pollutants from water using a newly  
developed atmospheric plasma reactor**

6.1 Introduction.....	88
6.2 Experimental section.....	89
6.2.1 Materials .....	89
6.2.2 Experimental Apparatus .....	90
6.2.3 Schlieren Imaging .....	91

6.2.4 Emission spectroscopy .....	91
6.2.5 Determination of Species produced by Plasma in Solution .....	92
6.2.6 Treatment of Organic Pollutants .....	92
6.3 Results and discussion.....	94
6.3.1 Characterization of the reactor .....	94
6.3.2 Removal of persistent organic pollutants.....	101
6.4 Conclusions .....	104

**Chapter 7.1 - Comparative study on the influence of two discharge sources on GapDH activity**

7.1.1 Introduction .....	110
7.1.2 Experimental procedures .....	112
7.1.2.1 Plasma sources.....	112
7.1.2.2 GapDH activity.....	113
7.1.2.3 Inhibition zone test .....	114
7.1.2.4 Oxidative thiol modifications (Ellman's assay) .....	114
7.1.2.5 SDS-PAGE .....	114
7.1.3 Results .....	114
7.1.3.1 Inhibition tests .....	114
7.1.4 Discussion.....	117

**Chapter 7.2 - Effect of ions of cold atmospheric plasma on biological substrates**

7.2.1 Introduction .....	124
7.2.2 Experimental procedures .....	124
7.2.3 Characterization of the source .....	125
7.2.4 GapDH activity assay .....	128
7.2.5 <i>E.coli</i> test .....	130

8 Conclusions .....	132
---------------------	-----

**APPENDIX A**

**Application of Slater and Douglas-Hamilton kinetic model ..... 134**



## Summary

My Ph.D. activity developed along four lines of research dealing with non-thermal plasma (NTP) induced chemical processes for water remediation and biomedical applications.

Specifically, I studied the effectiveness of atmospheric air plasma treatment in decomposing emerging organic contaminants (EOCs). The experimental setup used was a dielectric barrier discharge (DBD) reactor, a prototype developed in collaboration with the Department of Industrial Engineering of the University of Padova. Among EOCs, I chose six different contaminants, notably sulfamethoxazole, a veterinary antibiotic, triclosan, an antibacterial agent, perfluorooctanoic acid (PFOA), a perfluorinated organic contaminant, and the herbicides irgarol, metolachlor and mesotrione. Kinetics of their removal by plasma, intermediates of oxidation, possible degradation pathways and conversion to CO<sub>2</sub> were evaluated. The achievement of more than 93% of conversion was observed for all the contaminants used at the initial concentration of 5 μM, except for PFOA (42%).

An important advancement in my research involved the assessment of residual toxicity of plasma treated water samples. For this purpose, in collaboration with Prof. Giovanni Libralato (University of Naples), we tested the efficiency of plasma treatment in producing water free from ecotoxicological effects due to potentially toxic by-product residues. We tested one of the pollutants mentioned above, sulfamethoxazole (SMZ), an antibiotic listed among the most important emerging organic contaminants. A battery of acute and chronic toxicological test were employed: *Daphnia magna*, *Raphidocaeilis Subcapitata* and *Vibrio Fischeri*. It was found that toxicity of SMZ 5×10<sup>-4</sup> M is minimized (*V.fischeri*) or reduced to zero (*D. magna*, *R. Subcapitata*) after 4 h of plasma treatment.

To improve the efficiency of our DBD reactor, we tested the effect of addition of a photocatalyst, TiO<sub>2</sub>. We compared the kinetics of degradation of Irgarol in photocatalytic plasma process with those obtained when TiO<sub>2</sub> was not included. The results obtained suggest that the effect of photoactivation by titanium dioxide in our reactor was negligible under the conditions employed.

Possible reciprocal effects of different organic pollutants dissolved in water subjected to plasma induced advanced oxidation in our dielectric barrier discharge (DBD) reactor were then evaluated. As case study for this investigation, I chose the herbicides S-metolachlor and mesotrione, which are commonly applied in mixture. Results revealed that metolachlor does not affect mesotrione kinetics and viceversa when they are in solution, in 1:1 ratio.

A new reactor was developed in our lab, in collaboration with Dr. Bosi from the Department of Industrial Engineering (University of Padova) with improved design and features with respect to the existing DBD reactor. The new reactor, operating in streamer discharge regime, was exhaustively characterized in collaboration with Dr. Gabriele Neretti (University of Bologna) and Dr. Barbara Zaniol (Consorzio RFX), and tested on phenol and metolachlor.

Finally, during a four-month stage at the University of Bochum (Germany) I had the opportunity to work on a project dealing with plasma applications in the biomedical field under the supervision of Profs. Julia Bandow and Jan Benedikt. In particular, the effects of two plasma sources were tested *in vitro* on glyceraldehyde 3-phosphate dehydrogenase and *E. coli*. The results obtained for the enzyme suggest the importance of oxidation of the thiol group of the active site in plasma mode of action. The same approach was applied to assess the effect of ionic components of plasma by a new source developed by Prof. Benedikt (University of Bochum). The study of inactivation of the enzyme via plasma, with and without ions, showed a synergic effect between radicals and ions.

## Riassunto

La Tesi riporta e discute i risultati ottenuti nell'applicazione di plasmi non termici per il trattamento ossidativo di inquinanti modello e ulteriori risultati relativi all'utilizzo del plasma in campo biomedico.

L'apparato sperimentale impiegato è stato progettato e realizzato in collaborazione con il Dipartimento di Ingegneria Elettrica e produce una scarica a barriera di dielettrico (reattore DBD). Il sistema era già in uso nel periodo antecedente l'inizio della mia attività di dottorato. Le specie reattive che si generano a causa della scarica elettrica nell'aria umida sovrastante la fase liquida entrano in contatto con essa e possono reagire con l'inquinante organico in soluzione. Le specie reattive possono essere distinte in primarie, cioè generate direttamente dalla scarica per reazione del gas con gli elettroni energetici formando radicali, ioni e specie eccitate altamente reattive ed instabili, e secondarie prodotte per reazione delle stesse specie con le molecole del gas oppure con l'umidità presente.

Il primo passo è stato quello di applicare tali scariche elettriche per il trattamento di diverse categorie di inquinanti emergenti allo scopo di valutare le potenziali applicazioni di questa tecnologia in relazione alle proprietà chimico fisiche degli inquinanti trattati. Sono stati selezionati i seguenti contaminanti organici persistenti: il sulfametossazolo, un antibiotico veterinario, il triclosan, un antibatterico, l'acido perfluoroacetico e tre erbicidi, l'irgarol, il metolachlor ed il mesotrione. Per tutti i composti in esame ho ottenuto profili esponenziali di degradazione in funzione del tempo di trattamento, da cui sono state ricavate le costanti cinetiche di pseudo-primo ordine. L'analisi HPLC-MS ha consentito l'identificazione degli intermedi e prodotti di degradazione, compatibili con possibili reazioni dovute all'azione dell'ozono e dei radicali  $\cdot\text{OH}$ . Sono stati proposti inoltre i meccanismi di degradazione dei composti organici trattati.

Lo scopo finale nell'uso di processi di degradazione avanzata è la completa conversione della componente organica a  $\text{CO}_2$ . In seguito al trattamento al plasma, sono state riscontrate percentuali di mineralizzazione pari o maggiori al 93% per tutti gli inquinanti considerati, usati in concentrazione pari a 5  $\mu\text{M}$ , fatta eccezione per l'acido perfluorooctanoico per cui la percentuale di mineralizzazione è stata considerevolmente più bassa (42%).

Lo studio dei processi di degradazione al plasma è inoltre servito in alcuni casi da punto di partenza per ulteriori approfondimenti. E' questo il caso dell'irgarol, in cui si è cercato di implementare l'effetto del plasma aggiungendo un fotocatalizzatore ampiamente utilizzato,  $\text{TiO}_2$ . Non sono stati

riscontrati tuttavia miglioramenti nell'effetto della scarica su tale inquinante indicando un trascurabile effetto fotocatalitico nelle condizioni sperimentali adottate. Un ulteriore avanzamento nelle ricerche in questo ambito è consistito nell'applicazione della scarica DBD su una miscela di inquinanti, il metolachlor e il mesotrione, solitamente utilizzati in combinazione in diverse formulazioni agricole. Gli studi cinetici effettuati hanno evidenziato che i due composti non si influenzano reciprocamente quando subiscono il trattamento al plasma in soluzioni miste in cui sono presenti in rapporto molare 1:1.

Un importante parametro nella valutazione di una tecnica di depurazione consiste nell'analisi ecotossicologica del campione acquoso dopo il trattamento. A tale scopo, in collaborazione con il Prof. Giovanni Libralato del Dipartimento di Biologia dell'Università di Napoli, sono stati effettuati test tossicologici su campioni contenenti sulfametossazolo (SMZ), prima e dopo il trattamento nel reattore DBD. Allo scopo è stata utilizzata una batteria di test acuti e cronici per *Vibrio Fischeri*, *Daphnia magna* e *Raphidocaelis subcapitata*. I dati ottenuti a partire da una soluzione di SMZ  $5 \cdot 10^{-4}$  M hanno mostrato un elevato livello di tossicità della soluzione iniziale e la riduzione (*V.fischeri*) o l'azzeramento di tali effetti (*D.magna* e *R.subcapitata*) a seguito del trattamento nel reattore al plasma.

Un nuovo reattore è stato inoltre ideato e realizzato in collaborazione con il Dr. Franco Bosi, del Dipartimento di Ingegneria Industriale dell'Università di Padova. La sorgente di plasma utilizza una scarica di tipo *streamer* ed è stata realizzata allo scopo di favorire un migliore trasporto delle specie reattive prodotte dalla scarica e ottimizzare la loro interazione con la soluzione da trattare. Il reattore è stato quindi caratterizzato in collaborazione con il Dr. Gabriele Neretti (Università di Bologna) e la Dr.ssa Barbara Zaniol (Consorzio RFX, Padova) e collaudato nel trattamento di due inquinanti organici, il fenolo ed il metolachlor.

Infine nel corso di un periodo di quattro mesi di attività di ricerca presso il laboratorio della Prof.ssa Bandow dell'Università di Bochum (Germania) ho avuto modo di approfondire alcuni aspetti legati alle applicazioni del plasma atmosferico in campo biomedico. In particolare ho partecipato a studi sugli effetti di due diverse sorgenti al plasma su un enzima, gliceraldeide-3-fosfato deidrogenasi, *in vitro* e sul batterio *E. coli*. Il sito di attacco principale è risultato essere il sito attivo cisteina con conseguente ossidazione del gruppo -SH. Lo stesso approccio è stato applicato, in collaborazione con il Prof. Benedikt per lo studio degli effetti del plasma, in assenza e in presenza delle specie ioniche. I risultati ottenuti hanno evidenziato un effetto sinergico dovuto alla copresenza di specie neutre e ioniche.

# **Personal contribution statement**

## **Chapter 2**

I conceived the study, I designed and performed the experiments, except for toxicological tests, derived the models and analysed the data. I wrote the manuscript.

## **Chapter 3**

I conceived of the presented idea, verified the analytical methods, investigated and supervised the findings of this work. I wrote the final manuscript, whose results were discussed by all the authors.

## **Chapter 4**

I carried out all the experiments. I contributed to the interpretation of the results and I wrote the manuscript with inputs from all the authors.

## **Chapter 5**

I conceived the idea, performed the experiments and analyzed the results.

## **Chapter 6**

I contributed to the design and implementation of the research, to some experiments and to the analysis of the results. I contributed to the final version of the manuscript.

## **Chapter 7**

I performed the measurements, processed the experimental data, the analysis, drafted the manuscript and designed the figures.

# Chapter 1 – Introduction

## 1.1 Non thermal plasma

Plasma is the fourth state of matter. This ionized state is characterized by electrons, positive and negative ions, radicals and excited species in mixture with neutrals present in the gas, resulting in an overall electrically neutral mixture. Plasmas can be distinguished in thermal and non-thermal (NTP). The former indicate that all species (electrons, ions and neutral species) are in a thermal equilibrium state and can be described by a single temperature at each point of space [1]. In NTPs (or *cold* plasmas), ions and neutrals are characterized by close to or equal to room temperature ( $T_i$  and  $T_0$ , respectively); the temperature of the electrons ( $T_e$ ) rather may range from 10000 to 250000 K (1-20 eV) [2]. Indicating as  $T_v$  the temperature of vibrational excitation of molecules and as  $T_r$  that of their rotational excitation, it is possible to underline the differences between the reactive species of the plasma:

$$T_e > T_v > T_r \approx T_i \approx T_0$$

Ionization and chemical processes in such cold plasmas are not determined by thermal properties of the entire gas, they are induced by energetic electrons. It was reported that “NTP is considered to be highly efficient because little energy is lost in heating the surrounding fluid, which allows the energy to be focused on the excitation of electrons” [3]. Besides, in many applications heating of the gas represents a drawback, making non thermal discharges a most convenient option. Compared to thermal discharges, cold discharges have shorter duration, reduced current intensity and a lower ionization level ( $10^{-6}$ ) and electron density ( $10^{13} \text{ cm}^{-3}$ ); however, they are more efficient with limited power and more selective as regards chemical reactions produced [4]. With the appropriate electron energy distribution, it is possible to trigger specifically some reactions: this means that, by varying gas composition and electrodes configurations it is possible to induce specific excitations and reactions, thus “tuning” the plasma characteristics according to the purpose.

## 1.2 Atmospheric pressure plasma discharges

In general, a plasma discharge is generated by applying a high voltage between two electrodes separated by a gas, thus producing an electrical field. A large variety of discharges is known. They can be classified according to their time dependence (stationary or transient), distance between the discharge and the surface or heating of the gas species [1, 4]. Some examples are represented by corona, dielectric barrier (DBD) discharges, streamers and plasma jets. Corona and DBD were the first most common sources operating at atmospheric pressure and room temperature to be indicated

as non thermal discharges. This physical mode of operation represents a significant advantage: it enables to eliminate expensive setup requirements for vacuum control and thus makes the technique more cost-effective and feasible for biological treatment [5]. Corona is generated when a voltage of some kV is applied and a discharge expands from a (driven) electrode, usually a needle or a wire, to an extended surface (counter electrode). Corona discharges can be continuous or pulsed: the former is produced when DC or low frequency AC voltages are applied between the electrodes; the latter occurs for short voltage pulses (usually submicroseconds). The most common configurations are the point-plane, with a needle placed above a grounded plane, wire-cylinder and wire-plate. Depending on its polarity and geometry, it is possible to distinguish streamer corona, glow corona, spark (usually positive point-to-plane discharge) and pulse corona. Streamer and glow discharges are examples of cold discharges while at higher pressures and currents they can change into spark or arc discharges. Corona owes its name to the presence of several “ionic filaments” (*streamers*) that, with crownlike appearance, are initiated from one (driven) electrode and, depending on the configuration, may or not reach the counter electrode [4].

DBD is the typical plasma setup used in ozonizers. In barrier discharges one or both the electrodes consist of a dielectric material, usually glass, plastics or ceramics [6]. This is due to avoid instabilities in the discharge, crucial for commercial applications. The presence of a dielectric material avoids a discharge in continuous operation mode. For this reason, barrier discharges operate at alternating voltage, from a few V to about 10 kV, depending on the distance between the electrodes. The best distance between the electrodes is usually of a few millimeters; with larger gaps the discharge becomes inhomogeneous.

Contrary to corona discharge, streamer discharges are transient and filamentary. Streamers are defined as rapidly extending ionized fingers, at high electric fields. Developing a discharge, streamer initiation occurs when free charge carriers multiply in regions where the field is above the breakdown value and an additional electric field is created by them. The streamers represent the early stage of electric breakdown of large nonionized regions. In fact, thanks to the strong field enhancement, streamer penetration occurs into areas where the background electric field is below the ionization threshold. In most cases streamers are generated from a tip- or wirelike electrodes, in order to enhance the electric field and to initiate easily the streamer. The advantage of this geometry lies in the fact that the required voltages for streamer initiation are reduced, making the process cheaper [4].

The operation gas can vary according to the specific plasma treatment application. Many cold atmospheric pressure plasma operate in helium or argon. Helium shows a thermal heat conductivity about 10 times larger than that of most other gases, thus enhancing heat removal from the discharge.

Helium is often used in atmospheric-pressure plasma jets, a new concept of plasma sources, usually applied for local treatment in biomedical applications [7], surface cleaning and coating processes [8]. Especially for the first application mentioned above, an important requirement is related to the gas temperature, that has to be close to room temperature [9]. They exhibit many characteristics of a conventional, low-pressure glow discharge and can be driven by RF and AC high voltage. Compared to other sources, plasma jets blow plasma outside the device, overcoming the disadvantage of conventional plasmas confined between electrodes [10]. In my thesis work I had the opportunity to use two DBD and a streamer plasma sources and also a plasma jet.

### 1.3 Plasma chemistry

The reactions occurring in a plasma depend on the gas and the configuration used to produce the discharge. In general, the main process in a discharge is represented by ionization, in particular, electron impact ionization. This process leads to ionization of the background gas by interaction with the electrons accelerated in the electric field:



When the electrical discharge occurs in air:



Other relevant phenomena concern the electron loss due to the attachment on gas components possessing high electron affinity.



This interaction can lead to dissociation, i.e. dissociative attachment



or three-body attachment



where M indicates an arbitrary species, needed for energy and momentum conservation. The field at which impact ionization and electronic attachment precisely balance is called *breakdown field* [4].

Non thermal plasma is characterized by a high chemical efficiency. As mentioned in the previous paragraph, almost all the energy provided by the system is converted into energy of the electrons (~10 eV), that in turn can trigger many different chemical reactions.

Fragmentation processes can occur, with the consequent formation of free radicals:





as well as excitation of atomic or molecular species:



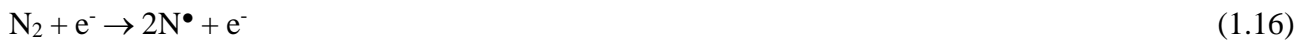
Molecular excitation can lead to radical species formation through bond dissociation



Homolytic bond dissociation can be also induced by electron impact:



Specifically, in air:



Besides, reactive species can undergo recombination:



The above chemical reactions lead to the formation of secondary reactive species, like ozone in the case of air non thermal plasma:



where M is molecular nitrogen or oxygen. Nitrogen oxides, NO and NO<sub>2</sub>, are formed as a result of the following reactions:



Plasma causes ionization reactions of NO and O<sub>3</sub> by exothermic charge exchange with primary ions:



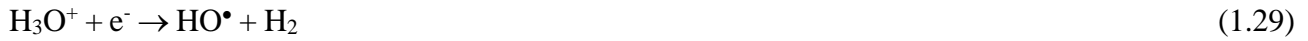
NO can also be removed in non thermal plasma through the following reaction:



In the presence of humidity, hydroxyl radicals are also formed. This strong oxidant can be produced by the electron-induced dissociation of water



by its dissociative electron recombination



by ionic pathways



Hydrogen peroxide is also formed by the reaction of atomic oxygen in the presence of water



or by recombination of hydroxyl radicals



The main reactive oxygen species (ROS) and nitrogen species (RNS) present in air NTPs are thus: metastable states of molecular oxygen and nitrogen, excited and ground state atomic oxygen,  $\text{O}^*$  and  $\text{O}$ ; ionic species  $\text{O}_2^{+\bullet}$ ,  $\text{N}_2^{+\bullet}$ ,  $\text{NO}^+$ ,  $\text{O}_2^{-\bullet}$ ,  $\text{O}^{-\bullet}$ ,  $\text{O}_3^{-\bullet}$ ; OH radical, ozone,  $\text{H}_2\text{O}_2$  and NO.

These reactive nitrogen and oxygen species (RONS) will be considered in evaluating the performance of all the sources employed in this thesis. In the case of helium plasma jets operating at atmospheric pressure, excited  $\text{He}^*$  is important for energy transfer to create RONS [11, 12].

#### 1.4 Plasma and liquid: reactions induced by air NTP in water

Chemical processes induced by low temperature plasmas in gas-liquid environment and in liquids have become an important research topic due to recent developments in many different fields, especially plasma medicine [13] and nanomaterials synthesis [14, 15]. Plasmas produce a wide variety of species, that can dissolve into and react at the gas-liquid interface or within the bulk of the liquid [16, 17]. An example is represented by hydroxyl and hydroperoxyl ( $\text{HO}_2$ ) radicals, formed in the plasma phase in contact with the liquid and that can dissolve in water to react and form  $\text{H}_2\text{O}_2$ . Similarly,  $\text{NO}_x$  species will readily dissolve in aqueous solution to form  $\text{HNO}_2$  and  $\text{HNO}_3$  [17].

When non thermal plasma is in contact with the aqueous solution, reactive species can produce secondary radicals:



The hydroxyl radical is one of the major species produced by electrical discharges with water. It is the strongest oxidant in aqueous environment ( $E^0 = 2.85\text{V}/\text{SHE}$ ), it is highly reactive, unselective and reacts with organic and inorganic species. Important  $\bullet\text{OH}$  scavengers in natural systems are represented by carbonates and phosphates. It is possible to distinguish three main oxidation pathways

of organic species, hydrogen abstraction, hydroxyl radical electrophilic addition to unsaturated systems and direct electron transfer [18]:



Organic radicals may be further oxidized to peroxy radicals and successively transformed in oxy and hydroperoxy radicals. The following formation of organic peroxides, aldehydes and acid can lead in some cases to complete mineralization ( $\text{CO}_2$  as final product). Ozone is also a precursor of  $\bullet\text{OH}$  in water. It is a powerful oxidant ( $E^0=2.07\text{ V}$ ) and it is formed in the gas-phase. It can transfer into the liquid but it is not stable in water and, particularly at basic pH, it undergoes a series of chain reactions that can be initiated by hydroxide ion [19]:

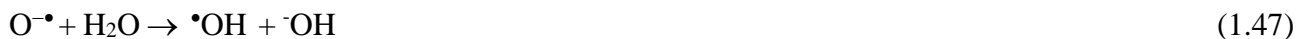


The ozone radical anion,  $\text{O}_3^{\bullet-}$ , reacts further along reaction paths which depends on the pH of the solution. In all cases, however, it gives rise to the formation of  $\bullet\text{OH}$ :

At  $\text{pH} < 8$ :

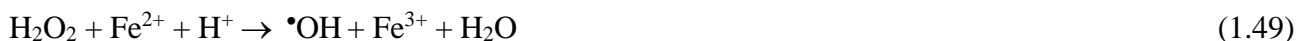


At  $\text{pH} > 8$ :



Ozone reacts with specific functional groups of organic compounds by cycloaddition, electrophilic substitution and, more rarely, nucleophilic substitution reactions. It can react also with inorganic species like  $\text{Fe}^{2+}$  and nitrites [20].

Hydrogen peroxide is a long-lived species ( $E^0 = 1.78\text{ V}$ ). Due to its water solubility it can react in the gas phase, at the interphase and in the bulk target solution. It is able to oxidize many organic compounds by direct reaction or indirectly. The indirect oxidation includes interaction with transition metals, i.e.  $\text{Fe}^{2+}$ , in the Fenton's reaction [4]:



It is known that the presence of hydrogen peroxide can contribute to PAW, plasma activated water, a post discharge aqueous solution with proven beneficial effects, for example on seeds germination and sterilization [21, 22].

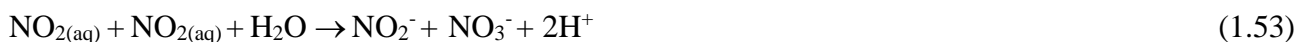
Most of the various reactive species produced by plasma in water and at the gas-liquid interface are able to release hydronium ion into aqueous solution. Thus, a pH decrease is typically observed, accompanied by an increase in solution conductivity. This acidic environment is largely attributed to the formation of nitrous and nitric acid in the liquid phase and can be explained starting from reactions of NO in the gas phase:



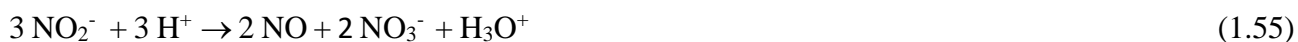
NO e NO<sub>2</sub> may react with hydroxyl radical to produce nitrous and peroxyntrous acid, respectively:



Nitrogen dioxide can dissolve in water and undergo the following reactions:



Nitrites can be subjected to disproportionation into nitrates and nitric oxide:



In acidic conditions, HNO<sub>2</sub> can produce nitrosonium ion NO<sup>+</sup>, responsible of nitrosilation of primary and secondary amines and substitution reactions on aromatic compounds [23]:



Peroxyntrous acid can also form by the reaction of NO<sub>2</sub><sup>-</sup> with H<sub>2</sub>O<sub>2</sub> or by reaction of NO with superoxide anion [24, 25]:



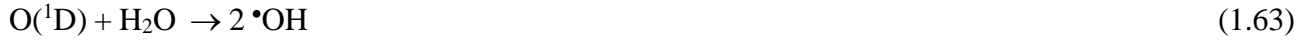
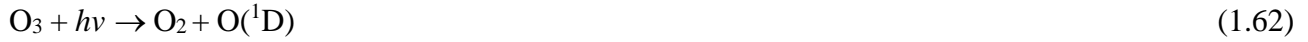
Peroxynturate is a very strong oxidant species, with a short half-life (~10-20 ms). It can oxidize organic molecules directly, usually at neutral or basic pH, or through proton- or CO<sub>2</sub> catalyzed homolysis, which promotes the release of NO<sub>2</sub> and •OH in the liquid [4].

The energy produced during the electrical discharges may be also converted to UV light. UV radiation can react directly with the organic species (direct photolysis) although, in aqueous solution, this process is in competition with absorption by water in the vacuum UV region. Alternatively, UV light can induce the decomposition of ozone, hydrogen peroxide or a photocatalyst (indirect photolysis). Direct photolysis occurs according to the following reactions:





Indirect photolysis may involve photodegradation of ozone (200-280 nm region) to form excited oxygen atom



or  $H_2O_2$  (200-300 nm)



Besides, nitrite and nitrate can photodissociate leading to secondary oxidants formation:



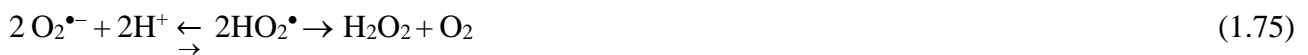
The presence of a photocatalyst can in some cases enhance the efficiency of plasma oxidation. The most common photocatalyst is  $TiO_2$ . By suspending titania particles in water solutions treated by plasma, it is possible to activate the catalyst if energy of UV photons is greater than 3.2 eV ( $\lambda < 390$  nm) [4]. This energy corresponds to the bandgap energy of  $TiO_2$  ( $E_{bg}$ ) and enables to form charge carriers on its surface upon illumination, specifically conduction band electrons ( $e_{cb}^-$ ) and valence band holes ( $h_{vb}^+$ ),



that, in the presence of oxygen and water, may react according to the following equations:



It was demonstrated that hydroxyl radical is the most important species involved and that the presence of  $TiO_2$  enhances plasma process, since the amount of  $H_2O_2$  is greater in liquid-plasma/ $TiO_2$  systems compared to plasma without the catalyst [4]. Hydrogen peroxide is produced from superoxide radical ion



or by recombination of OH radicals produced from charge carriers reactions (eq 1.73 and 1.74).  $e_{cb}^-$  and  $h_{vb}^+$  can convert hydrogen peroxide to  $\bullet\text{OH}$  and  $\text{HO}_2\bullet$ . It is possible to further increase  $\text{H}_2\text{O}_2$  production, adding to the solution suitable electron donor compounds that hinder the  $e_{cb}^-/h_{vb}^+$  recombination of  $\text{TiO}_2$  [4].

## **1.5 Applications of non thermal plasmas**

Non-thermal plasma represents a unique source of energetic electrons in a gas under atmospheric conditions. These energetic electrons can efficiently generate radicals and atomic species, ions, excited species and photons. The field of plasmas is exceptionally interdisciplinary [26]: air NTP is a form of advanced oxidation technology enabling the breakdown of organic and inorganic compounds in water [27]. The fluxes of ions of non thermal plasmas, with adjustable energies ranging from a few to several hundreds of eV, enable surface modification by sputtering, etching, activation and deposition that are essential to technological devices ranging from the etching and deposition of materials in microelectronics fabrication to medical implants [28, 29]. Among the various plasma fields, “Plasma Medicine”, combining plasma physics with life science and medicine, has been rapidly developing [5]. This thesis dealt with plasma applications in water purification and, to a lesser extent, sterilization.

### **1.5.1 Water remediation by non thermal plasma**

#### **1.5.1.1 Water pollution emergency**

“In a world where demands for freshwater are continuously growing and where limited water resources are increasingly stressed by over-abstraction pollution and climate change, neglecting the opportunities arising from improved wastewater management is nothing less than unthinkable in the context of a circular economy”. This is the take-home message of the last United Nations World Water Development Report [30], focused on reducing pollution and its impact on ambient water quality by increasing the treatment and safe use of wastewater globally. It is known that water is essential to life but the rapid population growth and the increment of agricultural and industrial activities caused an increased water demand and wastewater production. Thus, new considerations on reuse of wastewater are fundamental to face the hydric emergency. Poverty and water are closely linked: “in 2012, an estimated 842,000 deaths in middle-and low-income countries were caused by contaminated drinking water, inadequate handwashing facilities, and inappropriate or inadequate sanitation services”[30]. Data of 2015 reported also that 844 million people still lacked even a basic drinking water service and 263 million people spent over 30 minutes per round trip to collect water from an improved (limited) drinking water source. The management of water resources requires

therefore a sustainable approach in order to maintain the economic, social and environmental functions it provides in contributing to the livelihoods of people.

#### **1.5.1.2 Emerging organic contaminants (EOCs)**

The availability of water resources is intrinsically linked to water quality, as the pollution of water sources may prohibit different types of uses. Recently, the improvement of chemical analytical instrumentations has led to the detection of organic micro contaminants at very low concentration in water sources [31-33]. Among these micropollutants there are some referred to as “emerging organic contaminants” (EOCs) [34]. EOCs are defined as natural or synthetic substances that are not commonly monitored in the environment but that can induce known or suspected undesirable effects on humans and ecosystems [35]. These contaminants are originated from several kinds of products including pharmaceuticals, veterinary medicines, detergents and personal care products. In Europe, the regulation of surface water and groundwater quality standards is based on the Groundwater Daughter Directive [36] and the Directive 2008/105/EC [37]. In 2015, a watch list of substances for European Union-wide monitoring, including EOCs, was reported in the Decision 2015/495/EU [38]. These directives refer to the monitoring of volatile organic compounds, pesticides, chlorinated solvents, polycyclic aromatic hydrocarbons. With regard to Italian water resources, Zuccato et al. reported a study of some pharmaceuticals in surface water, drinking water and effluents of wastewater treatment plants (WWTPs) [39] and a list of 298 EOCs (including 137 pesticides) found in Italian surface water and groundwater was compiled recently [32]. The lack of information on toxicity and environmental impacts for a large number of contaminants, especially organic compounds, make it difficult to include them in the list of chemicals to be monitored, although the number of compounds regulated by the legislation is growing. Despite EOC concentrations encountered in the environment are quite low, in the range between ng/L and µg/L, chronic exposure of the aquatic communities may cause potentially harmful effects. The increasing concern about these chemicals as aquatic pollutants is due also to their persistence [40] and the impact of mixtures of EOCs on aquatic environment [41, 42].

#### **1.5.1.3 Advanced Oxidation Processes (AOPs)**

Wastewater treatment plants may employ conventional treatments or advanced oxidation processes (AOPs) for remediation. The first are usually based on treatment with activated sludge. Elimination of the pollutant occurs in this case by the metabolic activity of living organisms, usually microorganisms and in particular, bacteria and fungi that live in natural waters and soil [43]. It was demonstrated that conventional remediation technologies often only partially remove selected drugs

(20–90%), discharging a significant amount of them in the effluent [44, 45]. In some cases, derivatives present in wastewater effluents can also be converted back to their parent form upon entering surface waters [46]. A feasible option to remove such biologically persistent compounds is the use of AOP. Advanced oxidation processes are defined as water treatment processes performed at room temperature and normal pressure and based on the *in situ* generation of a powerful oxidizing agent, the OH radical, at a sufficient concentration to effectively decontaminate waters [47]. Organic contaminants can be effectively removed by hydroxyl radicals [48-50] which are known to be very reactive and non selective [51, 52]. It is possible to have chemical, photochemical, electrochemical and sonochemical AOPs depending on the way hydrogen peroxide is produced [53, 54]. The oldest and most used chemical AOP is the Fenton method, which uses a mixture of a soluble iron(II) salt and H<sub>2</sub>O<sub>2</sub>, known as the Fenton's reagent. However, heterogeneous photocatalysis, using TiO<sub>2</sub> suspensions as well as ozonolysis (O<sub>3</sub> + UV irradiation) have been reported [54]. Since it enables the creation of a highly reactive environment (OH radicals, ozone, hydrogen peroxide, UV radiation, etc...), plasma technology can be considered a synergic combination of all the above described processes [55].

#### **1.5.1.4 Non thermal plasma for water remediation: state of the art**

The first employment of non-thermal plasma for environmental purposes was related to air pollution control; in particular for treating NO<sub>x</sub>, short- and long-chained hydrocarbons, volatile organic compounds (VOCs) and elementary mercury [26, 56, 57]. It has shown great promise in treating vehicle exhaust gas, both gasoline and diesel. The reactive environment created in non thermal plasma has been applied next to eliminate a variety of organic compounds from water. In the search for a cost-effective solution, plasma processes have recently gained more attention since they are one of the most effective available techniques to decompose recalcitrant organics [26, 58, 59].

Beyond the classification based on plasma discharges (see 1.2 section), plasma reactors for water treatment can be distinguished according to their electrode configuration. Electrical discharges can be generated: directly in the water bulk, directly in the water bulk with externally applied bubbles (bubble discharge reactors), in the gas phase over water bulk or film, in the gas phase with water drops or mist, as a combination of the previous types, or not in direct contact with the solution under treatment [60]. A wide number of homogeneous and heterogeneous catalysts were introduced into plasma systems for water treatment, in order to enhance the effects of plasmachemical processes. Some examples are represented by metallic electrodes, like platinum or tungsten, by the addition of iron or the introduction of TiO<sub>2</sub>. It was also shown that activated carbon may operate both as adsorbant and catalyst in the liquid phase and that the process efficiency increases if plasma is associated to



ultrasonication [4, 61]. Additionally, several working gas are used, influencing significantly plasma chemistry and therefore treatment efficiency and by-product formation: oxygen generally enhances the process efficiency, argon often performs better for phenol degradation [60]. However, they are not economically feasible for use on large scale and atmospheric air is more often preferred due to its wide availability.

The major drawbacks of non thermal plasma AOP are the energy efficiency, preventing in some cases the implementation of plasma systems on a larger scale and the incomplete understanding of plasma interaction mechanisms with the various classes of organic pollutants [60]. An extensive study of generated oxidation by-products and long-living oxidants in treated water is necessary to verify that overall toxicity is consistently and sufficiently decreased by the plasma treatment. The present thesis aimed at investigating the above mentioned aspects and answering some of the questions regarding the prospects of electrical discharges for environmental applications.

### **1.5.2 Biological applications of plasma: sterilization**

The innovative field of plasma medicine is emerging as a hot multidisciplinary topic, involving the physics, chemistry, biology and engineering community. For over 20 years now, cold plasma has been investigated on live organisms, proteins, DNA, infectious agents, single microbial cell and viruses, eukaryotic cells, biofilms [62]. Plasma has recently generated considerable attention due to promising applications in contamination control and medicine [63, 64]. Although significant progress on its molecular mechanisms has been made in the past decade, the literature is still lacking in understanding of the role of oxidants and in cells and tissues relating to the effects of plasma [65]. In this work, particular emphasis was given to the effect of some components of cold plasma on biological macromolecules and on inactivation of bacteria, since this is the most common studied cell type.

Non thermal atmospheric pressure plasma is needed to treat heat-sensitive biological systems. Cold plasma for biological applications can be classified into dry gas plasma, humid gas plasma, gas plasma in contact with liquid and plasma formed in the liquid phase. The discharge configurations can vary from corona discharges, DBD, gliding arc discharges, microwave, RF discharges and plasma jets. Three new cold atmospheric plasma devices (PlasmaDerm® of Cinology GmbH, kINPen Med of neoplasm tools GmbH and plasma ONE of plasma MEDICAL SYSTEMS®) have been certified as medical devices and are currently used for the treatment of patients. Moreover, the plasma physics community, within the EU COST plasma medicine project, has developed a reference microscale atmospheric pressure plasma jet [66]. RONS produced by the discharge depend on the type of plasma contacting with the liquid and the chemical composition of the operating gas and the liquid

environment [67]. Bacterial degradation can be attributed to chemical effects, since the oxidizing plasma components can attack the bacteria external membrane and degrade specific components [68]. This process is strongly influenced by the type of bacteria: gram-positive have much thicker cell walls, consisting mainly in peptidoglycan, teichoic acids and surface proteins. Gram-negative membrane is thinner but more complex, richer in lipids and lipopolysaccharides compared to that of gram-positive bacteria [69]. Reactive species can attack the functional groups of the outer membrane compounds (“etching process”) and once inside the cell, they can attack RNA bases or proteins [70]. In addition, physical mechanisms related to the electrical discharge can contribute to plasma interactions with living organisms. It is well known, for example, that UV radiation can inhibit the replication of cells, by causing the dimerization of thymine bases in DNA strands [71, 72]. Possible effects due to local thermal heating enhance the microorganisms inactivation, e.g. by increasing the rate of RONS chemical reactions or by denaturation of proteins. Finally, pulsed electrical field related to plasma can contribute to changes in cell morphology, inducing lethal effects. It is worth to cite the process of electroporation: it occurs when a potential difference is generated across the cell membrane by a pulsed electrical field. If the field reaches the voltage across the membrane of approximately 1V, the membrane becomes permeable to macromolecules. This effect can be reversible or irreversible, with the consequence of cell death, according to the diameters of the pores (that in turn depends on the electric field and on the pulse duration) [73].

## References

1. Fridman A. Plasma chemistry. Cambridge university press. 2008
2. Meichsner J, Schmidt M, Schneider R, Wagner H. Nonthermal plasma chemistry and physics. CRC Press. 2012
3. Gerrity D, Stanford BD, Trenholm RA, Snyder SA. An evaluation of a pilot-scale nonthermal plasma advanced oxidation process for trace organic compound degradation. *Water Res.* 2010; 44(2):493-504
4. Parvulescu VI, Lukes P, Magureanu M. Plasma Chemistry and Catalysis in Gases and Liquids. Wiley-VCH, US. 2012
5. von Woedtke T, Metelmann H-, Weltmann K. Clinical Plasma Medicine: State and Perspectives of in Vivo Application of Cold Atmospheric Plasma. *Contributions to Plasma Physics.* 2014; 54(2):104–117
6. Kogelschatz U (2003) Dielectric-barrier discharges: their history, discharge physics, and industrial applications. *Plasma Chem Plasma Process* 23:1
7. Bekeschus S, Schmidt A, Weltmann K, von Woedtke T The plasma jet kINPen – A powerful tool for wound healing. *Clinical Plasma Medicine* 2016; 4:19-28

8. Schäfer J, Foest R, Quade A, Ohl A, Weltmann K. Local deposition of SiO<sub>x</sub> plasma polymer films by a miniaturized atmospheric pressure plasma jet (APPJ). *J Phys D: Appl Phys.* 2008; 41(19): 194010
9. Conrads H, Schmidt M. Plasma generation and plasma sources. *Plasma Sources Sci Technol.* 2000; 9 (4):441
10. Laroussi M, Akan T. Arc-Free Atmospheric Pressure Cold Plasma Jets: A Review. *Plasma Processes and Polymers.* 2007; 4(9):777–788
11. Jun-Seok Oh and Endre J Szili and Nishtha Gaur and Sung-Ha Hong and Hiroshi Furuta and Hirofumi Kurita and Akira Mizuno and Akimitsu Hatta and Robert, D Short. How to assess the plasma delivery of RONS into tissue fluid and tissue. *J Phys D: Appl Phys.* 2016; 49(30): 304005
12. J Benedikt and D Schröder and S Schneider and G Willems and A Pajdarová and J Vlček and V Schulz-von, der Gathen. Absolute OH and O radical densities in effluent of a He/H<sub>2</sub>O micro-scaled atmospheric pressure plasma jet. *Plasma Sources Sci Technol.* 2016; 25(4):045013
13. K-D Weltmann and Th, von Woedtke. Plasma medicine-current state of research and medical application. *Plasma Phys Controlled Fusion.* 2017;59(1): 014031
14. Pai DZ, (Ken) Ostrikov K, Kumar S, Lacoste DA, Levchenko I, Laux CO. Energy efficiency in nanoscale synthesis using nanosecond plasmas. *Scientific Reports.* 2013; 3:1221
15. Mariotti D., Sankaran R M. Perspectives on atmospheric-pressure plasmas for nanofabrication. *J Phys D: Appl Phys.* 2011; 44(17): 174023
16. Rumbach P, Bartels DM, Sankaran RM, Go DB. Corrigendum: The solvation of electrons by an atmospheric-pressure plasma. *Nature Communications.* 2015; 6:7248
17. Bruggeman PJ, Kushner MJ, Locke BR, Gardeniers JGE, Graham WG, Graves DB, Hofman-Caris RCHM, Maric D, Reid JP, Ceriani E, Fernandez Rivas D, Foster JE, Garrick SC, Gorbanev Y, Hamaguchi S, Iza F, Jablonowski H, Klimova E, Kolb J, Krcma F, Lukes P, Machala Z, Marinov I, Mariotti D, Mededovic Thagard S, Minakata D, Neyts EC, Pawlat J, Lj Petrovic Z, Pflieger R, Reuter S, Schram DC, Schröter S, Shiraiwa M, Tarabová B, Tsai PA, Verlet JRR, von Woedtke T, Wilson KR, Yasui K, Zvereva G. Plasma–liquid interactions: a review and roadmap. *Plasma Sources Sci Technol* 2016; 25(5) [053002]
18. Tarr MA. *Chemical Degradation Methods for Wastes and Pollutants: Environmental and Industrial Applications.* Marcel Dekker, Inc., New York, NY. 2003
19. Gottschalk C, Libra JA, Saupe A. *Ozonation of Water and Waste Water: A Practical Guide to Understanding Ozone and its Application.* Wiley-VCH Verlag GmbH. Weinheim, Germany 2007
20. Hoigné J, Bader H. Rate constants of reactions of ozone with organic and inorganic compounds in water—II: Dissociating organic compounds. *Water Research.* 1983; 17:185-194
21. Sivachandiran L, Khacef A. Enhanced seed germination and plant growth by atmospheric pressure cold air plasma: combined effect of seed and water treatment. *RSC Adv.* 2017;7 (4):1822-1832

22. Ma R, Wang G, Tian Y, Wang K, Zhang J, Fang J. Non-thermal plasma-activated water inactivation of food-borne pathogen on fresh produce. *J Hazard Mater.* 2015;300:643-651
23. Clayden J, Greeves N, Warren S. *Organic chemistry.* Oxford University Press, Oxford. 2012
24. Lukes P, Dolezalova E, Sisrova I, Clupek M. Aqueous-phase chemistry and bactericidal effects from an air discharge plasma in contact with water: evidence for the formation of peroxyxynitrite through a pseudo-second-order post-discharge reaction of H<sub>2</sub>O<sub>2</sub> and HNO<sub>2</sub>. *Plasma Sources Sci Technol.* 2014; 23(1): 015019
25. Brisset J, Hnatiuc E. Peroxyxynitrite: A Re-examination of the Chemical Properties of Non-thermal Discharges Burning in Air Over Aqueous Solutions. *Plasma Chem Plasma Process.* 2012;32(4): 655–674
26. Adamovich I, Baalrud S D, Bogaerts A, Bruggeman P J, Cappelli M, Colombo V, Czarnetzki U, Ebert U, Eden J G, Favia P, Graves D B, Hamaguchi S, Hieftje G, Hori M, Kaganovich I, Mizuno A, Moreau E, Murphy A B, Niemira B A, Oehrlein G S, Lj Petrovic Z, Pitchford L C, Pu Y-K, Rauf S, Sakai O, Samukawa S, Starikovskaia S, Tennyson J, Terashima K, Turner M M, and M C M van de Sanden M C M, Vardelle A. The 2017 Plasma Roadmap: Low temperature plasma science and technology. *J Phys D: Appl Phys.* 2017; 50(32): 323001
27. Foster JE. Plasma-based water purification: Challenges and prospects for the future. *Phys Plasmas.* 2017; 24:055501
28. Fridman G, Friedman G, Gutsol A, Shekhter AB, Vasilets VN, Fridman A. Applied Plasma Medicine. *Plasma Processes and Polymers.* 2008; 5(6):503–533
29. Fricke K, Steffen H, von Woedtke T, Schröder K, Weltmann K (2011) High Rate Etching of Polymers by Means of an Atmospheric Pressure Plasma Jet. *Plasma Processes and Polymers.* 2011;8(1):51–58
30. The United Nations World Water Development Report 2017. 2017
31. Kong L, Kadokami K, Duong HT, Chau HTC. Screening of 1300 organic micro-pollutants in groundwater from Beijing and Tianjin, North China. *Chemosphere.* 2016;165:221-230
32. Meffe R, de Bustamante I. Emerging organic contaminants in surface water and groundwater: A first overview of the situation in Italy. *Science of The Total Environment.* 2014; 481:280-295
33. Richardson SD, Ternes TA. Water analysis: emerging contaminants and current issues. *Anal Chem.* 2014; 86 (6):2813–2848
34. Pal A, Gin KY, Lin AY, Reinhard M. Impacts of emerging organic contaminants on freshwater resources: Review of recent occurrences, sources, fate and effects. *Science of The Total Environment.* 2010; 408:6062-6069
35. Lapworth DJ, Baran N, Stuart ME, Ward RS. Emerging organic contaminants in groundwater: A review of sources, fate and occurrence. *Environmental Pollution.* 2012; 163:287-303
36. EU [Groundwater Directive \(2006/118/EC\)](#)

37. Directive SF. Directive 2008/56/EC of the European Parliament and of the Council. Journal. 2008
38. Barbosa MO, Moreira NFF, Ribeiro AR, Pereira MFR, Silva AMT. Occurrence and removal of organic micropollutants: An overview of the watch list of EU Decision 2015/495. *Water Research*. 2016; 94:257-279
39. Zuccato E, Castiglioni S, Fanelli R, Reitano G, Bagnati R, Chiabrando C, Pomati F, Rossetti C, Calamari D. Pharmaceuticals in the environment in Italy: causes, occurrence, effects and control. *Environmental Science and Pollution Research*. 2006; 13(1):15-21
40. Benotti MJ, Trenholm RA, Vanderford BJ, Holady JC, Stanford BD, Snyder SA. Pharmaceuticals and endocrine disrupting compounds in US drinking water. *Environ Sci Technol*. 2008; 43 (3):597–603
41. Daughton CG, Ternes TA. Pharmaceuticals and personal care products in the environment: agents of subtle change? *Environ Health Perspect*. 1999; 107 (Suppl 6): 907–938
42. Pal A, He Y, Jekel M, Reinhard M, Gin KY. Emerging contaminants of public health significance as water quality indicator compounds in the urban water cycle. *Environment International*. 2014; 71:46-62
43. Rajasulochana P, Preethy V. Comparison on efficiency of various techniques in treatment of waste and sewage water – A comprehensive review. *Resource-Efficient Technologies*. 2016; 2:175-184
44. Karthikeyan KG, Meyer MT. Occurrence of antibiotics in wastewater treatment facilities in Wisconsin, USA. *Sci Total Environ*. 2006; 361(1-3):196-207
45. Clara M, Strenn B, Gans O, Martinez E, Kreuzinger N, Kroiss H. Removal of selected pharmaceuticals, fragrances and endocrine disrupting compounds in a membrane bioreactor and conventional wastewater treatment plants. *Water Research*. 2005; 39:4797-4807
46. Stackelberg PE, Furlong ET, Meyer MT, Zaugg SD, Henderson AK, Reissman DB. Persistence of pharmaceutical compounds and other organic wastewater contaminants in a conventional drinking-water-treatment plant. *Sci Total Environ*. 2004; 329(1-3):99-113
47. Glaze WH, Kang J, Chapin DH. The chemistry of water treatment processes involving ozone, hydrogen peroxide and ultraviolet radiation. *The Journal of the International Ozone Association*. 1987 9(4):335-352
48. Wols BA, Hofman-Caris CHM. Review of photochemical reaction constants of organic micropollutants required for UV advanced oxidation processes in water. *Water Research*. 2012; 46:2815-2827
49. Garca-Montao J, Ruiz N, Munoz I, Domenech X, Garca-Hortal JA, Torrades F, Peral J. Environmental assessment of different photo-Fenton approaches for commercial reactive dye removal. *J Hazard Mater*. 2006; 138(2):218-225
50. Schulze-Hennings U, Pinnekamp J. Response surface method for the optimisation of micropollutant removal in municipal wastewater treatment plant effluent with the UV/H<sub>2</sub>O<sub>2</sub> advanced oxidation process. *Water Sci Technol*. 2013; 67(9):2075-82

51. Pignatello JJ, Oliveros E, MacKay A. Advanced oxidation processes for organic contaminant destruction based on the Fenton reaction and related chemistry. *Crit Rev Environ Sci Technol*. 2006;36(1): 1-84
52. Shannon MA, Bohn PW, Elimelech M, Georgiadis JG, Marias BJ, Mayes AM. Science and technology for water purification in the coming decades. *Nature*. **2008**; 452:301–310
53. Oller I, Malato S, Sánchez-Pérez JA. Combination of Advanced Oxidation Processes and biological treatments for wastewater decontamination—A review. *Science of The Total Environment*. 2011; 409:4141-4166
54. Oturan MA, Aaron J. Advanced oxidation processes in water/wastewater treatment: principles and applications. A review. *Crit Rev Environ Sci Technol*. 2014; 44(23):2577-2641
55. Jiang B, Zheng J, Qiu S, Wu M, Zhang Q, Yan Z, Xue Q. Review on electrical discharge plasma technology for wastewater remediation. *Chemical Engineering Journal*. 2014; 236:348-368
56. Byun Y, Koh DJ, Shin DN. Removal mechanism of elemental mercury by using non-thermal plasma. *Chemosphere*. 2011; 83:69-75
57. Feng X, Liu H, He C, Shen Z, Wang T. Synergistic effects and mechanism of a non-thermal plasma catalysis system in volatile organic compound removal: a review. *Catal Sci Technol*. 2018; Advance article
58. Hijosa-Valsero M, Molina R, Schikora H, Müller M, Bayona JM. Removal of priority pollutants from water by means of dielectric barrier discharge atmospheric plasma. *Journal of Hazardous Materials*. 2013;262:664-673
59. Magureanu M, Mandache NB, Parvulescu VI. Degradation of pharmaceutical compounds in water by non-thermal plasma treatment. *Water Research*. 2015; 81:124-136
60. Vanraes P, Nikiforov AY, Leys C. Plasma Science and Technology-Progress in Physical States and Chemical Reactions. InTech, Tetsu Mieno (ed). 2016
61. Tomohiro Takahashi and Noriharu Takada and, Hirotaka Toyoda. Synergistic effect of microwave plasma and ultrasonic wave on decomposition of organic compounds in water. *Japanese Journal of Applied Physics*. 2014; 53:07KE01
62. Mizuno A. Destruction of biological particles using non-thermal plasma. *Journal of Clinical Biochemistry and Nutrition*. 2016. Doi:10.3164/jcbrn.16-64
63. Machala Z, Hensel K, Akishev Y. Plasma for Bio-Decontamination, Medicine and Food Security. Springer, Dordrecht. 2012
64. Laroussi M. From Killing Bacteria to Destroying Cancer Cells: 20 Years of Plasma Medicine. *Plasma Processes and Polymers*. 2014. Doi:10.1002/ppap.201400152
65. David BG. The emerging role of reactive oxygen and nitrogen species in redox biology and some implications for plasma applications to medicine and biology. *J Phys D: Appl Phys*. 2012;45(26): 263001

66. Beijer P A C, Sobota A, van Veldhuizen E M, Kroesen G M W. Multiplying probe for accurate power measurements on an RF driven atmospheric pressure plasma jet applied to the COST reference microplasma jet. *J Phys D: Appl Phys.* 2016; 49(10): 104001
67. Chauvin J, Judée F, Yousfi M, Vicendo P, Merbahi N. Analysis of reactive oxygen and nitrogen species generated in three liquid media by low temperature helium plasma jet. *Scientific Reports.* 2017. Doi:10.1038/s41598-017-04650-4
68. Machala Z, Tarabova B, Hensel K, Spetlikova E, Sikurova L, Lukes P. Formation of ROS and RNS in Water Electro-Sprayed through Transient Spark Discharge in Air and their Bactericidal Effects. *Plasma Processes and Polymers.* 2013. Doi:10.1002/ppap.201200113
69. Silhavy TJ, Kahne D, Walker S. *The Bacterial Cell Envelope.* Cold Spring Harbor Perspectives in Biology. 2010. Doi:10.1101/cshperspect.a000414
70. Lu H, Patil S, Keener KM, Cullen PJ, Bourke P. Bacterial inactivation by high-voltage atmospheric cold plasma: influence of process parameters and effects on cell leakage and DNA. *J Appl Microbiol.* 2014. Doi:10.1111/jam.12426
71. Sinha RP, Hader D. UV-induced DNA damage and repair: a review. *Photochem Photobiol Sci.* 2002. Doi:10.1039/B201230H
72. Schneider S, Lackmann J W, Narberhaus F, Bandow J E, Denis B, Benedikt J. Separation of VUV/UV photons and reactive particles in the effluent of a He/O<sub>2</sub> atmospheric pressure plasma jet. *J Phys D: Appl Phys.* 2011; 44(29): 295201
73. Leduc M, Guay D, Leask R L, Coulombe S. Cell permeabilization using a non-thermal plasma. *New Journal of Physics.* 2009; 11:115021

# Chapter 2 - Non-thermal plasma oxidation: degradation, kinetics, intermediate products and toxicity studies of sulfamethoxazole in aqueous solution

Agata Giardina<sup>1</sup>, Ester Marotta<sup>1</sup>, Giovanni Libralato<sup>2</sup>, Antonia Siciliano<sup>2</sup>, Cristina Paradisi<sup>1</sup>

<sup>1</sup> Department of Chemical Science, University of Padova, Via Marzolo 1, 35131 Padova, Italy

<sup>2</sup> Department of Biology, University of Naples Federico II, Naples, Italy

## Abstract

Aqueous solutions of Sulfamethoxazole (4-amino-N-(5-methylisoxazol-3-yl)-benzenesulfonamide, SMZ), an antibiotic largely employed for humans and animals and widely found in waters and wastewaters, were subjected to air non-thermal plasma treatment in a dielectric barrier discharge reactor. The effect of the pollutant initial concentration and of the solution pH on the decomposition kinetics, residual carbon in solution and products and intermediates formation was investigated. It was found that the lowest the pollutant concentration the highest is the rate of its removal. Mineralization is reached for longer treatment times with respect to the decomposition of the initial compound. For solution  $8 \cdot 10^{-6}$  M complete mineralization is obtained, a result never observed before in plasma treatments and seldom reached also with different advanced oxidation processes. From the HPLC-UV/Vis and LC-ESI-MS<sup>n</sup> analyses, it was found that the same intermediate compounds are formed regardless of the pH of the solution, but they are characterized by a different ratio distribution. Finally, toxicological analyses of the final solutions when mineralization is not complete, show the removal of harmful SMZ derivatives after plasma treatment.

## 2.1 Introduction

Advanced oxidation processes (AOPs) have demonstrated to be highly effective in removing non-biodegradable and/or toxic contaminants, like anti-inflammatory drugs, hormones, pesticides and other. These methods are based on use of hydroxyl radicals ( $\cdot\text{OH}$ ) and include ozonation UV photolysis and photocatalytic treatment [1].

Among the AOPs, non-thermal plasma (NTP), in most studies, is based on either dielectric barrier discharges (DBD) or corona discharges to produce reactive species (e.g. electrons, ions, atomic oxygen, ozone, OH radicals) in gas phase in contact with a thin layer of liquid [2]. Other approaches



are based on use of direct electrical liquid discharges and discharge in bubbles/vapor in liquid [3,4]. NTP has gained interest due to diverse oxidant species produced and because no catalysts are required, making remediation procedure cost effective and feasible for a wide range of contaminants categories. In this regard, the massive use of pharmaceuticals is causing increasing concern due to their potential toxic impact to the environment. Together with personal care products and a variety of endocrine disrupting compounds, they are included in a relatively new category of micropollutants, defined as Emerging Organic Contaminants (EOCs). These synthetic compounds belong to different categories that are biologically active but still unregulated or not commonly monitored in the environment. As a consequence of their nature, drugs often exhibit some physicochemical properties that facilitate their presence in wastewater and surface water, as polarity, significant hydrosolubility and high stability and half-life [5]. The effects of unintended chronic pharmaceutical exposure on human and animal health, as well as the ecological communities, are not yet well understood, although it is known how some of the substances detected can affect organisms in the environment. In this context, antibiotics are the most common pharmaceuticals detected in aquatic ecosystem. Their antimicrobial action makes them hard to be eliminated through conventional oxidation methods. Plasma based oxidation technology demonstrated to be a perspective alternative to the existing approaches in the remediation of antibiotics-contaminated water and soil [6]. Sulfamethoxazole (4-amino-N-(5-methylisoxazol-3-yl)-benzenesulfonamide, SMZ) is considered a typical representative. It is a widespread antibiotic, originally designed for humans but recently sharing a large global consumption in animal food industry. It is known from literature that natural degradation of SMZ by means of biological processes usually give unsatisfactory results. The treatment of conventional activated sludge enables to decompose SMZ in the range 32-49% and produces more toxic byproducts [7].

Sulfamethoxazole can be considered as a suitable model for the study of sulfamidic compounds removal from water. Boreen *et al.* [8] demonstrated that, among a group of sulfa drugs, SMZ was the slowest to degrade as result of AOP treatment, compared to analogous compounds. The same observations were reported by Kim *et. al.* specifically for plasma treatment [9]. In this work NTP generated by a dielectric barrier discharge (DBD) reactor was used to remove SMZ from water solution. The aim of this study was to investigate the removal of this sulfamidic drug from water and to compare its toxicity in the aquatic environment, before and after plasma treatment. To tackle the problem, a multi-step approach was applied: first, we defined the degradation mechanisms underlying this process, then we performed the toxicity assessment of plasma treated SMZ solutions and finally we evaluated the mineralization extent of SMZ aqueous solutions at different initial concentrations. To this purpose, the degradation products formed by NTP treatment of SMZ were identified. A few

of them were also monitored during the time course experiments at different pH. Moreover, for the first time, the toxicity of plasma treated SMZ samples was evaluated. Partially oxidized SMZ solutions were assessed for *Daphnia magna*, *Vibrio fischeri* and *Raphidocaelis subcapitata* using standardized bioassays. Complete mineralization was achieved for lower initial concentrations of SMZ and longer treatment times.

## **2.2 Materials and methods**

### **2.2.1 Materials**

Sulfamethoxazole and H<sub>3</sub>PO<sub>4</sub> (85 wt. % in H<sub>2</sub>O) were purchased from Sigma-Aldrich while KH<sub>2</sub>PO<sub>4</sub> and K<sub>2</sub>HPO<sub>4</sub>·3H<sub>2</sub>O from Carlo Erba. Ultrapure grade water (milliQ a Millipore system), obtained by filtration of distilled water with a Millipore system, was employed for all the experiments. Pure air used in the experiments was a synthetic mixture (80% nitrogen e 20% oxygen) from Air Liquid with specified impurities of H<sub>2</sub>O (<3 ppm) and of C<sub>n</sub>H<sub>m</sub> (<0.5 ppm).

### **2.2.2 Experimental apparatus**

The experimental apparatus employed in this work is a dielectric barrier discharge (DBD) reactor and it was described exhaustively in a previous paper [10]. Briefly, the reactor is made of a glass vessel (i.d.=95x75 mm, h=60 mm) with a teflon cover including four passing stainless steel electrodes. The electrodes support two parallel wires of 75 mm length and 0.15 mm diameter fixed upon their tips. The wires, made of stainless steel, are placed at a distance of 38 mm between each other and 15 mm above the aqueous solution. A volume of 70 mL of SMZ solution was employed for all the experiments and the height of the liquid inside the reactor was 10 mm. The outside bottom surface of the reactor base is covered with a film of silver and connected with the ground. The discharge is generated by an AC high voltage transformer with effective voltage of 18 kV and a frequency of 50 Hz. For all the experiments the voltage was kept constant and voltage-current measurement were performed with a digital oscilloscope (TDS5032B, bandwidth 350 MHz, sample rate 5 G/s) to verify the reproducibility of the electrical conditions.

A flow of air of 30 mL·min<sup>-1</sup> was allowed through the reactor and the discharge occurred in the gas phase above the liquid surface. To minimize evaporation phenomena from the solution to be treated, the air was humidified by passing it through a water bubbler placed before the reactor. Control experiments assured that the concentration of sulfamethoxazole remains constant in the solution when the humidified air is flowing in the absence of the discharge.

### 2.2.3 Sulfamethoxazole treatment experiments

Aqueous sulfamethoxazole solutions (70 mL) were prepared in milliQ water and phosphate buffer at pH 2, 7 and 11 and were subjected to plasma treatment. For experiments carried out at fixed pH, aqueous solutions were buffered by addition of suitable amounts of Na<sub>2</sub>HPO<sub>4</sub>, KH<sub>2</sub>PO<sub>4</sub> and H<sub>3</sub>PO<sub>4</sub>, with a buffer concentration of 2·10<sup>-2</sup> M. The efficiency of the decomposition process was determined by measuring the antibiotic conversion as a function of treatment time. To this purpose, at desired reaction times, the discharge was interrupted and a 0.5 mL aliquot of the treated solution was withdrawn and analyzed by HPLC (Thermo Scientific Products instrument with P2000 pump and UV6000LP Diode array detector). A Phenomenex Kinetex C18 column (5u C18 100A, 150x4.6 mm) was used and a mobile phase composed of water with 0.1% of formic acid (eluent A) and acetonitrile with 0.1% of formic acid (eluent B). The LC gradient for the separation was: from 0 to 20 min, a linear increase of B from 5 to 100. Then 2 minutes of isocratic elution and finally the initial conditions were re-established in 10 min. The elution was followed at 270, 314 and 370 nm. The fraction of residual drug expressed as C/C<sub>0</sub> was plotted against treatment time and the data were fitted by Equation (2.1)

$$C=C_0 \cdot e^{-kt} \quad (2.1)$$

to obtain k, the rate constant of the process.

pH of the initial and final solutions was monitored during the experiments with a pH meter Seven Compact, S220 (Mettler Toledo).

The antibiotic decomposition products were identified through the analysis of selected samples by liquid chromatography (Agilent Technologies 1100 series) connected to a diode array and a mass spectrometer detector (MSD Trap SL model G2245D). The conditions (column, eluents, gradient) were the same described above. The ionization was performed within an electrospray (ESI) source alternating positive and negative polarity with the following parameters: nebulizer 50 psi, dry gas flow rate 11 L/min, dry gas temperature 350 °C. The assignment of the oxidation products was performed by comparison of their retention time, UV/Vis and MS spectra with those obtained from standard compounds, when available. Otherwise, peaks were tentatively attributed to specific intermediate products based on MS/MS spectra and comparison with data reported in the literature.

The total carbon (TC) amount of SMZ solutions, before and after NTP treatment, was determined by a TOC analyzer (Shimadzu TOC-VCSN instrument). It operates in the range of 50 µg/L–25 g/L and is equipped with an autosampler and an automatic diluter. Calibration of the instrument was carried out by using solutions of standard potassium hydrogen phthalate automatically diluted in the range of interest.

## 2.2.4 Toxicity assessment

The toxicity tests were performed for the untreated solutions of sulfamethoxazole, the SMZ solutions treated with non-thermal plasma for 4 h and milliQ water after the same treatment. Two initial concentrations of the antibiotic were tested:  $5 \cdot 10^{-6}$  M and  $5 \cdot 10^{-4}$  M. Median effect concentrations were calculated according to each test protocol. All experiments were performed in duplicate or triplicate at temperature in the range of  $15-20 \pm 5$  °C and pH  $7 \pm 0.01$ . A battery of acute (A) and chronic (C) toxicity tests were used including biological models belonging to various trophic levels, notably *Daphnia magna*, a crustacean, (A), *Raphidocelis subcapitata*, a microalga (C), and the marine gram negative bacterium, *Vibrio fischeri* (A).

### 2.2.4.1 Toxicity assessment on *Daphnia magna*

Acute toxicity tests with *D. magna* were carried out according to ISO (2013). Five new born daphnids (0-24 h old) were exposed to each sample solution and experiments were performed in two replicates. Daphnids were bred with *R. subcapitata* in a culture medium that imitates natural fresh water. Number of mobile and immobile specimens were registered after 24 and 48 h at 20°C under continuous illumination. The daphnids were considered immobile after 48 h of incubation if not swimming within 15 s of observation. Effect data are expressed as percentage of dead organisms compared to a control containing only the neonates in the saline medium.

### 2.2.4.2 Toxicity assessment on *R. subcapitata*

The chronic test with *R. subcapitata* was carried out according to ISO (2012). Cultures were kept in Erlenmeyer flasks. The initial inoculum contained  $10^4$  cells·mL<sup>-1</sup>. The specific growth inhibition was calculated considering 3 replicates exposed at 20°C for 72 h. Tests were carried out under continuous uniform illumination ( $\geq 4300$  lx at the surface of the exposure medium). The cell density was inferred after 24, 48, and 72 h spectrophotometrically applying a Cell Density Factor (CDF). Effect data are expressed as percentage of growth inhibition.

### 2.2.4.3 Toxicity assessment on *Vibrio Fischeri*

This acute test is based on bioluminescence inhibition of the marine gram negative bacterium, *Vibrio fischeri* (earlier referred as *Photobacterium phosphoreum*). The commercial test kit, Microtox®, used in our case, is based on the specific strain, NRRL B- 11177. A Microtox analyzer M500 (Azur Environmental) was used to read light emissions. Light production is directly proportional to the metabolic activity of the bacterial population and any inhibition of enzymatic activity corresponds to the decrease in bioluminescence. The assay provides a measure of sub-lethal response of the

bacterium in the presence of pollutant agents in water, the natural bioluminescence of *V. fischeri* is reduced and the toxicity is expressed as EC<sub>50</sub> counted according the standard procedure ISO 11348-3. Luminescence inhibition of the samples was assessed for 5, 10 and 15 min of exposure. The light output of the luminescent bacteria from SMZ untreated and treated water was compared with the light output of a blank control sample.

## 2.3 Results and discussion

### 2.3.1 Effect of SMZ initial concentration

Solutions with three different concentrations, [SMZ]<sub>0</sub>, namely  $5 \cdot 10^{-4}$ ,  $5 \cdot 10^{-5}$  and  $1 \cdot 10^{-5}$  M, were prepared in milliQ water. The decomposition profile was monitored by measuring the organic pollutant conversion as a function of treatment time maintaining constant the applied voltage. Figure 1 shows the degradation curves obtained.

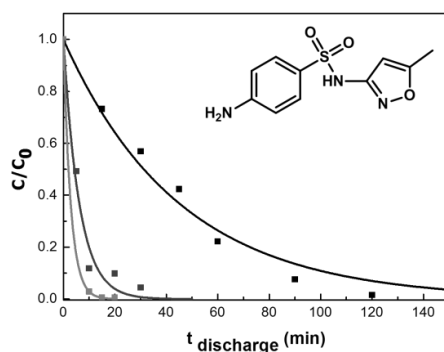


**Figure 1.** Decay curves for different initial concentrations of SMZ:  $5 \cdot 10^{-4}$  M (black)  $5 \cdot 10^{-5}$  M (dark grey) and  $1 \cdot 10^{-5}$  M (light grey)

It is evident that the rate of SMZ decomposition depends on its initial concentration (see Table 1). As it can be observed, the lower the pollutant initial concentration the faster is its degradation. This phenomenon is analogous to that observed in previous studies of NTP decomposition of volatile organic compounds in air and for phenol in water [11,12] and it can be explained according to the kinetic model proposed by Slater and Douglas-Hamilton [13].

**Table 1.** Decomposition constants for different initial concentrations of SMZ

[SMZ] <sub>0</sub> /M	$k \cdot 10^2$ /min <sup>-1</sup>	t <sub>1/2</sub> /min
$5 \cdot 10^{-4}$	$2.2 \pm 0.1$	31
$5 \cdot 10^{-5}$	$16 \pm 2$	4
$1 \cdot 10^{-5}$	$35 \pm 2$	2

### 2.3.2 Effect of pH

Experiments were carried out in buffered solutions, using  $\text{Na}_2\text{HPO}_4$ ,  $\text{KH}_2\text{PO}_4$  and  $\text{H}_3\text{PO}_4$ , to study the influence of pH on the degradation efficiency of SMZ. In the absence of a buffering system, the pH of 70 mL of milliQ water changed from neutrality to 2.8 after 240 min of plasma treatment. Previous studies demonstrated that this phenomenon is caused by the production of nitric acid dissolved in solution, as result of reactions initiated by discharge in air above the solution [12]. Moreover, the changes in the solution pH can be explained also by the production of organic acids, such as formic and oxalic acid, during the remediation process [14]. SMZ samples with the same initial concentration ( $5 \cdot 10^{-4}$  M) were prepared in three distinct buffers, at pH 2, 7 and 11 and then treated with plasma. As it can be observed in Figure 2, the degradation curves show in all cases an exponential decay while the decomposition constants are different, with removal efficiency following the pH sequence,  $k(\text{pH } 11) > k(\text{pH } 7) > k(\text{pH } 2)$  (see Table 2).

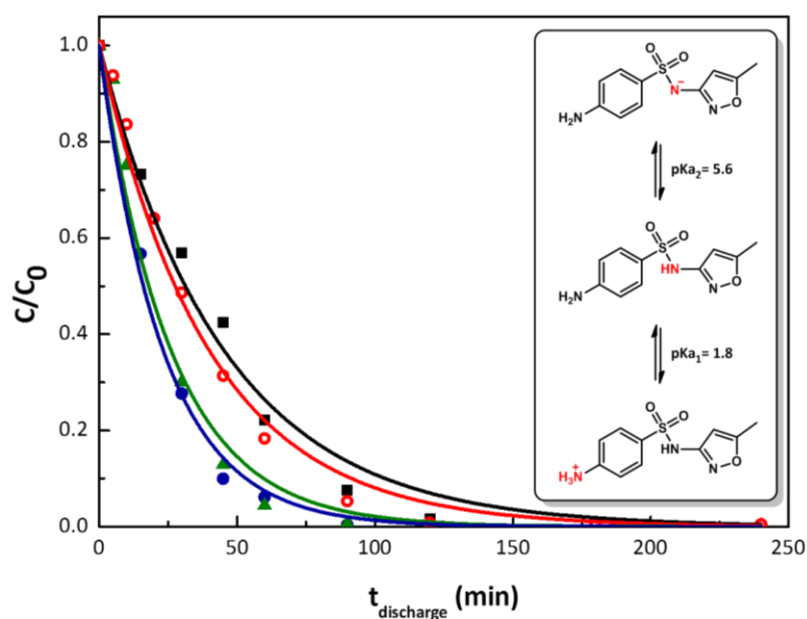


**Figure 2.** Decomposition of SMZ under different pH conditions. (■) milliQ water; (○) buffer at pH = 2; (▲) buffer at pH = 7; (●) buffer at pH = 10

The change of the degradation rate constant as a function of pH (Figure 2) can be related to the speciation of SMZ. Sulfamethoxazole presents three different species in water depending on the pH ( $\text{pK}_{a1} = 1.8$ ,  $\text{pK}_{a2} = 5.6$ ). For very acidic aqueous solutions the protonated form is predominant, with the protonation at the aniline group. At neutral pH the sulfanilamidic nitrogen of sulfamethoxazole is deprotonated. At pH 11, at which the maximum efficiency was obtained, SMZ is completely deprotonated (see ref 15).

**Table 2.** Removal efficiency of SMZ under different pH conditions.

Condition	$k \cdot 10^2 / \text{min}^{-1}$	$t_{1/2} / \text{min}$
milliQ water	$2.2 \pm 0.1$	31
buffer pH = 2	$2.5 \pm 0.1$	28
buffer pH = 7	$3.8 \pm 0.3$	18
buffer pH = 11	$4.3 \pm 0.2$	16

The significant increase of the decomposition efficiency observed going from neutral to basic pH can be explained as the sum of two contributions: the oxidant species present in solution and the reactivity of the pollutant towards them. In our plasma reactor, it is well known that ozone and hydroxyl radicals are the main species involved in the oxidation process of organic pollutants [16,17]. OH radicals can be generated directly in humid air plasma via reaction of water with atomic oxygen or via electron induced dissociation of water [18] or indirectly from decomposition of ozone in water [19]. Ozone is a selective oxidant which reacts with SMZ with a rate constant  $k_{O_3} = 3.3 \cdot 10^5$ ,  $4.7 \cdot 10^5$  and  $5.7 \cdot 10^5 \text{ M}^{-1} \text{ s}^{-1}$  with the protonated, neutral and conjugate base of SMZ, respectively [20,21]. Apparent reaction rate of SMZ with OH radicals was determined as  $(7.63 \pm 0.85) \cdot 10^9 \text{ M}^{-1} \text{ s}^{-1}$  in the range of pH 3-8, suggesting similar reactivity for neutral and anionic form of SMZ [22]. The main reactive sites of sulfamethoxazole are constituted by nitrogen at the aniline group and by the isoxazole ring. Since protonated amino groups do not react with ozone, the reactivity of amines is strongly influenced by their pKa values [20]. As already mentioned, SMZ is predominantly dissociated at pH 7 and completely deprotonated at pH 11. At a pH value corresponding to higher percentage of deprotonated sulfonamide the kinetic constant of ozone is higher, due to the increase of electron density into the oxazole ring. Vice versa, this causes a decrease in rate constants at  $\text{pH} < 7$ . Considering that ozone is one of the major reactive species in our system, it is possible to justify the similar trend in degradation constants obtained after SMZ degradation at different pH. Besides, it is known that hydroxyl radicals exhibit high reactivity with olefinic double bonds and anilines [23]. At basic pH, decomposition of ozone in water produces hydroxyl radicals increasing the amount of reactive species provided to treated solution [24].

### 2.3.3 Transformation products characterization

Mineralization of a complex organic molecule proceeds via numerous steps and involves many oxidation intermediates and byproducts. This is the case also for NTP induced advanced oxidation. These degradation intermediates and byproducts may persist after the total removal of the parent

compound. Coupled analysis by HPLC-UV/Vis and LC-MS/MS allowed for the identification of several intermediates during SMZ degradation by NTP. The same intermediates were detected under all the experimental conditions tested (pH 2, pH 7 and pH 11).

It is known that hydroxylation, cleavage of S-N bond, nitration of amino group, and isomerization are the main pathway of degradation for most AOPs [9,25-27]. The MS<sup>2</sup> spectrum of sulfamethoxazole (Figure 3a) can be very useful to interpret the MS<sup>2</sup> spectra of the intermediates arising from plasma process and therefore to identify them. The most abundant byproduct, P-99 is 3-amino-5-methylisoxazole (m/z 99), generated by cleavage of the sulphonamide bond (Figure 3b). Two compounds with m/z 270 (Fig 3 b and c) were detected and attributed to products formed by the addition of a hydroxyl radical to SMZ structure in two different positions. Thanks to MS/MS analysis, it was possible to characterize their structure: the presence of the ionic fragments at m/z 156, 108 and 92 (Fig. 3c), detected also in the fragmentation of the parental compound (Fig. 3a), suggests that, for one of the two isomers, the moiety constituted by the aniline ring linked to the sulfoxide is not modified and that the hydroxylation occurred on the isoxazole ring. In the case of the other isomer (Fig 3d), the ionic fragment at m/z 156 was not present, indicating that the attack of ·OH occurs on the benzene ring. This hypothesis is supported by the fragment at m/z 99 typical of isoxazole ring, which is therefore not modified. Furthermore, substitution of the amino group by the hydroxyl group lead to the formation of a product at m/z 271 (P-271). This dihydroxylated compound (Figure 3e) is the result of the attack of hydroxyl radical on the aniline ring (absence of ion fragment m/z 156).

Intermediates originating from the reaction of SMZ with ozone were also detected: the products at m/z 318 (Fig. 4a) and 302 (Fig. 4c) originate by the addition of ozone to the aniline ring and the following breakdown of the resulting ozonide (Fig 6); the products at m/z 336 (Fig. 4b) and 320 (Fig. 4d) are due to the following addition of a water molecule, which is supposed to take place on the isoxazole ring. Addition of a water molecule on sulfamethoxazole produces also a compound at m/z 272, while the same reaction on m/z 270 product generates P-288, dihydroxylated sulfamethoxazole, whose fragmentation pattern is similar to SMZ (m/z 108, m/z 156).

Another interesting finding was identification of two isomeric compounds with m/z 284 but different elution time (Fig 4e and f). This byproducts can be differentiated through their fragmentation pattern: comparing P-284 MS/MS spectrum (Fig 4e) with those in literature [26], it is possible to confirm its structure, resulting from oxidation of p-sulfoaniline. The second isomer P-284 (Fig 4f) was attributed to the oxidation of the isoxazolic methyl, because of losses of 18 u (-H<sub>2</sub>O) and 28 u (-CO), typical fragmentations for carboxylic derivatives. No traces of the product with -NH<sub>2</sub> oxidized to -NO<sub>2</sub> with m/z 284 was detected, even if known as the primary degradation product of ozonation [26]. Finally a hypothesis about a product detected at m/z 282 (Fig. 5) was formulated: this could be formed by



oxidation of methyl to formyl group in the isoxazole ring and of the amino group of the aniline to -NO.

Some of the by-products found are known intermediates along the complex reaction scheme leading from SMZ to CO<sub>2</sub>, observed also in other advanced oxidation techniques [9,26-28]. Others were detected for the first time, as result of plasma induced oxidation.

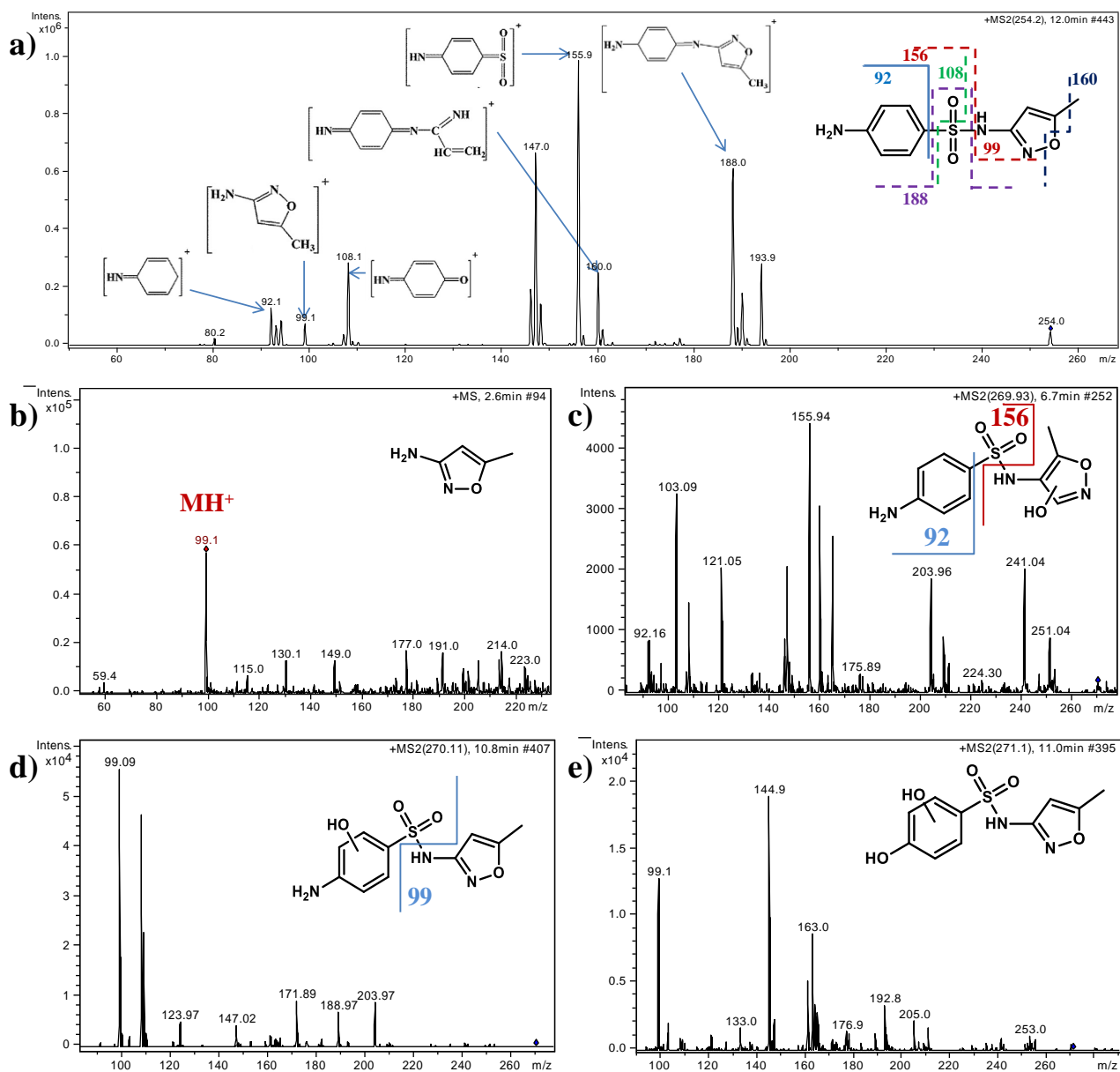


**Figure 3.** MS, MS<sup>2</sup> spectra and structures of SMZ, and of some intermediates of plasma treatment: (a) MS<sup>2</sup> spectrum of SMZ, (b) MS spectrum of the most abundant intermediate of SMZ oxidation at m/z 99, (c) and (d) MS<sup>2</sup> spectra of two isomeric intermediates detected at m/z 270 and (e) product at m/z 271

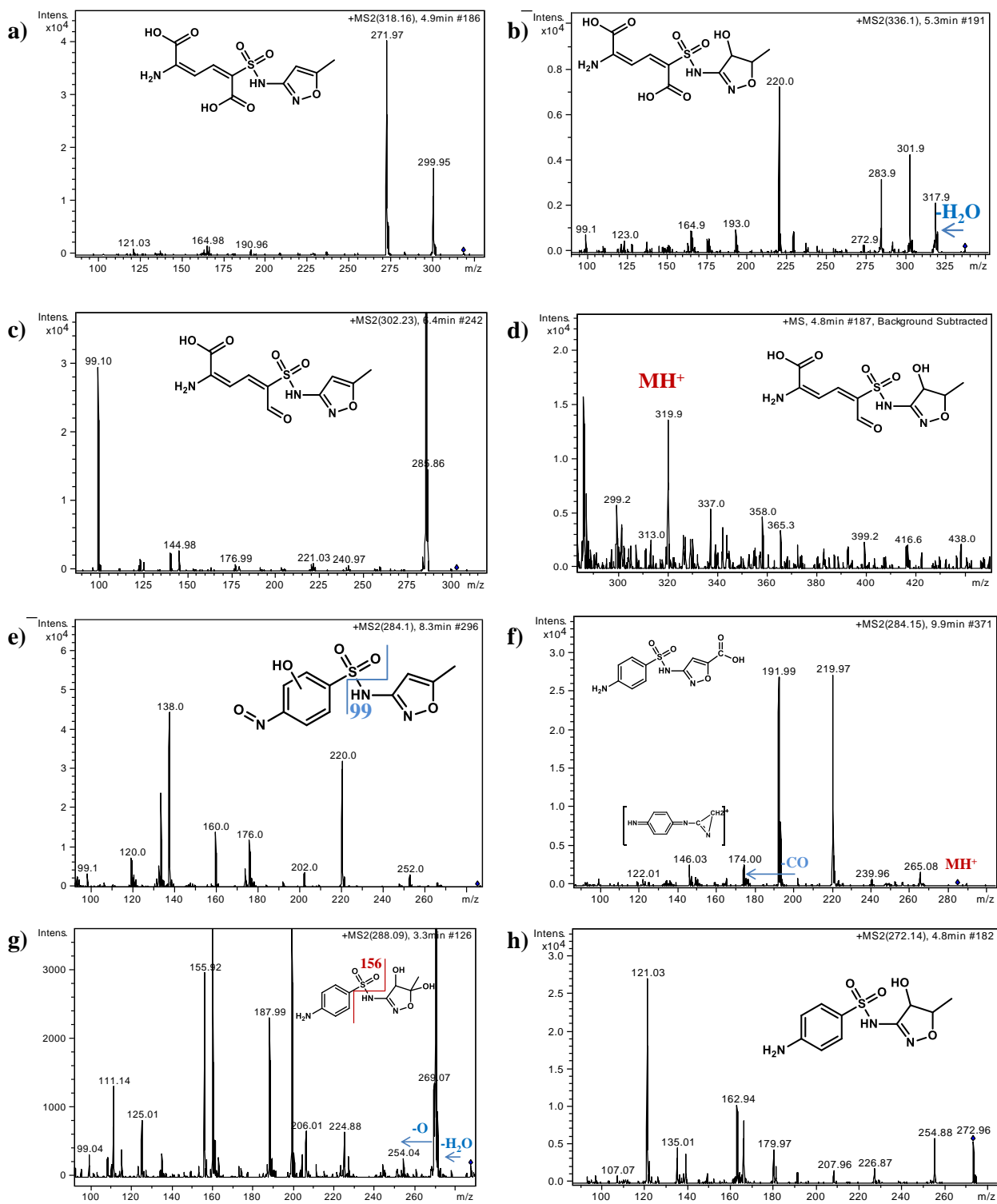


**Figure 4.** MS<sup>2</sup> spectra of some intermediates of SMZ degradation detected at (a) m/z 318, (b) m/z 336, (c) m/z 302, (e) and (f) m/z 284, (g) m/z 288, (h) m/z 272 and (d) MS spectrum of the intermediate with m/z 320

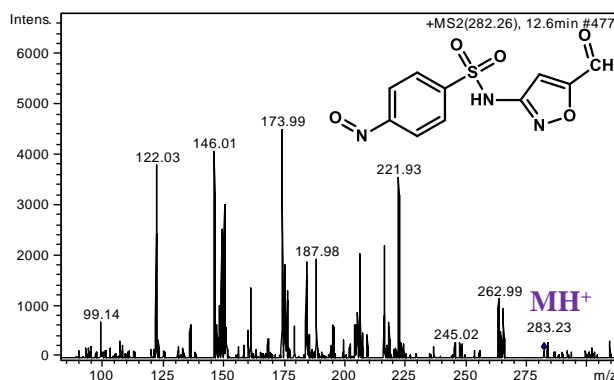


**Figure 5.** MS<sup>2</sup> spectrum of the intermediate of SMZ degradation detected at m/z 282

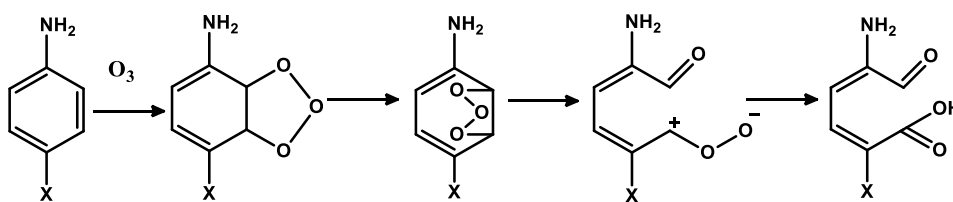


**Figure 6.** Mechanism of ozone attack on the aniline ring of SMZ

A few organic byproducts have been identified by means of HPLC analysis with UV/Vis and MS<sup>n</sup> detectors. The intermediates identified represent a further proof of the various degradation pathways of sulfamethoxazole, which may concern isoxazole ring, benzene ring or, in some cases, as the product at m/z 320 (Fig 4d), both of them. S-N bond cleavage, hydroxylation of the benzene ring or isoxazole ring, oxidation of the amine group or the methyl group at isoxazole moiety are reactions that took place in all experimental pH conditions studied, although prevailing paths occurred depending on such parameters [20]. Besides, LC-MS analysis confirmed no nitration or nitrosation of SMZ and decomposition products, not unlikely observed with plasma operation in air [6].

As above mentioned, due to its two pK<sub>a</sub>-values (1.7 and 5.6) SMZ has a cationic, neutral or anionic form. However, under environmental conditions only the latter two species are of relevance. The speciation of SMZ strongly influences the kinetics of degradation which demonstrates the necessity of separate investigation of both relevant species. It was interesting to observe how pH can affect not only the reactivity of SMZ, but also its byproducts distribution.

A key example is represented by the hydroxylated intermediate with m/z 284: hydroxyl radical attack at the benzene ring is promoted at pH > 7, when the formation of ·OH is favored and the amino group of aniline moiety is not protonated.

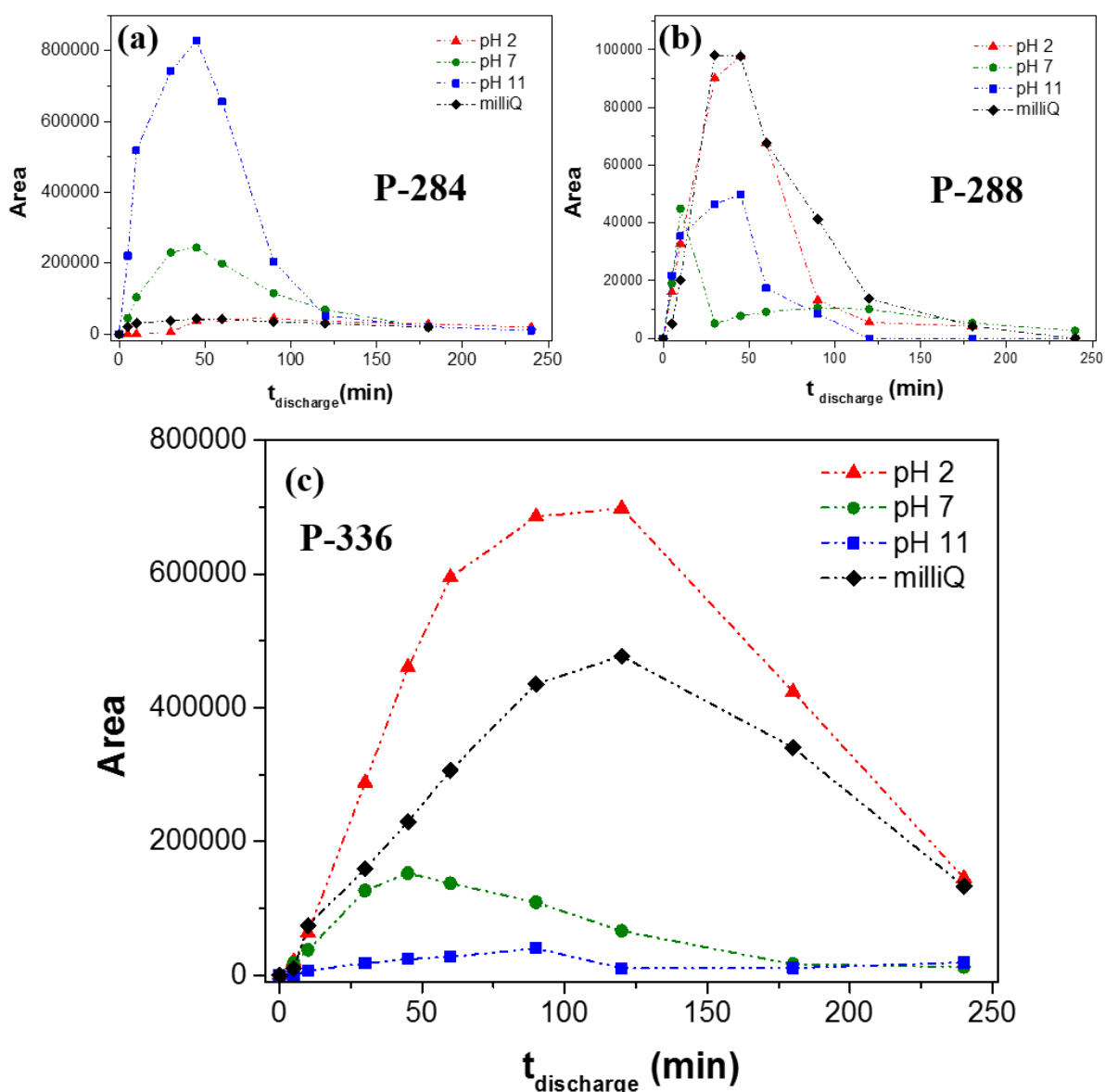


**Figure 7.** UV-HPLC areas of P-284, P-288 and P-336 as a function of treatment time.

On the contrary, addition of a water molecule on the double bond of isoxazole ring is enhanced at more acidic pH values, as shown for m/z 336 and m/z 288. Figure 7 above describes the profile changes of chromatographic MS areas (270 nm) of the products as a function of time, under different pH conditions. It can be immediately noted as, for by-products at m/z 288 and m/z 336, areas are higher at acidic pH while the opposite trend is observed for P-284. Nevertheless, to decompose all of them the best pH condition is neutral pH, at which all species described are removed in less than 240 min of plasma treatment.

As mentioned above, the desired goal in treating organic pollutants is their exhaustive oxidation to  $\text{CO}_2$ . Qualitative FT-IR online analysis confirmed formation of  $\text{CO}_2$  from the oxidation of

sulfamethoxazole. To quantify the extent of mineralization, total carbon was measured before and after plasma treatment, for initial concentration of SMZ of  $1 \cdot 10^{-5}$  M. By extending the treatment time to 360 min, CO<sub>2</sub> produced corresponds to 46% of the total organic carbon subjected to the oxidation process. In other words, 54% of the total organic carbon originally present as sulfamethoxazole remains dissolved in solution. Although SMZ is completely decomposed after 15 min of plasma treatment, some carbon-containing organic compounds are present in the system, which are more slowly oxidized than the precursor SMZ. However, this result is encouraging if compared with data already present in literature for similar treatments [9]. Mineralization extent was assessed also for lower initial concentration of the antibiotic, in particular  $8 \cdot 10^{-6}$  M. This concentration is still significantly higher than that found in the worst case scenario of poultry wastewater treatment [29] but more adequate to simulate the effect of NTP on real SMZ contaminated water samples. For this concentration values complete mineralization was achieved after 6 h of treatment. Although the treatment time can be a limitation, it is worth to note that, to our knowledge, in literature only one study reports total mineralization of SMZ, notably after catalyzed ozonation [27]. These findings may be useful in evaluation NTP as an alternative approach for persistent organic contaminants remediation in water.

#### 2.3.4 Toxicity assessment

The evaluation of SMZ solutions toxicity before and after plasma treatment is particularly interesting, since oxidation products more toxic than the target contaminant may be generated. Many case studies are described in literature about the increase of toxicity observed during the oxidation of organic contaminants in water [30-32]. Therefore, in this work, samples of SMZ solutions collected before and after plasma treatment were subjected to three different assays: *D. magna*, *R. subcapitata* and *V. fischeri*. The toxicity characterization was based on the exposure of *V. fischeri*, *R. subcapitata*, and *D. magna*, and, widely used for SMZ study with other AOP technologies [33,34]. Our study revealed the impact of SMZ solution of  $5 \cdot 10^{-4}$  M and the effect of oxidation products of SMZ formed after 4 h of plasma treatment. This condition corresponds indeed to the complete depletion of mother compound but at the same time to the presence of its degradation products.

Figure 8 shows the results about the toxicity of untreated sulfamethoxazole sample. Percentage of inhibition is quite high: EC<sub>50</sub> is 46.67% for *Daphnia magna*, 43% for *R. subcapitata* and 31% for the bacterium bioassay. After 4 h of plasma treatment, toxicity is reduced to zero for the *D. magna* assay.

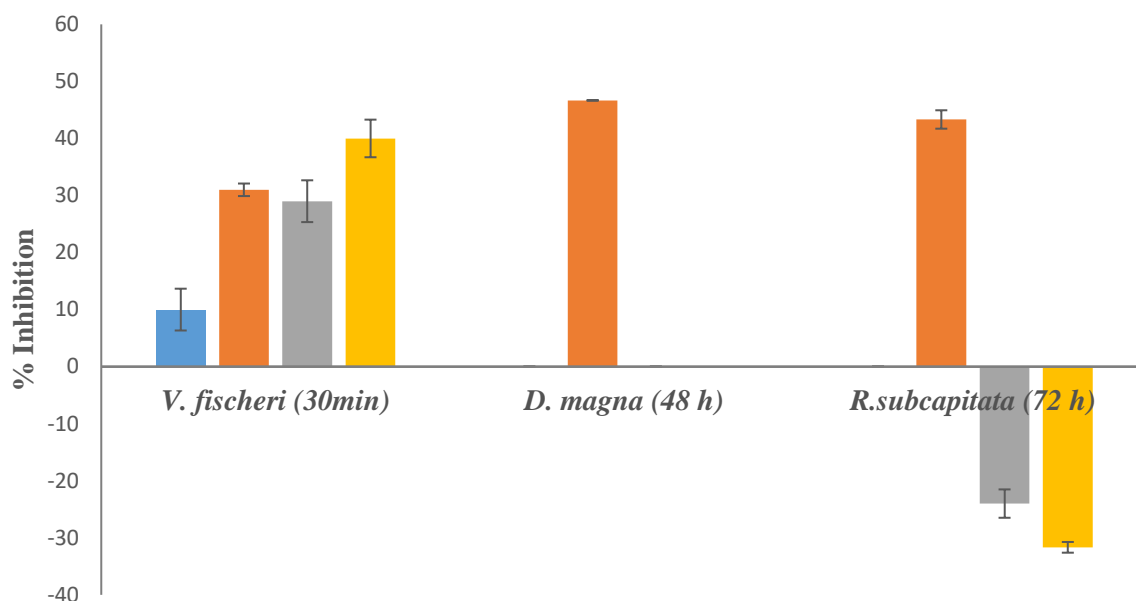


**Figure 8.** Results of the toxicological assessment of a SMZ  $5 \cdot 10^{-4}$  M in aqueous solution before (orange) and after 4 h of plasma treatment (grey). MilliQ water was subjected to the same treatment: blue rectangles indicate the untreated samples while yellow one stands for results plasma treated water

This means that the oxidation products formed during the plasma treatment are not toxic. It is worthy to note that the same test on milliQ water subjected to plasma treatment revealed no toxic potential. The effect on *R. subcapitata* was even more stunning. Compared to the untreated solution, which induces 43% of growth inhibition in microalgae, plasma treated solution is responsible of a stimulation effect in microalga growth. It is also possible to observe the same trend also for milliQ water previously subjected to NTP. This can be attributed to species produced from SMZ molecule as result of its oxidation routes.

In particular,  $\text{SO}_4^{2-}$   $\text{NH}_4^+$  and  $\text{NO}_3^-$  ions, in addition to inorganic carbon and carbon source released by the organic contaminant, may serve as nutrient for algae growth.  $\text{NH}_4^+$  are also formed during plasma treatment and its detection was already reported in literature for plasma [9] and other advanced oxidation processes [35]. Moreover, nitrate ions are produced by air non-thermal plasma in water. An effect of 29% was found for plasma treated samples of SMZ  $5 \cdot 10^{-4}$  M on *V. fischeri*, confirmed also by a similar behavior of the bacterium when in contact with plasma treated water (40% of inhibition). This suggests the importance of a toxicological characterization of AOP treated samples as complete as possible, involving different categories of organisms. Even at low level, the organic pollutants escaping from the wastewater treatment can adversely affect the balance of ecosystem.

The above observations demonstrated that, in the case of water contaminated by SMZ, plasma approach represents a feasible technology and opens new scenarios for perspective uses of plasma

treated water. Non-thermal plasma could be used as a preliminary step before biological treatment in the water treatment plants, shortening the time of application of this advanced oxidation step.

## References

ISO,2012. Water Quality– Fresh water Algal Growth Inhibition Test with Unicellular Green Algae.8692.ISO,Geneva 2012.

ISO,2013. Water Quality: Determination of the Inhibition of the Mobility of *Daphnia magna* Straus(Cladocera, Crustacea) – Acute Toxicity Test.

ISO,1998. Water quality : Determination of the inhibitory effect of water samples on the light emission of *Vibrio fischeri* (Luminescent bacteria test). Part 3: Method using freeze-dried bacteria.

1. Oturan MA, Aaron J. Advanced oxidation processes in water/wastewater treatment: Principles and applications. A review. *Crit Rev Environ Sci Technol*. 2014;44(23):2577-2641.

2. - Bruggeman PJ, Kushner MJ, Locke BR, Gardeniers JGE, Graham WG, Graves DB, Hofman-Caris RCHM, Maric D, Reid JP, Ceriani E, Fernandez Rivas D, Foster JE, Garrick SC, Gorbanev Y, Hamaguchi S, Iza F, Jablonowski H, Klimova E, Kolb J, Krcma F, Lukes P, Machala Z, Marinov I, Mariotti D, Mededovic Thagard S, Minakata D, Neyts EC, Pawlat J, Lj Petrovic Z, Pflieger R, Reuter S, Schram DC, Schröter S, Shiraiwa M, Tarabová B, Tsai PA, Verlet JRR, von Woedtke T, Wilson KR, Yasui K, Zvereva G. Plasma–liquid interactions: a review and roadmap. *Plasma Sources Sci Technol* 2016; 25(5) [053002]

3. Lukes P, Locke BR. Plasmachemical oxidation processes in a hybrid gas–liquid electrical discharge reactor. *J Phys D*. 2005;38(22):4074.

4. Bosi FJ, Tampieri F, Marotta E, Bertani R, Pavarin D, Paradisi C. Characterization and comparative evaluation of two atmospheric plasma sources for water treatment. *Plasma Processes and Polymers*. 2017. doi: 10.1002/ppap.201700130

5. Andreozzi R, Raffaele M, Nicklas P. Pharmaceuticals in STP effluents and their solar photodegradation in aquatic environment. *Chemosphere*. 2003;50(10):1319-1330.

6. Magureanu M, Mandache NB, Parvulescu VI. Degradation of pharmaceutical compounds in water by non-thermal plasma treatment. *Water Research*. 2015;81(Supplement C):124-136.

7. Dirany A, Aaron SE, Oturan N, Sirés I, Oturan M, Aaron J. Study of the toxicity of sulfamethoxazole and its degradation products in water by a bioluminescence method during

application of the electro-fenton treatment. *Analytical and bioanalytical chemistry*. 2011;400(2):353-360.

8. Boreen A L, Arnold W A, McNeill K. Photochemical fate of sulfa drugs in the aquatic environment: Sulfa drugs containing five-membered heterocyclic groups. *Environ. Sci. Technol.*, 2004; 38 (14):3933–3940

9. Kim K, Kam SK, Mok YS. Elucidation of the degradation pathways of sulfonamide antibiotics in a dielectric barrier discharge plasma system. *Chemical Engineering Journal*. 2015;271(Supplement C):31-42.

10. Marotta E, Ceriani E, Shapoval V, Schiorlin M, Ceretta C, Rea M, Paradisi C. Characterization of plasma-induced phenol advanced oxidation process in a DBD reactor. *Eur Phys J Appl Phys*. 2012; 55(1):13811

11. Schiorlin M, Marotta E, Kim H, Paradisi C, Ogata A. Determination of atomic oxygen in atmospheric plasma from oxygen isotope exchange. *Plasma Processes and Polymers*. 2011;8(9):859-866.

12. Marotta E, Ceriani E, Schiorlin M, Ceretta C, Paradisi C. Comparison of the rates of phenol advanced oxidation in deionized and tap water within a dielectric barrier discharge reactor. *Water Res*. 2012;46(19):6239-6246.

13. Slater RC, Douglas-Hamilton DH. Electron-beam-initiated destruction of low concentrations of vinyl chloride in carrier gases. *J Appl Phys*. 1981; 52(9):5820 14. - Plasma Chemistry and Plasma Processing. (- 6):- 677.

15. Dodd M C, HUang C-H. Transformation of the antibacterial agent sulfamethoxazole in reactions with chlorine: Kinetics, mechanisms, and pathways. *Environ Sci Technol*. 2004; 38 (21):5607–5615

16. Marotta E, Schiorlin M, Ren X, Rea M, Paradisi C. Advanced oxidation process for degradation of aqueous phenol in a dielectric barrier discharge reactor. *Plasma Processes Polym*. 2011;8(9):867-875.

17. Krishna S, Ceriani E, Marotta E, Giardina A, Špatenka P, Paradisi C. Products and mechanism of verapamil removal in water by air non-thermal plasma treatment. *Chemical Engineering Journal*. 2016;292(Supplement C):35-41.



18. Marotta E, Callea A, Ren X, Rea M, Paradisi C. DC corona electric discharges for air pollution control, 2—ionic intermediates and mechanisms of hydrocarbon processing. *Plasma Processes and Polymers*. 2008;5(2):146-154.
19. Staehelin J, Bühler R, Hoigné J. Ozone decomposition in water studied by pulse radiolysis. 2. OH and HO/sub 4/as chain intermediates. *J.Phys.Chem.:(United States)*. 1984;88(24):5999–6004
20. Dodd M C, Buffle M O, von Gunten U. Oxidation of antibacterial molecules by aqueous ozone: Moiety-specific reaction kinetics and application to ozone-based wastewater treatment. - *Environ Sci Technol*. 2006; 40 (6):1969–1977
21. Qiang Z, Adams C, Surampalli R. Determination of ozonation rate constants for lincomycin and spectinomycin. *Ozone: Science & Engineering*. 2004 ;26(6):525-537
22. Yang Y, Lu X, Jiang J, et al. Degradation of sulfamethoxazole by UV, UV/H<sub>2</sub>O<sub>2</sub> and UV/persulfate (PDS): Formation of oxidation products and effect of bicarbonate. *Water Research*. 2017;118(Supplement C):196-207
23. Buxton V. Critical review of rate constants for reactions of hydrated electrons, hydrogen atoms and hydroxyl radicals ( $\cdot\text{OH}/\cdot\text{O}^-$  in aqueous solution. - *Journal of Physical and Chemical Reference Data*. 1988; 17 (2): 513
24. Staehelin J, Hoigné J. Decomposition of ozone in water in the presence of organic solutes acting as promoters and inhibitors of radical chain reactions. - *Environ Sci Technol*. 1985;19 (12): 1206–1213
25. Peleyeju MG, Umukoro EH, Tshwenya L, Moutloali R, Babalola JO, Arotiba OA. Photoelectrocatalytic water treatment systems: Degradation, kinetics and intermediate products studies of sulfamethoxazole on a TiO<sub>2</sub>-exfoliated graphite electrode. *RSC Adv*. 2017; 7 (64): 40571-40580
26. Gómez-Ramos MdM, Mezcua M, Agüera A, et al. Chemical and toxicological evolution of the antibiotic sulfamethoxazole under ozone treatment in water solution. *Journal of Hazardous Materials*. 2011;192(1):18-25.
27. Shahidi D, Moheb A, Abbas R, Larouk S, Roy R, Azzouz A. Total mineralization of sulfamethoxazole and aromatic pollutants through Fe<sup>2+</sup>-montmorillonite catalyzed ozonation. *Journal of Hazardous Materials*. 2015;298(Supplement C):338-350

28. Liu X, Garoma T, Chen Z, Wang L, Wu Y. SMX degradation by ozonation and UV radiation: A kinetic study. *Chemosphere*. 2012;87(10):1134-1140
29. Asha R C, Kumar M. Sulfamethoxazole in poultry wastewater: Identification, treatability and degradation pathway determination in a membrane-photocatalytic slurry reactor. *Journal of Environmental Science and Health, Part A*. 2015; 50(10): 1011-1019
30. Hübner U, von Gunten U, Jekel M. Evaluation of the persistence of transformation products from ozonation of trace organic compounds-A critical review. *Water Research*. 2015;68(Supplement C):150-170
31. Huang H, Liu G, Lv W, Yao K, Kang Y, et al. Ozone-Oxidation Products of Ibuprofen and Toxicity Analysis in Simulated Drinking Water. *J Drug Metab Toxicol* 2015; 6:181
32. Zazo J A, Casas J A, Mohedano A F, Gilarranz M A, RODRIGUEZ J J. Chemical pathway and kinetics of phenol oxidation by fenton's reagent. - *Environ Sci Technol*. 2005;39 (23):9295–9302
33. Gómez-Ramos MdM, Mezcua M, Agüera A, et al. Chemical and toxicological evolution of the antibiotic sulfamethoxazole under ozone treatment in water solution. *Journal of Hazardous Materials*. 2011;192(1):18-25
34. Gong H, Chu W. Determination and toxicity evaluation of the generated products in sulfamethoxazole degradation by UV/CoFe<sub>2</sub>O<sub>4</sub>/TiO<sub>2</sub>. *Journal of Hazardous Materials*. 2016; 314(Supplement C):197-203
35. Calza P, Medana C, Pazzi M, Baiocchi C, Pelizzetti E. Photocatalytic transformations of sulphonamides on titanium dioxide. *Applied Catalysis B: Environmental*. 2004;53(1):63-69

# Chapter 3 - Air non-thermal plasma treatment of Irgarol deposited on TiO<sub>2</sub>

Agata Giardina, Francesco Tampieri, Ester Marotta, Cristina Paradisi

Department of Chemical Sciences, University of Padova, Via Marzolo 1, 35131 Padova, Italy

## Abstract

The herbicide 2-(methylthio)-4-(*tert*-butylamino)-6-(cyclopropylamino)-s-triazine (tradename Irgarol 1051, abbreviated here as Irg), widely used in antifouling paints as biocide inhibiting seaweeds growth, is found in coastal waters in the vicinity of ports and harbors. In this work, Irg was subjected to air non-thermal plasma (NTP) treatment, alone and in the presence of TiO<sub>2</sub>. A dielectric barrier discharge reactor was used, powered by AC voltage (18 kV, 50 Hz) to produce air-NTP directly above the surface of the aqueous Irg solution to be treated. Due to the very high rate of Irg degradation under the experimental conditions used, the results of kinetic experiments failed to detect any rate enhancement due to titania induced photodegradation. We show, however, that pre-adsorption of Irg on titania provides a means to significantly increase Irg NTP induced degradation throughput, a result which might have useful practical consequences. This phenomenon is due to the acidic character of TiO<sub>2</sub> which brings more Irg in solution by increasing  $[\text{IrgH}^+]/[\text{Irg}]$ , the ionization ratio. Product analysis, performed by LC/ESI-MS<sup>n</sup>, allowed us to detect and identify numerous intermediates of Irg degradation and to propose different competing reaction pathways for the investigated NTP induced Irg advanced oxidation process. The extent of mineralization to CO<sub>2</sub> was assessed by Total Carbon analysis. It was found to reach 95% after 5 h treatment of Irg solutions with an initial concentration of  $5 \cdot 10^{-6}$  M. These results confirm the capability of our NTP prototype reactor to mineralize persistent organic pollutants.

## 3.1 Introduction

Emerging Organic Contaminants (EOCs) are raising increasing concern because of their known or suspected undesirable effects on humans and ecosystems, even if present at low concentration [1]. This wide class of contaminants includes pharmaceuticals, personal care products, surfactants, herbicides, various industrial additives and endocrine disruptors [2]. Many EOCs which have been detected in wastewaters and surface waters [3] are characterized by high chemical stability and, consequently, are not amenable

to conventional removal methods [4]. An important family of EOCs is that of s-triazine compounds, which are widely used as herbicides for weed and grass control [5]. The herbicide 2-(methylthio)-4-(*tert*-butylamino)-6-(cyclopropylamino)-s-triazine (tradename Irgarol 1051, abbreviated here as Irg) is widely used in antifouling paints as biocide inhibiting seaweeds growth [6-8]. It has a low solubility in water (7 mg/L), a high hydrophobicity ( $K_{ow} = 3.95$ ) and is found in lakes and coastal waters [6,9-12]. The environmental fate and behavior of Irgarol 1051 [8,13] and its transformation in biological wastewater treatments [14] have been reviewed. Recent studies report on hazard and risk of Irgarol 1051 and related biocides for marine microalgae and other marine organisms [15-17].

Conventional processes for wastewater treatment are often inadequate to degrade recalcitrant EOCs and there is an urgent demand for more effective oxidation methods. Advanced oxidation processes (AOPs) are the most effective approach to tackle this problem [18]. They are based on  $H_2O_2$ , UV radiation and ozone, used alone or in combination. More recently non-thermal plasma has become a new promise as a novel means to induce AOPs for water treatment, as documented by the impressive number of papers recently published on the topic [19,20].

Non-thermal plasmas (NTP) are generated by electric discharges in a gas at room temperature and ambient pressure and are characterized by non-equilibrium conditions. Thus, high energy electrons are present within the “cold” gas, along with reactive species including ions, atoms and radicals and excited molecules. In addition, UV–Vis radiation is also generated by the relaxation of molecular and atomic excited species. When the gas is air in contact with water, reactive oxygen species are produced ( $O_3$ ,  $H_2O_2$ , superoxide, OH radicals, etc.) which act as a powerful oxidant mixture for water purification, especially useful for the removal of resistant organic compounds like EOCs.

In this paper we report the results of a study of air non-thermal plasma induced degradation of Irgarol 1051 in water. To the best of our knowledge, there are no previous reports in the literature on the application of this novel approach for the removal of Irgarol 1051 and related biocides. In view of the known photodegradation behavior of Irgarol 1051 [21] and of the fact that UV-vis radiation is emitted by excited species in air plasmas [22], we also investigated the possibility of synergic effects when plasma treatment is applied in combination with a common and extensively studied photocatalyst,  $TiO_2$ . Conduction band electrons ( $e^-$ ) and valence band holes ( $h^+$ ) are generated when aqueous  $TiO_2$  suspensions are irradiated with light energy greater than this material band gap energy (e.g. 3.2 eV). The photo generated electrons and holes reduce and oxidize organic molecules and produce reactive species, mainly superoxide radical anion  $O_2^{\bullet-}$  and  $\bullet OH$  radicals [23]. We used a dielectric barrier discharge (DBD) reactor developed and tested previously in our laboratory, which generates an air-NTP right above the surface of the water to

be treated by means of and AC voltage (18 kV, 50 Hz) [24, 25]. We have shown in previous work that in this air-NTP reactor the main reactive species initiating the oxidation of organic pollutants in solution are •OH radicals and ozone [24]. We report here on the implementation of a combined NTP/TiO<sub>2</sub> process by the addition of suspended titania in the aqueous layer.

The results of kinetic and product studies on the degradation of Irgarol 1051, including the extent of mineralization achieved, are described and discussed also with reference to mechanisms reported in the literature for treatment of Irgarol 1051 in other AOPs.

## **3.2 Experimental section**

### **3.2.1 Materials**

Irgarol (Sigma-Aldrich, 98.4% purity) solutions were prepared in MilliQ water, obtained by filtration of deionized water with a Millipore system. Titanium dioxide (Degussa P25), a known mixture of 65% anatase and 35% rutile form with an average particle size of 30 nm, nonporous with a reactive surface area (BET) of  $50 \pm 15 \text{ m}^2 \text{ g}^{-1}$  was heated at 200 °C before the use. Pure air used in the experiments was a synthetic mixture (80% nitrogen and 20% oxygen) from Air Liquid with specified impurities of H<sub>2</sub>O (<3ppm), of C<sub>n</sub>H<sub>m</sub> (<0.5ppm), of CO<sub>2</sub> (< 1 ppm) and of CO (< 1 ppm).

### **3.2.2 Preparation of Irgarol on TiO<sub>2</sub>**

Samples of Irgarol on TiO<sub>2</sub> were prepared by adding 4 mg of the herbicide dissolved in acetone to 100 mg of TiO<sub>2</sub>. The solvent was removed under vacuum at 45 °C for 1h.

### **3.2.3 Plasma degradation procedure**

For each experiment, a suspension was prepared adding 70 mL of water to the desired amount of pollutant included-TiO<sub>2</sub>. In the plasma reactor, solutions of Irgarol containing the TiO<sub>2</sub> powder were magnetically stirred 30 min before treatment and during each experiment.

Plasma degradation was carried out using a DBD reactor, composed of a glass vessel (95×75×60 mm) covered with a Teflon lid. It is equipped with inlet and outlet connectors of a flow (30 mL×min<sup>-1</sup>) of a humidified mixture of 80% N<sub>2</sub> and 20 % O<sub>2</sub> (“pure air” above the liquid surface). Discharge is produced in the gas above the water surface: AC effective voltage of 18 kV and 50 Hz was applied to two parallel stainless steel wires, at a distance of 10 mm from the liquid surface. The wires are fixed upon the tips of

four electrodes passing through the cover. The counter electrode is made of a grounded metallic layer out of the silver-painted-base of the reactor.

### **3.2.4 Analytical procedures.**

The efficiency of plasma treatment was determined by measuring Irgarol conversion as a function of treatment time. To this purpose, at selected reaction times the discharge was interrupted and a 0.5 mL aliquot of the treated suspension was collected from the reactor. To separate TiO<sub>2</sub> particles from the solution, samples were centrifuged (Eppendorf Minispin® Plus with Blackline Rotor, AC input 230 V). The supernatant was analyzed by HPLC (Shimadzu LC-10AT pump with a UV and Vis Shimadzu SPD-10 detector). A Phenomenex column Kinetex 5u C18 100A 150×4.6 mm was used with water (eluent A) and methanol (eluent B). The gradient for B was as follows: 20% at the beginning, 75% in 25 minutes. The elution was followed at 226 nm. Extent of mineralization was measured with a TOC analyzer (Shimadzu Inc., Japan).

For the identification of the intermediates, selected samples were analyzed using the same eluents, column and gradient but a different HPLC system (Agilent Technologies 1100 series) connected to a diode array and a mass spectrometer detector (MSD Trap SL model G2245D). The ionization was performed within the electrospray (ESI) source in positive polarity with the following parameters: nebulizer 50 psi, dry gas flow rate 8 L·min<sup>-1</sup>, dry gas temperature 350°C, capillary voltage 3.5 kV, capillary exit 113.5 V, and skimmer 40 V.

The final solution was analyzed by total carbon analysis using a Shimadzu TOC-V<sub>CSN</sub> instrument, equipped with an autosampler and an automatic diluter. The instrument was calibrated using solutions of standard potassium hydrogen phthalate automatically diluted in the range of interest.

pH of the solutions were monitored during the experiments with a pH meter Seven Compact, S220 (Mettler Toledo).

## **3.3 Results and discussion**

### **3.3.1 Kinetic experiments**

Since UV radiation is emitted from excited species of air non-thermal plasma, we first checked for the possibility that TiO<sub>2</sub> might be photoactivated in our reactor and act in synergy with other reactive species of the plasma to initiate the oxidation of Irgarol. Figure 1 shows the results of two experiments in which a 2.1·10<sup>-2</sup> mM aqueous solution of Irgarol was treated in our reactor alone and in the presence of TiO<sub>2</sub> (178 mg/L). It is evident that the results obtained in these two experiments are about the same, indicating

that photoactivation of TiO<sub>2</sub> is not appreciable under the experimental conditions used. This conclusion is consistent with the observation that both experiments yielded the same degradation products (vide infra).

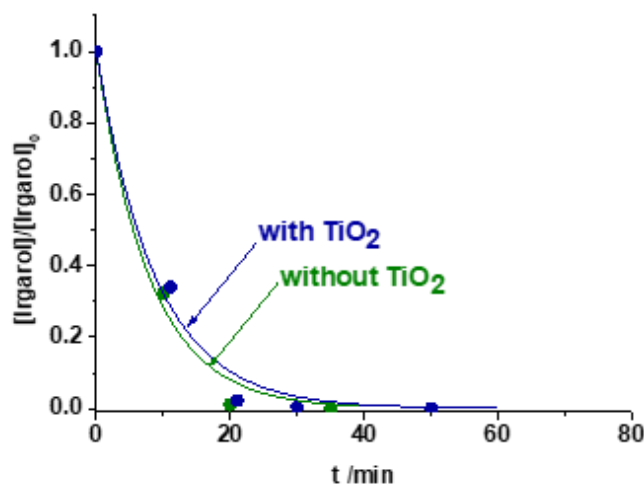


**Figure 1.** Plasma treatment of an aqueous solution of Irgarol  $2.1 \cdot 10^{-2}$  mM without (•) and with addition of 178 mg/L of TiO<sub>2</sub> (•). The line are the best exponential fit of the experimental data

The data in Figure 1 also show that the process is too fast to allow for kinetic analysis by the sampling procedure described in the Experimental Section. Thus, although the concentration/time data can be fitted with a first-order exponential equation (eq. 3.1)

$$[\text{Irg}]/[\text{Irg}]_0 = e^{-kt} \quad (3.1)$$

where [Irg]<sub>0</sub> and [Irg] are the concentrations of Irg at time zero and t, respectively, these interpolations certainly do not warrant an accurate determination of k, but only provide an estimate for the process half-life time, which is about 6 min.

There are reports in the literature showing that the pseudo-first order rate constant (k) of air non-thermal plasma induced oxidation of organic pollutants is inversely proportional to the initial concentration of the pollutant itself [24]. Thus, for the determination of kinetic data with our reactor we usually adjust the pollutant concentration so as to make the reaction rate suitable for accurate experimental determinations by the sampling procedure. Due to the very low solubility of Irgarol, however, it was not possible to slow down the reaction rate by increasing its initial concentration.

A different set of experiments was then carried out in which Irgarol was not dissolved in water but deposited on TiO<sub>2</sub>, as described in the Experimental Section, to obtain a mixture which was then added to water in the plasma reactor.

In all these experiments the ratio between Irgarol and TiO<sub>2</sub> was maintained the same (4% in weight), but different amounts of this Irgarol plus TiO<sub>2</sub> mixture, hereafter abbreviated as Irg/TiO<sub>2</sub>, were used, namely 23, 56, 100 and 200 mg. The results of these experiments are presented in Figure 2, which shows for each experiment the concentration of Irgarol, [Irg], measured in solution at different treatment times. It is seen that both the shape of the [Irg] vs time profiles as well as the values of [Irg] strongly depend on the amount of Irg/TiO<sub>2</sub> used.

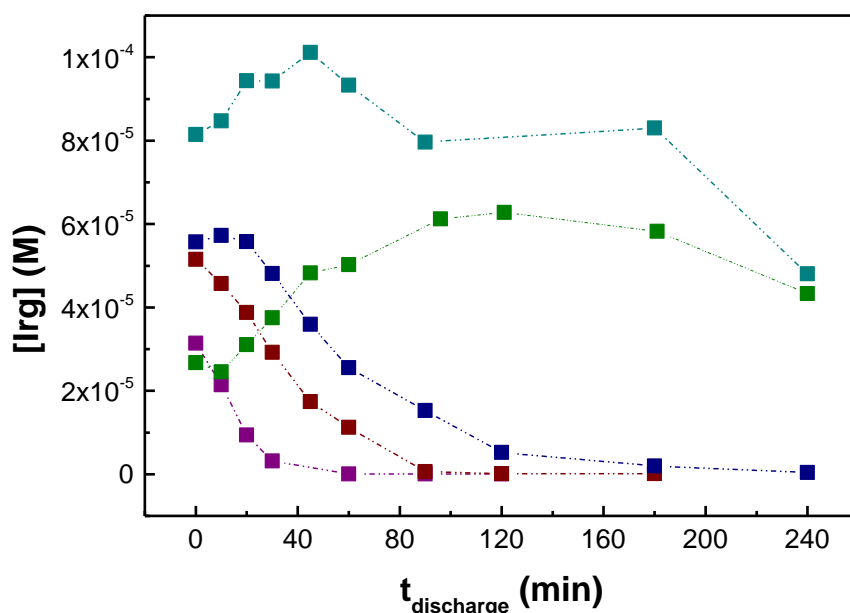
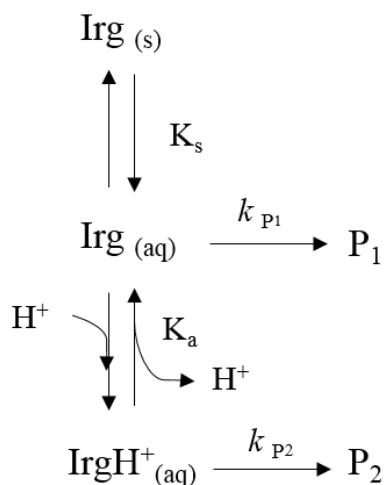


**Figure 2.** Concentration of Irgarol as a function of treatment time in the DBD reactor under the following loading conditions: Irg on TiO<sub>2</sub>: 200 mg (■); 100 mg (■); 56 mg (■); 23 mg (■). Saturated solution of Irgarol without TiO<sub>2</sub> (■)

The first effect, i.e. that on the concentration profile shape, is explained considering that Irg/TiO<sub>2</sub> serves as a reservoir releasing Irgarol in solution in response to consumption due to plasma induced oxidation. The second effect, i.e. that on the effective Irg concentration in solution, is associated with changes in the acidity of the medium which are expected to affect the solubility of Irgarol. Thus, although to the best of our knowledge the pK<sub>b</sub> of Irgarol has not been reported so far, it is expected to be within 9.8-13, the typical range found for other triazines. Since the pH of the solution decreases during the plasma treatment from neutral to ca. 3 [24], the ionization ratio [IrgH<sup>+</sup>]/[Irg], which is equal to pK<sub>b</sub>·[H<sup>+</sup>], is



expected to increase accordingly. The amount of dissolved Irgarol will consequently increase since the ionized species,  $\text{IrgH}^+$ , is certainly more soluble in water than its conjugate base,  $\text{Irg}$ . Scheme 1 describes a simplified mechanistic proposal for the system under study, which considers solubility and acid-base equilibria as well as plasma induced irreversible oxidation reactions.



**Scheme 1.** Mechanistic scheme for Irgarol reactions in the DBD reactor.

In this scheme  $\text{Irg(s)}$  and  $\text{Irg(aq)}$  represent undissolved and dissolved Irg, respectively. The two equilibria shown, i.e. solubilization and protonation of Irg, both respond to variations of pH. Specifically, lowering of pH associated with NTP production of nitric acid and with the presence of titania in the system shifts both equilibria to the right and brings about higher amounts of dissolved Irg in solution.

Support for this interpretation of the results obtained with different amounts of the  $\text{Irg/TiO}_2$  mixture came from the following experiments. First, we treated Irgarol alone, without any  $\text{TiO}_2$ , in a saturated solution in the presence of a large excess (7.8 mg in 70 mL of milliQ water) of undissolved solid Irgarol. The results of this experiment, reported in Figure 2, show that undissolved Irgarol acted in a similar way as  $\text{Irg/TiO}_2$ , as a reservoir replenishing the amount of compound in solution in response to consumption by plasma induced oxidation. Qualitatively, the Irgarol concentration profile in this experiment resembles that found with the  $\text{Irg/TiO}_2$  mixture (200 mg). Quantitatively, however, the two curves do not match. Specifically, the concentration of Irgarol at time zero is significantly larger in the experiment run with  $\text{Irg/TiO}_2$  than in that run with excess undissolved Irgarol. The reason for this difference is attributed to the acidic character of  $\text{TiO}_2$  which thus favors the dissolution of Irgarol by increasing the  $[\text{IrgH}^+]/[\text{Irg}]$  ratio. The macroscopic effect on the solution pH due to  $\text{TiO}_2$  was experimentally determined and is clearly evident in the plot of Figure 3. The same figure also reports the concentration of Irgarol measured

at time zero in solutions prepared by adding different amounts of the same Irg/TiO<sub>2</sub> mixture to milliQ water.

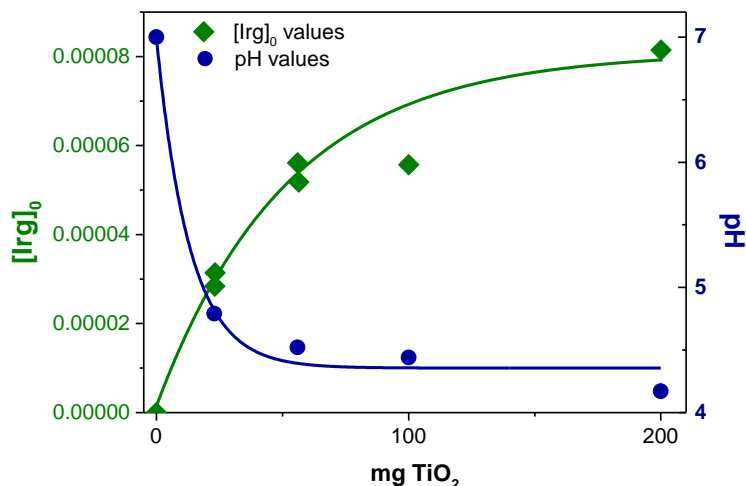


**Figure 1.** Irgarol initial concentration as a function of mg of TiO<sub>2</sub>. pH of water in the presence of different amounts of TiO<sub>2</sub>.

### 3.2 Products analysis

The chromatograms relative to the analyses HPLC-UV/Vis of the samples treated for different times show that, while the peak due to Irgarol decreases in time, many peaks of low abundance are formed. This suggests that Irgarol is oxidized through various competitive pathways, which can be ascribed to the presence of different reactive species in the system and to the presence in the molecule of multiple sites subjected to oxidation. It is known from the literature that OH radical and O<sub>2</sub> or superoxide ion are able to oxidize the side alkyl chain bonded on the nitrogen atoms and the sulfur atom. Oxidation of the side alkyl chains can result in the formation of a carbonyl substituent or in dealkylation [14,21,26-29]. The products which are at first observed in higher abundance in the plasma treatment are 2-methylthio-4-tert-butylamino-6-amino-s-triazine (**A**) and irgarol sulfoxide (**B**) (Scheme 2). **A** is known to be the main product of photodegradation of Irgarol [13,27-29], it is indicated as M1 in the studies of Lam et al. [27,28].

**B** was previously observed by Konstantinou et al. in photocatalytic degradation [21] and by Luft et al. in biological wastewater treatment [14]. As time passes, **A** and **B** are in their turn decomposed and the products most abundant in the UV-Vis chromatogram become 2-hydroxy-4-tert-butylamino-6-cyclopropylamino-s-triazine (**C**), 2-hydroxy-4-terbutylamino-6-ethylamino-s-triazine (**D**) and 2-hydroxy-4-terbutylamino-6-amino-s-triazine (**E**). According to the literature, **C** is formed from **B**. The formation of the hydroxy derivative **C** is a major pathway in direct photolysis but is attributed to a reaction with OH

radical [26]. This is consistent with the fact that this product is observed in our plasma system even if in our apparatus radiation does not seem to be involved in the process of decomposition of organic pollutants. **D** is formed from **C** through opening and partial dealkylation of the cyclopropyl group and **E** from **C** or from **D** through complete dealkylation. Analogous to **D**, but less abundant, is 2-methylthio-4-terbutylamino-6-ethylamino-s-triazine (**F**), which can be considered an intermediate between Irgarol and **B**, as suggested by Sakkas et al. in photodegradation [26] and by Konstantinou et al. in photocatalytic degradation [21]. Besides these main paths, various parallel pathways are proposed (Scheme 2) based on the identification of the products carried out through MS and MS/MS analyses (Figure 5 and 6). These additional pathways are characterized by a different outcome of the oxidation of the side alkyl chains and by consecutive oxidation. Terbutyl group can indeed be hydroxylated (**G**), partially dealkylated (**H**) and hydroxylated after partial dealkylation (**J**); for the cyclopropyl group oxidative ring opening with the formation of a carbonyl is instead generally observed (**K**), as found also in the photodegradation process [28].

From the MS/MS spectra (Figure 5 and 6) the presence of the t-butyl group is easily identified thanks to the characteristic loss of 2-methylpropene (56 u). This fragmentation is always observed, thus suggesting that requires a low energy content. When the t-butyl group is hydroxylated, loss of 2-methylpropenol (72 u) is observed, when it is dealkylated to isopropyl group, loss of propene (42 u) takes place. The loss of cyclopropene (41 u) from the cyclopropyl group is hypothesized to be instead more costly in terms of energy with respect to the loss of 2-methylpropene from the t-butyl group because it is not observed anytime the cyclopropyl group is present. When the cyclopropyl group is oxidized to carbonyl, loss of acrolein is generally observed in the ion fragmentation. This neutral loss is isobaric with the loss of 2-methylpropene (56 u), but, despite this mass coincidence, many structures of the products formed in the plasma treatment can be, however, reasonably inferred, considering the possible modifications on Irgarol previously characterized in the literature. Thus, some isomeric species were successfully distinguished (**A**, **G** and **K**, **H** and **L**, **M** and **N**, **O** and **P**).

Other general characteristics observed in the fragmentations of the molecules shown in Scheme 2 include the fact that no fragmentation of methylsulfide group is generally observed, while methyl sulfoxide group is subjected to thioformaldehyde loss (46 u) and to water loss (18 u), considering in the last case protonation on the oxygen bonded to the sulfur atom. The fragmentations of methyl sulfoxide group were proved by Luft et al. through high resolution MS/MS experiments carried out on synthesized Irgarol sulfoxide [14].

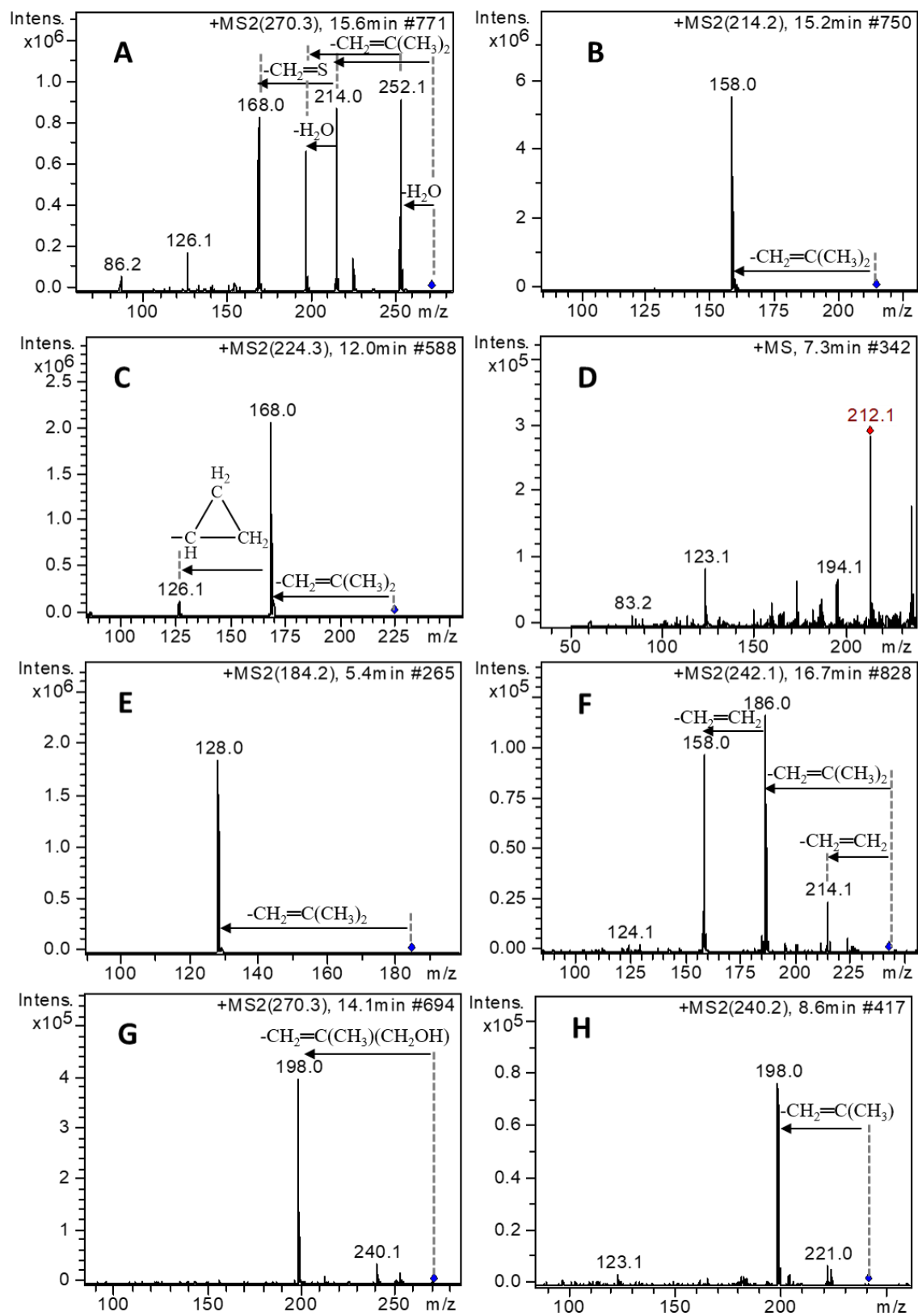


**Figure 5.** Positive MS/MS spectra of intermediates A, B, C, E, F, G, H and MS spectrum of D

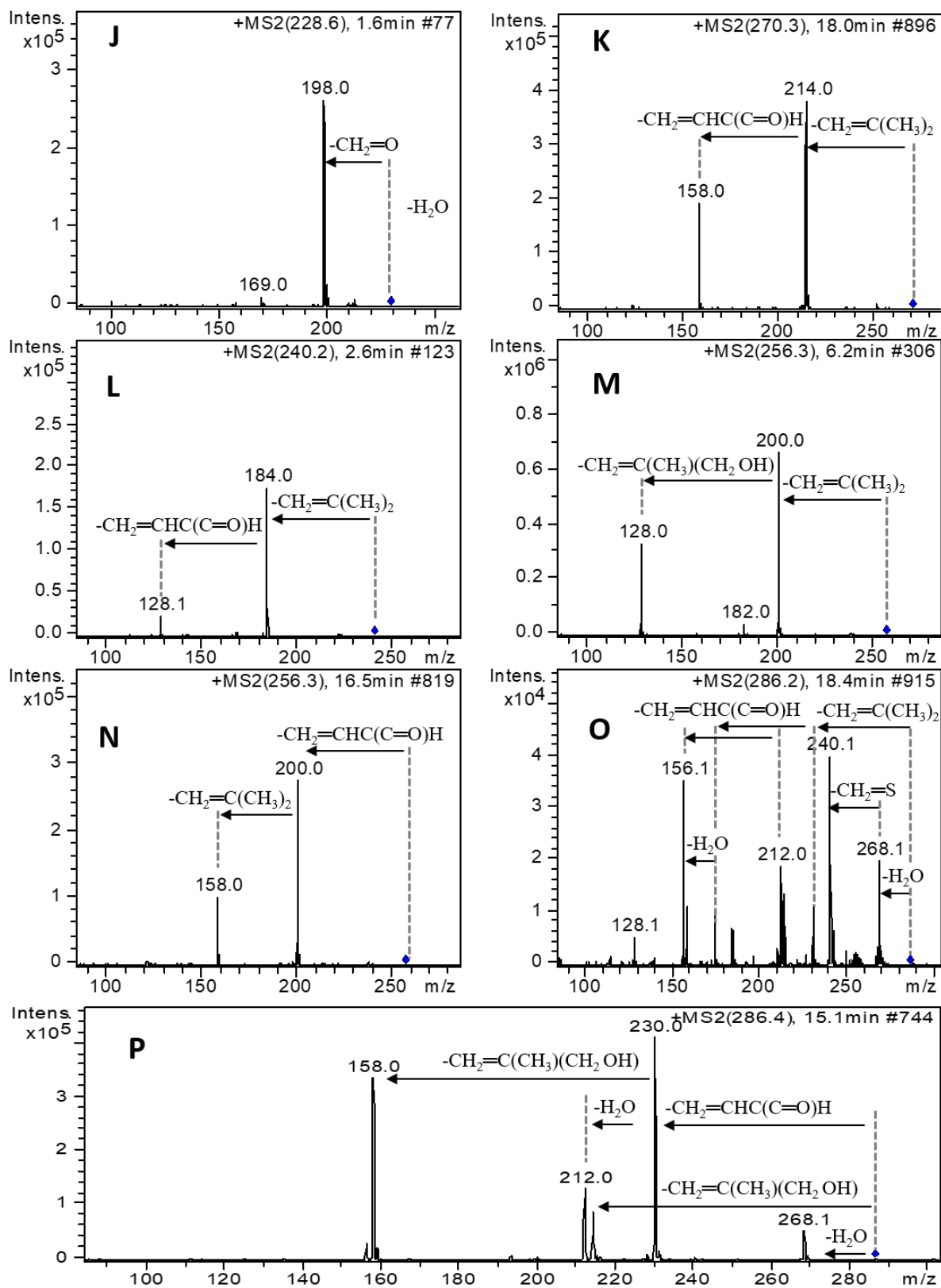
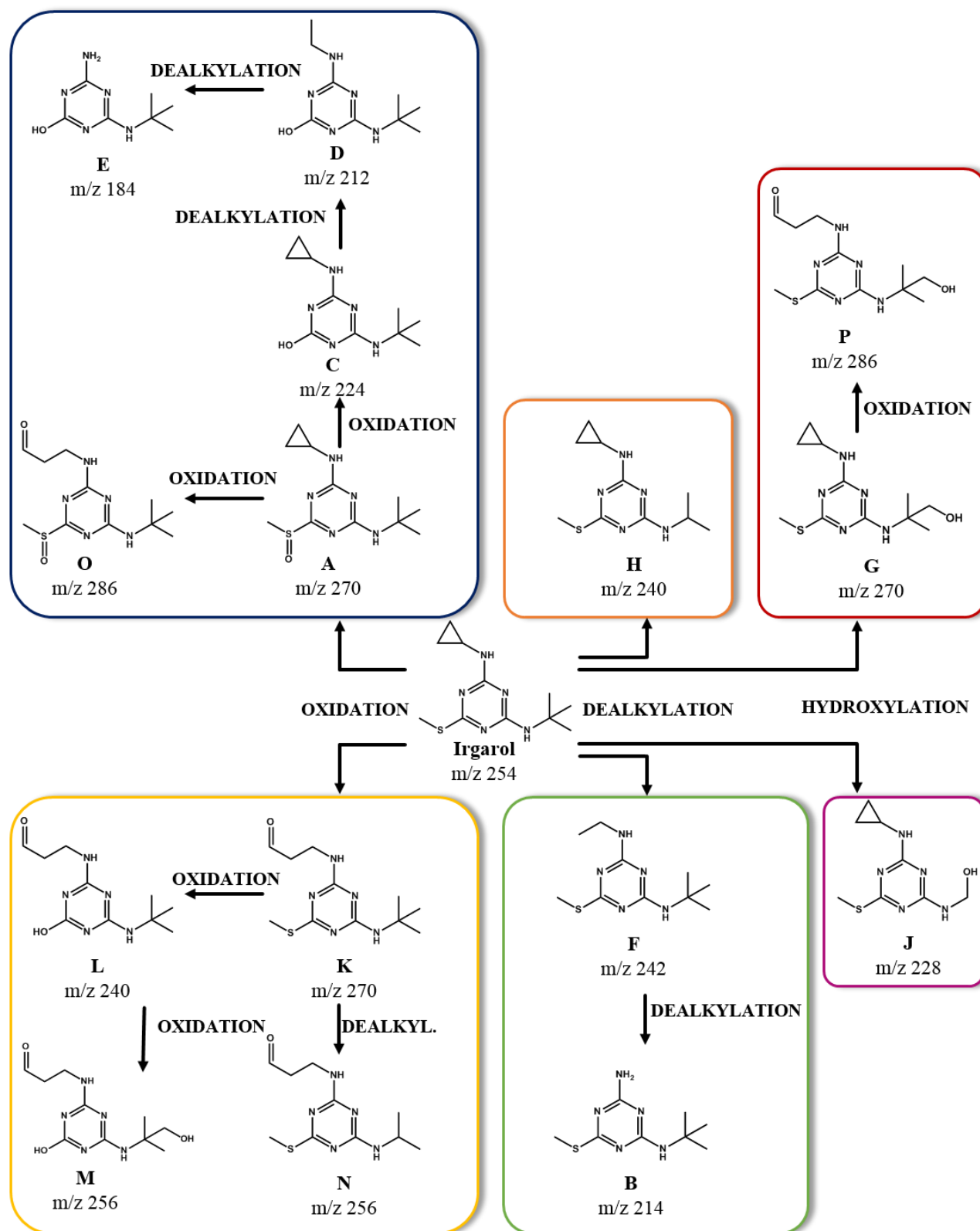


Figure 6. MS/MS spectra of Irgarol degradation products J, K; L, M, N, O, P.



**Scheme 2.** Degradation pathway of Irgarol in DBD reactor.

There are, however, some cases in which it was not possible to attribute the mass spectra to specific structures, as for example it is not clear if sulfoxide is further oxidized to sulfone group, thus we must specify that Scheme 2 is not fully complete. Moreover, the area of the peak exiting in correspondence of the dead volume of the HPLC system at first increases with the increase of treatment time and then decreases for still longer treatment times. This peak is reasonably due to products resulting from the triazine ring opening which are not retained by the HPLC column. The decrease of TOC in solution, and thus the formation of CO<sub>2</sub> as the final oxidation product, confirms this hypothesis. Mineralization degree was 40% for Irgarol solutions with a starting concentration of  $2.1 \cdot 10^{-5}$  M after 4 h of plasma treatment and 95% for Irgarol solutions with an initial concentration of  $5 \cdot 10^{-6}$  M after 5 h treatment.

### 3.4 Conclusions

Kinetic experiments on the NTP-induced degradation of Irgarol in the presence of TiO<sub>2</sub> failed to reveal any increase in reactivity which might be due to a contribution plasma stimulated photodegradation. Adsorption of the pollutant on the same semiconductor was studied by LC-UV and UV spectroscopy. It was demonstrated that the procedure of pre-adsorption of Irgarol on titania can significantly increase the throughput of NTP induced degradation, a result which might have some practical consequences. We believe that this phenomenon is due to the acidic character of TiO<sub>2</sub> which brings more Irg in solution by increasing the fraction of protonated Irg, i.e. the  $[\text{IrgH}^+]/[\text{Irg}]$  ionization ratio. For the first time the products of Irgarol formed under NTP induced advanced oxidation conditions are reported here. The high number of intermediates detected reveal a complex degradation scheme that involves as initial stages the oxidation of the side chains of the s-triazine ring. The extent of Irg mineralization in water was measured at two different Irg initial concentrations. The results show that almost total conversion to CO<sub>2</sub> was achieved for the lower concentration under study, that is about five orders of magnitude higher than that detected in real water samples. This confirms the efficiency of air NTP in oxidizing very recalcitrant pollutants present in water or wastewater.

### References

1. Lapworth DJ, Baran N, Stuart ME, Ward RS. Emerging organic contaminants in groundwater: A review of sources, fate and occurrence. *Environmental Pollution*. 2012;163(Supplement C):287-303
2. Meffe R, de Bustamante I. Emerging organic contaminants in surface water and groundwater: A first overview of the situation in Italy. *Science of The Total Environment*. 2014;481(Supplement C):280-295

3. Benotti MJ, Trenholm RA, Vanderford BJ, Holady JC, Stanford BD, Snyder SA. Pharmaceuticals and endocrine disrupting compounds in US drinking water. *Environ Sci Technol*. 2008;43(3):597-603.
4. Clara M, Strenn B, Gans O, Martinez E, Kreuzinger N, Kroiss H. Removal of selected pharmaceuticals, fragrances and endocrine disrupting compounds in a membrane bioreactor and conventional wastewater treatment plants. *Water Research*. 2005;39(19):4797-4807
5. Ridgway RL, Tinney JC, MacGregor JT, Starler NJ. Pesticide use in agriculture. *Environ Health Perspect*. 1978;27:103
6. Konstantinou IK, Albanis TA. Worldwide occurrence and effects of antifouling paint booster biocides in the aquatic environment: A review. *Environ Int*. 2004;30(2):235-248
7. Martinez K, Ferrer I, Hernando MD, et al. Occurrence of antifouling biocides in the spanish mediterranean marine environment. *Environ Technol*. 2001;22(5):543-552
8. Thomas KV, Fileman TW, Readman JW, Waldock MJ. Antifouling paint booster biocides in the UK coastal environment and potential risks of biological effects. *Mar Pollut Bull*. 2001;42(8):677-688
9. Kaonga CC, Takeda K, Sakugawa H. Antifouling agents and fenitrothion contamination in seawater, sediment, plankton, fish and selected marine animals from the seto inland sea, japan. *Geochem J*. 2015;49(1):23-37
10. Kaonga CC, Takeda K, Sakugawa H. Concentration and degradation of alternative biocides and an insecticide in surface waters and their major sinks in a semi-enclosed sea, japan. *Chemosphere*. 2016;145:256-264
11. Manzo S, Ansanelli G, Parrella L, et al. First evaluation of the threat posed by antifouling biocides in the southern adriatic sea. *Environmental Science: Processes & Impacts*. 2014;16(8):1981-1993
12. Laane R, Vethaak AD, Gandrass J, et al. Chemical contaminants in the wadden sea: Sources, transport, fate and effects. *J Sea Res*. 2013;82:10-53
13. Sakkas VA, Konstantinou IK, Albanis TA. Photochemical fate of organic booster biocides in the aquatic environment. In: *Antifouling paint biocides*. Springer; 2006:171-200



14. Luft A, Wagner M, Ternes TA. Transformation of biocides irgarol and terbutryn in the biological wastewater treatment. *Environ Sci Technol*. 2013;48(1):244-254
15. Dupraz V, Coquill N, Mnard D, Sussarellu R, Haugarreau L, Stachowski-Haberkorn S. Microalgal sensitivity varies between a diuron-resistant strain and two wild strains when exposed to diuron and irgarol, alone and in mixtures. *Chemosphere*. 2016;151:241-252
16. Sjollem SB, MartnezGarca G, van der Geest, Harm G, et al. Hazard and risk of herbicides for marine microalgae. *Environmental Pollution*. 2014;187:106-111
17. Mai H, Morin B, Pardon P, Gonzalez P, Budzinski H, Cachot J. Environmental concentrations of irgarol, diuron and S-metolachlor induce deleterious effects on gametes and embryos of the pacific oyster, *crassostrea gigas*. *Mar Environ Res*. 2013;89:1-8
18. Oturan MA, Aaron J. Advanced oxidation processes in water/wastewater treatment: Principles and applications. A review. *Crit Rev Environ Sci Technol*. 2014;44(23):2577-2641
19. Magureanu M, Mandache NB, Parvulescu VI. Degradation of pharmaceutical compounds in water by non-thermal plasma treatment. *Water Res*. 2015;81:124-136.
20. Reddy PMK, Mahammadunnisa S, Subrahmanyam C. Catalytic non-thermal plasma reactor for mineralization of endosulfan in aqueous medium: A green approach for the treatment of pesticide contaminated water. *Chem Eng J*. 2014;238:157-163.
21. Konstantinou IK, Sakellarides TM, Sakkas VA, Albanis TA. Photocatalytic degradation of selected s-triazine herbicides and organophosphorus insecticides over aqueous TiO<sub>2</sub> suspensions. *Environ Sci Technol*. 2001;35(2):398-405
22. Fridman G, Brooks AD, Balasubramanian M, et al. Comparison of direct and indirect effects of non-thermal atmospheric-pressure plasma on bacteria. *Plasma Processes and Polymers*. 2007;4(4):370-375
23. Hurum DC, Agrios AG, Gray KA, Rajh T, Thurnauer MC. Explaining the enhanced photocatalytic activity of degussa P25 mixed-phase TiO<sub>2</sub> using EPR. *The Journal of Physical Chemistry B*. 2003;107(19):4545-4549

24. Marotta E, Schiorlin M, Ren X, Rea M, Paradisi C. Advanced oxidation process for degradation of aqueous phenol in a dielectric barrier discharge reactor. *Plasma Processes and Polymers*. 2011;8(9):867-875
25. Marotta E, Ceriani E, Shapoval V, et al. Characterization of plasma-induced phenol advanced oxidation process in a DBD reactor. *Eur.Phys.J.Appl.Phys*. 2011;55(1)
26. Sakkas VA, Lambropoulou DA, Albanis TA. Photochemical degradation study of irgarol 1051 in natural waters: Influence of humic and fulvic substances on the reaction. *J Photochem Photobiol A*. 2002;147(2):135-141.
27. Lam K, Lei N, Tsang VW, Cai Z, Leung KM, Lam MH. A mechanistic study on the photodegradation of irgarol-1051 in natural seawater. *Mar Pollut Bull*. 2009;58(2):272-279.
28. Lam K, Lam MH, Lam PK, et al. Identification and characterization of a new degradation product of irgarol-1051 in mercuric chloride-catalyzed hydrolysis reaction and in coastal waters. *Marine Pollution Bulletin*. 2004;49(4):361-367
29. Peñela GA, Ferrer I, Barceló D. Identification of new photodegradation byproducts of the antifouling agent irgarol in seawater samples. *Int J Environ Anal Chem*. 2000;78(1):25-40.

# Chapter4 - Atmospheric plasma treatment of mesotrione and metolachlor in water

Agata Giardina, Ester Marotta, Cristina Paradisi

Department of Chemical Sciences, University of Padova, via Marzolo 1, 35131 Padova, Italy

## Abstract

The two common herbicides mesotrione and metolachlor, often used in combination, were subjected to advanced oxidation in water in a dielectric barrier discharge (DBD) reactor. In this reactor a strongly oxidizing plasma is produced in air at room temperature and atmospheric pressure just above the surface of the water to be treated. Experiments were conducted with each herbicide treated individually, at two different initial concentrations, as well as in 1:1 mixture with the other. The advanced oxidation process was monitored, by means of HPLC-MS/MS analysis, to obtain the herbicides rates of degradation and the products formed. The results show that air plasma is an efficient means to induce the degradation of both herbicides, that mesotrione is considerably more reactive than metolachlor and that, at sufficiently long treatment times, complete mineralization is achieved. Both product and kinetic studies also show that there is no appreciable reciprocal influence on the advanced oxidation of mesotrione and metolachlor when the two herbicides are treated together in our DBD air plasma reactor.

**Keywords:** mesotrione, metolachlor, non-thermal plasma, mixture, mineralization

## 4.1 Introduction

The widespread use of pesticides in agriculture has major impact on water quality and can lead to serious environmental consequences [1]. The pesticides currently in use include a variety of chemicals with widely different structures, modes of action and toxicity effects. The poor selectivity towards specific targets has led to the reconsideration of many first-generation synthetic pesticides and to their substitution with compounds of new generation, which are less dangerous to the environment [2]. A strategy to promote and broaden the efficacy of these new pesticides consists in using two or more of them in combinations called “cocktails” [3]. The direct and indirect impact of these mixtures on aquatic environments is not yet fully identified and is thus raising growing interest and concern. This is reflected by a rapidly increasing number of studies dealing with the harmfulness of pesticides cocktails as compared to single pesticides [4].

One important application of this approach, arising from the banning of atrazine [5], employs S-metolachlor [2-chloro-N-(2-ethyl-6-methylphenyl)-N-(methoxy-1-methylethyl) acetamide] in

combination with mesotrione [2-(4-mesy-2-nitrobenzoyl)cyclohexane-1,3-dione] on maize crops [6]. The choice to use metolachlor in combination with mesotrione was due mainly to its known difficult biodegradation [7] and because of its targets, which differ from those of mesotrione. Mesotrione acts on a critical enzyme, p-hydroxy-phenylpyruvate dioxygenase (HPPD), involved in carotenoid biosynthesis [7]. Metolachlor is an inhibitor of elongases and of the geranylgeranyl pyrophosphate (GGPP) cyclases, in plant hormones pathway [7]. It is persistent and capable of leaching to groundwater because of its significant water solubility (530 mg/L at 20° C [8]) and low log K<sub>oc</sub> (3.01 [9]). This is not the case for mesotrione but for its degradation products [10] that can be persistent under suboxic conditions such as subsoil and groundwater.

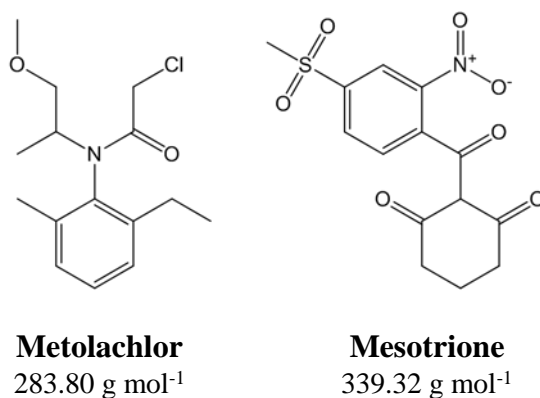


**Figure 1.** Chemical structures of metolachlor and mesotrione

It is reported in the literature that there is a different impact on soil when these two herbicides are used simultaneously, compared to that observed with the single compounds. Their persistence in the soil is prolonged, the environmental contamination increases, and more toxic effects are observed on biological microbial activity [11, 12]. However, it was recently stated that “the effects of mesotrione, metolachlor and terbuthylazine, applied in mixture, on soil biodegradation remain insufficiently researched” [12]. Interactions in combined herbicide mixtures may also occur in water during remediation treatments. Among the different approaches to water treatment, advanced oxidation processes (AOPs) are the most suitable to remove stable organic pollutants with low biodegradability, which is the case for the majority of pesticides. AOPs include treatment with H<sub>2</sub>O<sub>2</sub>/UV, ozonation, photo-Fenton and nonthermal plasma and are based on the generation and reaction of highly reactive oxygen-based oxidants, specifically the hydroxyl radical [13]. Nonthermal plasma (NTP) in air at room temperature and atmospheric pressure, also called *atmospheric plasma*, is particularly attractive as it produces strong oxidants, including O<sub>3</sub>, H<sub>2</sub>O<sub>2</sub> and ·OH, without the need for chemicals or UV lamps. There are many different experimental approaches to implement the action of nonthermal plasma and achieve the degradation of organic contaminants dissolved in water [14]. One convenient

and widely used approach, also adopted in the work reported here, generates atmospheric plasma by applying electrical discharges in the air above the liquid surface. Formed in the gas and at the gas-liquid interphase, primary and secondary reactive species produced by the discharge can either react with the dissolved organic contaminants at the liquid surface or transfer into the liquid and react in the bulk [14, 15].

NTPs have been successfully used to remove many emerging organic contaminants (EOCs), like pesticides, pharmaceuticals, and dyes [16-18]. Most studies found in the literature deal with treatment of a single contaminant at a time and there are very limited data on the behavior of mixtures of organic pollutants in AOP treatment processes [19, 20]. To the best of our knowledge, there are no reports on nonthermal plasma applied to treat mixtures of herbicides in water.

The aim of this work was, therefore, to study the efficacy of atmospheric air plasma treatment in the degradation of two persistent herbicides, metolachlor and mesotrione, processed individually and in mixture. Specifically, we searched for possible reciprocal effects on the herbicides degradation rates, products and mechanisms. A dielectric barrier discharge (DBD) reactor was used for this study, tested and described in previous work [21, 22], which generates an atmospheric plasma above the surface of the water to be treated. Specifically, this paper reports and discusses the extent of mineralization achieved, the oxidation kinetics and the intermediates and products obtained in experiments with both herbicides treated individually and in mixture.

## **4.2 Experimental Section**

### **4.2.1 Chemicals**

Mesotrione (Sigma-Aldrich, 99.9% purity) and metolachlor (Sigma-Aldrich, 97.6% purity) solutions were prepared in MilliQ water, obtained by filtration of deionized water with a Millipore system. Pure air used in the experiments was a synthetic mixture (80% nitrogen and 20% oxygen) from Air Liquide with specified impurities of H<sub>2</sub>O (<3ppm), of C<sub>n</sub>H<sub>m</sub> (<0.5ppm), of CO<sub>2</sub> (< 1 ppm) and of CO (< 1 ppm).

### **4.2.2 Dielectric Barrier Discharge (DBD) reactor**

The experimental setup was described in detail previously [23]. Briefly, the reactor consists of a glass vessel (95x75x60 mm) and a Teflon cover. A 70 mL volume of the aqueous solution to be treated is placed in the vessel and a flow (30 mL/min) of a humidified mixture of 80% N<sub>2</sub> and 20% O<sub>2</sub> (“pure air”) is established above the liquid surface through inlet/outlet ports in the reactor cover. Discharge is produced in the gas above the water surface by an AC high voltage of 18 kV and 50 Hz applied to two parallel stainless steel wires fixed upon the tips of four connected electrodes passing through the

cover. In the reactor the distance between the liquid surface and the wires is 10 mm. The counterelectrode is a grounded metallic plate in contact with the external surface of the reactor base, which is painted with a silver film.

### 4.2.3 Analytical procedures

The kinetics of decomposition of mesotrione and metolachlor, treated in the plasma reactor either individually or in mixture, were studied by measuring the herbicides conversion as a function of treatment time at constant applied voltage. At desired times the discharge was briefly interrupted and a 0.5 mL aliquot of the treated solution was sampled. The samples were thus quantitatively analyzed to obtain data of residual concentration (C) of the herbicide as a function of treatment time. The analyses were performed with an HPLC Thermo Scientific Products instrument with P2000 pump and UV6000LP Diode array detector at 270 nm, using a Phenomenex column Kinetex 5  $\mu$ m C18 100 Å 150x4.6 mm. The eluents were 0.1% formic acid in water (eluent A) and 0.1% formic acid in acetonitrile (eluent B). The gradient for B was as follows: from 10% to 95% in 25 min. The area of the chromatographic peak was converted into a concentration data by means of calibration curves. Data of  $C/C_0$ , where C and  $C_0$  represent the herbicide concentration at time t and zero, respectively, were plotted against treatment time and interpolated using the first order exponential function to obtain values of k, the pseudo first order rate constant. All the experiments were repeated in duplicate or triplicate. The reproducibility of the results was within 10%.

For the identification of the reaction intermediates, selected samples were analyzed using the same eluents and column but a different HPLC system (Agilent Technologies 1100 series) connected to a diode array and a mass spectrometer detector (MSD Trap SL model G2245D). The ionization was performed within the electrospray (ESI) source in positive (for metolachlor), negative (for mesotrione) and alternate polarity (for mixtures of both metolachlor and mesotrione) with the following parameters: nebulizer 50 psi, dry gas flow rate 11 L  $\text{min}^{-1}$ , dry gas temperature 350 °C, capillary voltage 3.5 kV, capillary exit 143.5 V, and skimmer 40 V. The eluents were 0.1% formic acid in water (eluent A) and 0.1% formic acid in acetonitrile (eluent B). The gradient for B was as follows: 10% for 2 min, to 75% in 25 min, 75% for 2 min and to 95% in 5 min.

To establish the extent of mineralization achieved at the end of the plasma treatment, the final solution was subjected to total carbon analysis using a Shimadzu TOC-VCSN instrument, with an operative range of 50  $\mu\text{g/L}$ –25 g/L. Calibration was carried out using solutions of standard potassium hydrogen phthalate automatically diluted in the range of interest.

## 4.3 Results and discussion

### 4.3.1 Degradation kinetics

All kinetic experiments were run in MilliQ water and involved monitoring of the herbicides conversion as a function of treatment time as detailed in the experimental section. The results of experiments in which each herbicide was treated individually are the necessary reference to evaluate any possible reciprocal effects occurring when the two herbicides are treated together. Therefore, the degradation of metolachlor and mesotrione was studied first in preliminary experiments in which each was treated individually, next in 1:1 mixtures including both. It was found in previous work that the rate of plasma induced degradation generally depends on the organic pollutant initial concentration [21, 22]. Thus, the single component experiments were run at two different initial concentrations,  $1 \cdot 10^{-4}$  and  $5 \cdot 10^{-5}$  M. The results were then compared with those obtained in experiments with both herbicides in a 1:1 mixture, each at an initial concentration of  $5 \cdot 10^{-5}$  M. The herbicide degradation as a function of treatment time is shown in Fig. 2a and 2b for mesotrione and metolachlor, respectively. The plots report the fraction of residual herbicide  $C/C_0$ , where  $C_0$  and  $C$  are the pollutant concentrations at time zero and  $t$ .

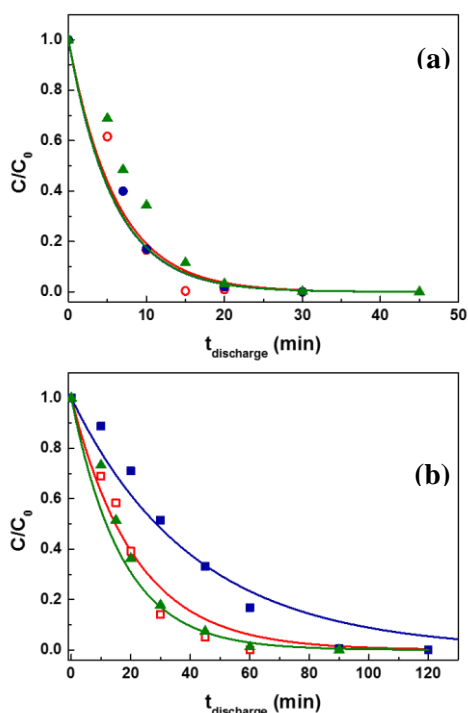


**Figure 2.** Degradation of mesotrione (a) and metolachlor (b) as a function of treatment time. Each herbicide was tested at two different initial concentrations,  $1 \cdot 10^{-4}$  (● and ■ respectively) and  $5 \cdot 10^{-5}$  M (○ and □ respectively) and in a 1:1 molar mixture with the other, each at  $5 \cdot 10^{-5}$  M (▲)

Fig. 2a and 2b show three sets of data each, pertaining to the herbicide treated alone at initial concentrations of  $1 \cdot 10^{-4}$  (filled symbols) and  $5 \cdot 10^{-5}$  M (open symbols) and in a 1:1 molar mixture with the other, each at  $5 \cdot 10^{-5}$  M. The data were analyzed according to the kinetic scheme described before [21, 23, 24] and interpolated with equation 4.1

$$C = C_0 \cdot \exp(-kt) \quad (4.1)$$

to obtain  $k$ , the process pseudo-first order rate constant. The kinetic results are collected in Table 1.

**Table 1.** Kinetic data for herbicides treated alone and in mixture in the plasma reactor

$C_0$ (M)	Mesotrione		Metolachlor	
	$10 \cdot k$ ( $\text{min}^{-1}$ )	$t_{1/2}$ (min)	$10 \cdot k$ ( $\text{min}^{-1}$ )	$t_{1/2}$ (min)
$1 \cdot 10^{-4}$	$1.8 \pm 0.1$	4.0	-	-
$5 \cdot 10^{-5}$	$1.7 \pm 0.2$	4.2	-	-
$1 \cdot 10^{-4}$	-	-	$0.28 \pm 0.03$	25
$5 \cdot 10^{-5}$	-	-	$0.50 \pm 0.04$	14
$5 \cdot 10^{-5} + 5 \cdot 10^{-5}$ (mixture)	$1.7 \pm 0.2$	4.0	$0.59 \pm 0.06$	12

Considering the results of the experiments with each herbicide treated individually, we can observe an evident difference in the degradation constants of the two compounds, that is in agreement with data of their persistence in soil and groundwater [6]. A second difference concerns the dependence of the observed rate constant on the herbicide initial concentration. Thus, while for mesotrione the rate of reaction appears not to depend on  $C_0$  within the range of concentrations tested, for metolachlor there was a significant increase in the rate of degradation when a lower  $C_0$  was used. Similar trends to that observed with metolachlor were found previously with other pollutants treated in the same reactor [23, 25].

The apparent insensitivity of the rate of mesotrione degradation on  $C_0$  is probably due to the fact that these reactions are too fast to be followed properly by the sampling procedure used in this work.

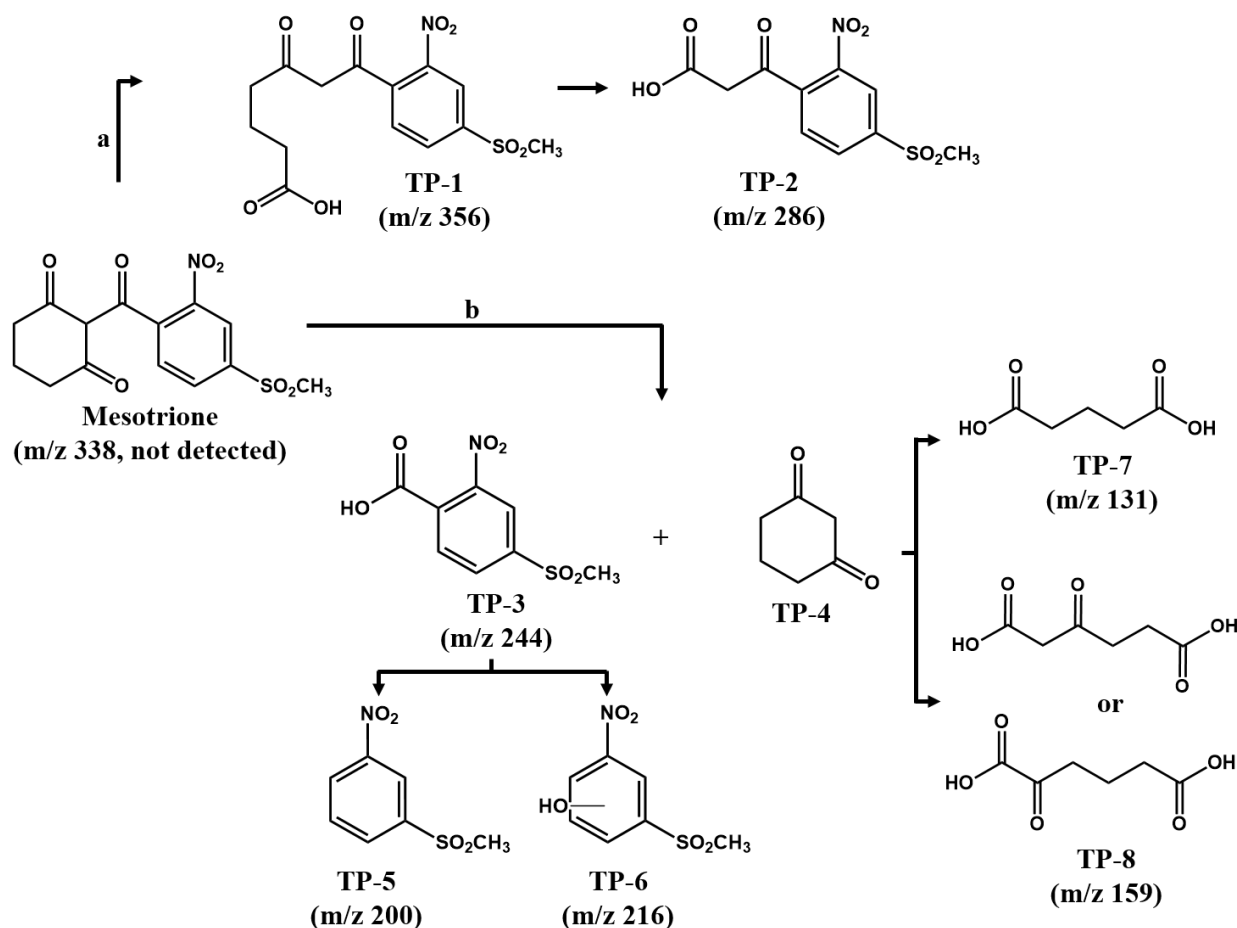
Finally, the results of the experiments with both herbicides treated together in a 1:1 mixture,  $5 \cdot 10^{-5}$  M each, are very interesting. In the case of mesotrione the three decay curves are almost coincident (Fig. 2a), showing that there is no appreciable influence by metolachlor on the rate of decay of mesotrione. Similarly, in the case of metolachlor (Fig. 2b) the decay curves for metolachlor treated at an initial concentration of  $5 \cdot 10^{-5}$  M in mixture and alone are almost coincident. Thus, it can be



concluded, both for mesotrione and metolachlor, that the rate of reaction of either is not appreciably affected by the presence of the other. We can therefore exclude that the two herbicides interact with each other in any way during the treatment and that competition for the plasma reactive species is not producing any evident effect in the reaction rate of either. This situation of no reciprocal interference is reasonably attributed to the significant difference in reactivity of the two herbicides.

#### 4.3.2 Transformation products (TPs) of metolachlor and mesotrione

Ozone and hydroxyl radicals are considered to be the major reactive species responsible for the degradation of the pesticides in our DBD reactor [21, 22]. Degradation of pesticides due to ozone can occur either by direct oxidation or by other oxidant species, notably peroxy and hydroxyl radicals, formed from ozone decomposition in water [26]. Together with OH radicals formed directly by the discharge, these species can attack organic molecules nonselectively.



**Scheme 1.** Proposed pathways for mesotrione oxidation. The data in parentheses are the m/z values of the corresponding deprotonated species formed in negative ESI ionization

This is a great advantage for wastewater treatment but may lead to a wide variety of oxidation products en route to complete conversion to CO<sub>2</sub>. In some cases, transformation products can be even more toxic than the parent compound [27-29]. For this reason, the identification of transformation products still present at the end of the process is a necessary task in the evaluation of any water treatment and of its applicability. Although complete mineralization was achieved for both herbicides tested in this work, it is important to characterize the degradation pathway of some model compounds in view of application of the approach for the degradation of structurally similar compounds.

Various transformation products were detected for mesotrione by LC/MS using negative electrospray ionization mode. Recently, the oxidation pathways of mesotrione have been investigated and described in experiments of advanced oxidation involving photolysis [30], photocatalysis [31,32], Fenton [31], electro-Fenton [33, 34] and photo-Fenton with peroxymonosulfate [32] processes, ozonation [31] and also DBD treatment [31]. The reactor previously used for the DBD treatment was significantly different from that used in the present paper, thus comparison of the obtained results is particularly interesting. Considering the acquired MS and MS/MS spectra of the degradation products (Fig. 3) and the products and degradation pathways proposed previously in the literature [30-34], we suggest that oxidative degradation of mesotrione in our plasma reactor occurs as shown in Scheme 1. Two main pathways are considered, leading, respectively, to the formation of 7-(4-(methylsulfonyl)-2-nitrophenyl)-5,7-dioxoheptanoic acid (TP-1), pathway **a**, and to 2-nitro-4 methylsulfonylbenzoic acid (TP-3) and 1,3-cyclohexanedione (TP-4), pathway **b**. TP-4 was not experimentally detected but deduced based on the observation of TP-3 and of glutaric acid (TP-7), reasonably formed from TP-4. As shown in Scheme 1, the difference between the two oxidation pathways consists in the C-C bond which is broken, to obtain TP-1 or TP-3. The species considered responsible for these reactions is ozone, because TP-3 was also observed in ozonation [31] and because it is known that ozone is able to react with diketones [35]. TP-1 can then be further oxidized to 3-(4-(methylsulfonyl)-2-nitrophenyl)-3-oxopropanoic acid (TP-2), as observed also in the photo-Fenton process with peroxymonosulfate [32]. TP-3 is instead converted to 3-methylsulfonyl-1-nitrobenzene (TP-5) and 2-nitro-4-methylsulfonylphenol (TP-6), as reported also in studies of photocatalysis [31], ozonation [31], DBD treatment [31], Fenton [31], electro-Fenton [34] and photo-Fenton with peroxymonosulfate processes [32]. A further product observed is a hydroxyhexenoic diacid (TP-8), reasonably originating from oxidative opening of TP-4 or from oxidation of TP-7. The structure of TP-6 cannot be attributed to a specific isomer.

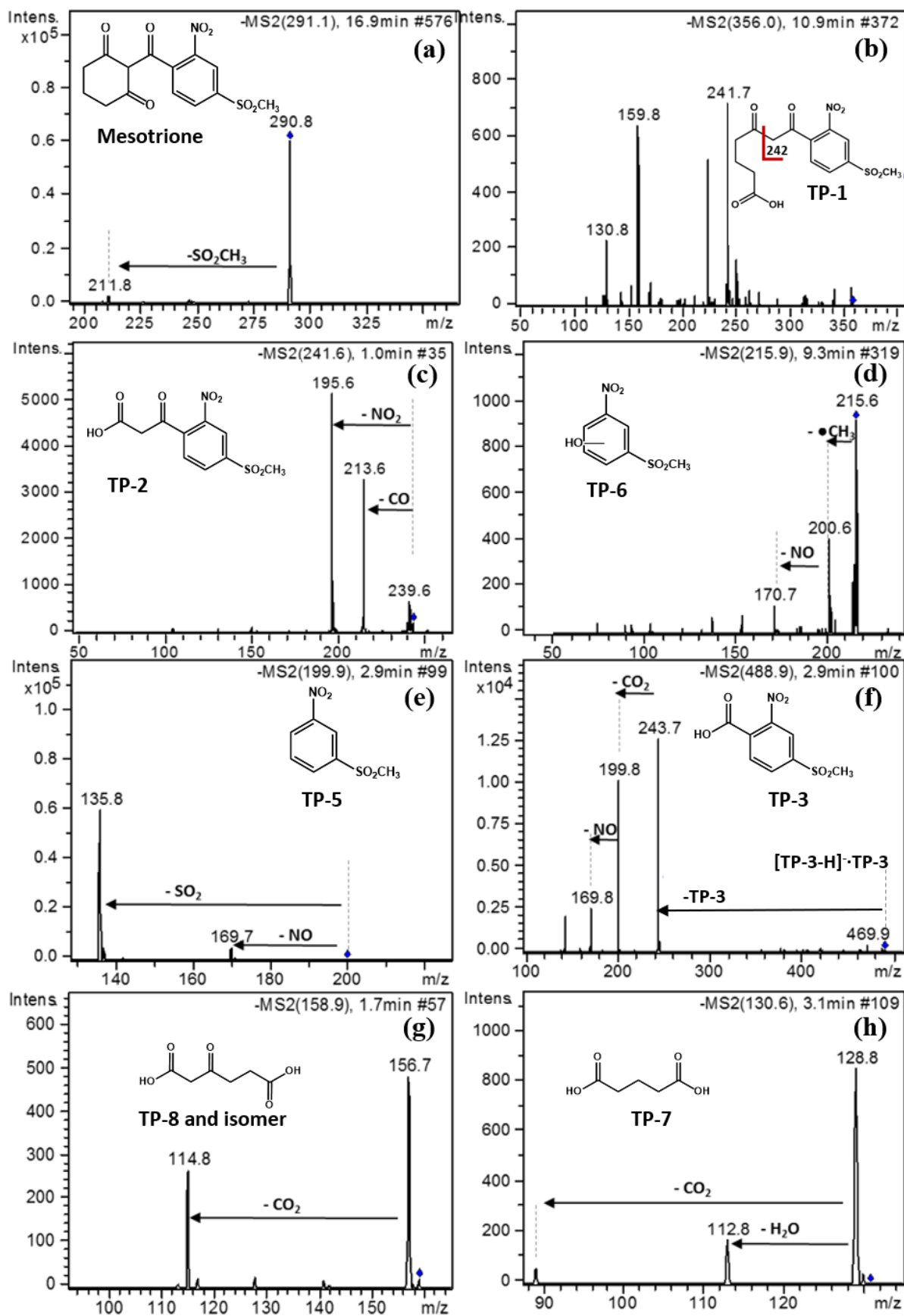


**Figure 3.** ESI-MS<sup>2</sup> spectra of mesotrione (a) and its oxidation products with m/z 356 (b), m/z 242 (c), m/z 216 (d), m/z 200 (e), m/z 489 (f), m/z 159 (g), m/z 131 (h)

The identification of the above mentioned products is based on MS and MS<sup>2</sup> spectra. As for mesotrione, the expected parent ion at m/z 338 was not detected in ESI- mode. Instead the [M-H-HNO<sub>2</sub>]<sup>-</sup> daughter ion at m/z 291 was observed. When isolated, it fragments by loss of the methylsulfonyl group, analogously to what was observed by Murati *et al.* [34] (Fig 3a). TP-1 was detected at m/z 356, corresponding to the deprotonated ion, which is fragmented in the MS<sup>2</sup> spectrum to form m/z 242, as shown in Fig. 3b. TP-2 was expected at m/z 286, but, as observed also in the paper dealing with the electro-Fenton process [34], it was fragmented in the ESI source and identified on the basis of the decarboxylated daughter ion at m/z 242, which in MS<sup>2</sup> experiments fragments by competing losses of CO and NO<sub>2</sub> (Fig. 3c). TP-3 is detected as deprotonated ion [TP-3-H]<sup>-</sup> at m/z 244 but also as deprotonated ion complexed with a neutral [TP-3-H]<sup>-</sup>·TP-3 at m/z 489. When fragmented in the MS<sup>2</sup> experiment, m/z 489 gives m/z 244 and the products of consecutive losses of CO<sub>2</sub> and NO, as shown in Fig. 3f. TP-6 is detected at m/z 216. Its MS<sup>2</sup> spectrum shows the loss of a methyl group followed by elimination of -NO (Fig 3d). Because of this primary methyl loss, we can conclude that TP-6 is either the *meta* or *para* isomer. Thus, the main primary fragmentation route of the *ortho* isomer would be hydroxyl loss, a well-known preferred fragmentation known as “ortho effect”, as observed in the spectrum of the products obtained by electro-Fenton process [34]. TP-5 is detected at m/z 200 and its characteristic fragmentations are competing losses of NO and of SO<sub>2</sub>, by a transposition process [36] (Fig 3e).

Aliphatic carboxylic acids TP-7 and TP-8 are also detected as deprotonated ions and both their MS<sup>2</sup> spectra are characterized by the loss of CO<sub>2</sub>. This characteristic fragmentation pathway does not allow us to infer the position of the oxidation site in TP-8.

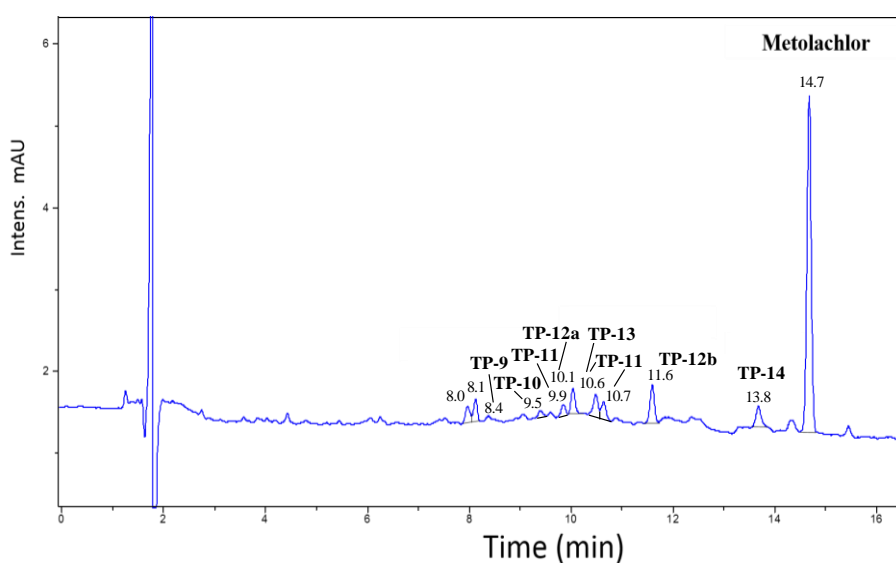
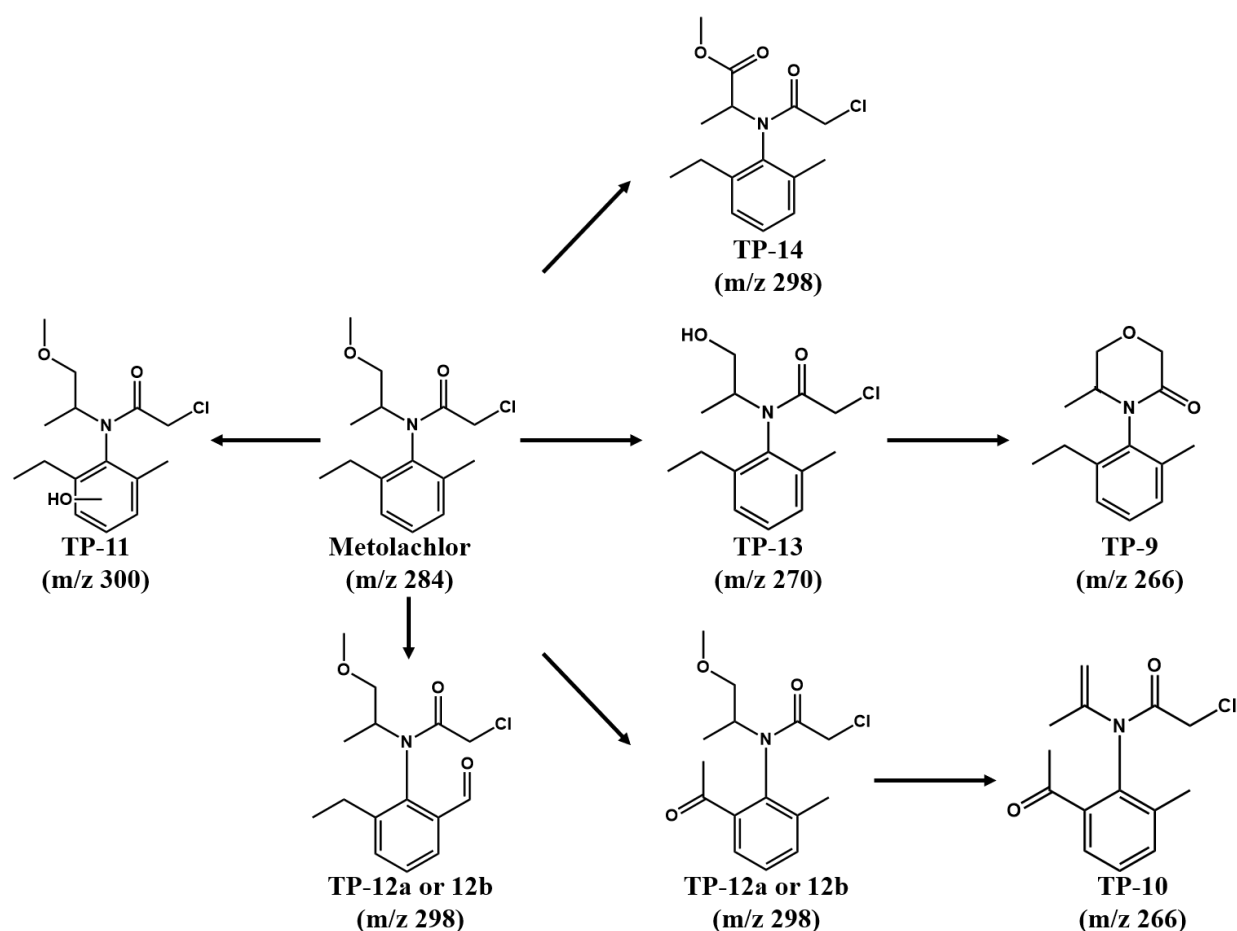


**Figure 4.** HPLC chromatogram acquired at 270 nm of a solution of metolachlor  $1 \cdot 10^{-4}$  M in MilliQ water, after 30 min of treatment in the DBD reactor



**Scheme 2.** Proposed pathways for metolachlor degradation. The data in parentheses are m/z values of the corresponding protonated species formed in positive ESI ionization

The acetamide-derived herbicide metolachlor reacts slowly with ozone ( $k_{\text{ozone}} = 3 \text{ M}^{-1} \text{ s}^{-1}$ ) [37] and much faster with OH radicals ( $k_{\text{OH}} = 6.67 \cdot 10^9 \text{ M}^{-1} \text{ s}^{-1}$ ) [38]. Reactions with OH radicals are not selective, thus it is difficult to identify distinctive pathways of degradation. Fig. 4 shows the HPLC-UV chromatogram acquired after 30 min of treatment of a  $1 \cdot 10^{-4} \text{ M}$  solution of metolachlor. Several peaks were attributed to metolachlor and its degradation products. ESI-MS(+) and MS<sup>2</sup> analyses (Fig. 5) allowed us to attribute them to products of hydroxylation, dechlorination and oxoquinoline-ring formation (Scheme 2). Hydroxylation of the aromatic ring leads to the formation of TP-11 at m/z 300 (Fig. 5b), that is also a product of metolachlor photoFenton oxidation [39]. Three isomers are detected with retention times of 9.9, 10.6 and 10.7 min, having identical MS/MS spectra, and thus ascribed to hydroxylation on different positions of the aromatic ring. Three peaks with m/z 298, which differs by 14 Da from metolachlor, can be ascribed to the oxidation of a >CH<sub>2</sub> group to >C(=O), process which was also observed in the photodegradation and Fenton treatment of metolachlor in water [39, 40]. Thanks to the different fragmentation patterns of the corresponding parent ions observed in the MS<sup>2</sup> spectra (Fig. 5), the isomers TP-12 and TP-14 were distinguished (Fig. 5c and e). The protonated ion

of TP-14 undergoes consecutive losses of two radicals,  $\bullet\text{OCH}_3$  and  $\bullet\text{CH}_3$ , while the protonated ions of the two isomers TP-12, indicated as TP12a and TP-12b in Figure 5a and in Scheme 2, fragment via methanol elimination, in analogy to the fragmentation observed for protonated metolachlor. Thus, in TP-12 the oxidized  $>\text{CH}_2$  groups are assigned to the methyl or ethyl group bound to the aromatic ring, which do not influence the main fragmentation path of the protonated ion. In TP-14 the oxidized  $>\text{CH}_2$  group is thought to be that of the *N*-(-2-methoxy-1-methylethyl) moiety. In this case the oxidation concerns the carbon atom involved in the bond which is broken in the fragmentation and for this reason a change in the fragmentation mechanism is observed. TP-12 is then further decomposed to TP-10, detected at  $m/z$  266 and with a retention time of 9.5 min. The compound TP-13 at  $m/z$  270 (Fig 5d), which coelutes with one of the TP-11 isomer at 10.6 min, can be attributed to 2-chloro-*N*-(2-ethyl-6-methylphenyl)-*N*-(1-hydroxypropan-2-yl)-acetamide, formed by OH attack on the O-methyl group [39]. Its fragmentation includes the loss of  $\text{H}_2\text{O}$  and thus the formation of a fragment at  $m/z$  252, analogously to what is observed with metolachlor, which forms  $m/z$  252 by the loss of  $\text{CH}_3\text{OH}$ . TP-9 with  $m/z$  234 is the major photolysis product [40, 41] and an important microbial degradation product [42]. Its fragmentation includes competitive losses of  $\text{H}_2\text{O}$  ( $m/z$  216), CO ( $m/z$  206),  $\text{HOCH}_2\text{C}\bullet\text{O}$  ( $m/z$  175) and of  $\bullet\text{CH}_3$  plus  $\bullet\text{CH}_2\text{OCHCO}$  ( $m/z$  146), as it is possible to observe in Fig. 5a.

It was of interest to compare the products formed when mesotrione and metolachlor were treated together in 1:1 mixture with those observed when the two herbicides were treated separately. The comparison shows that the same products were formed from each herbicide regardless of the presence of the other herbicide within the same solution. As an example, Fig. 6 shows the abundance *vs* time profile for three degradation products, two formed from metolachlor, namely hydroxylated metolachlor (TP-11) and *N*-(2-acetyl-6-methylphenyl)-2-chloro-*N*-(1-methoxypropan-2-yl)acetamide (TP-14) and TP-3, formed from mesotrione, whose MS/MS spectrum is reported in Fig 3f. For all three the characteristic profile of a reaction intermediate is observed, with the species concentration reaching a maximum and then decaying due to reaction of the intermediate itself. When comparing the data obtained in experiments with just one herbicide and with both herbicides in mixture it is interesting to note that not only the shape of the curves are very similar but also that the areas of the peaks are in agreement with the precursor herbicide initial concentration ( $1 \cdot 10^{-4}$  and  $5 \cdot 10^{-5}$  M when treated alone and in mixture, respectively).

Thus, the results of product studies confirm the conclusions of kinetic studies that there is no appreciable reciprocal influence on the advanced oxidation of mesotrione and metolachlor when the two herbicides are treated together in our DBD air plasma reactor.

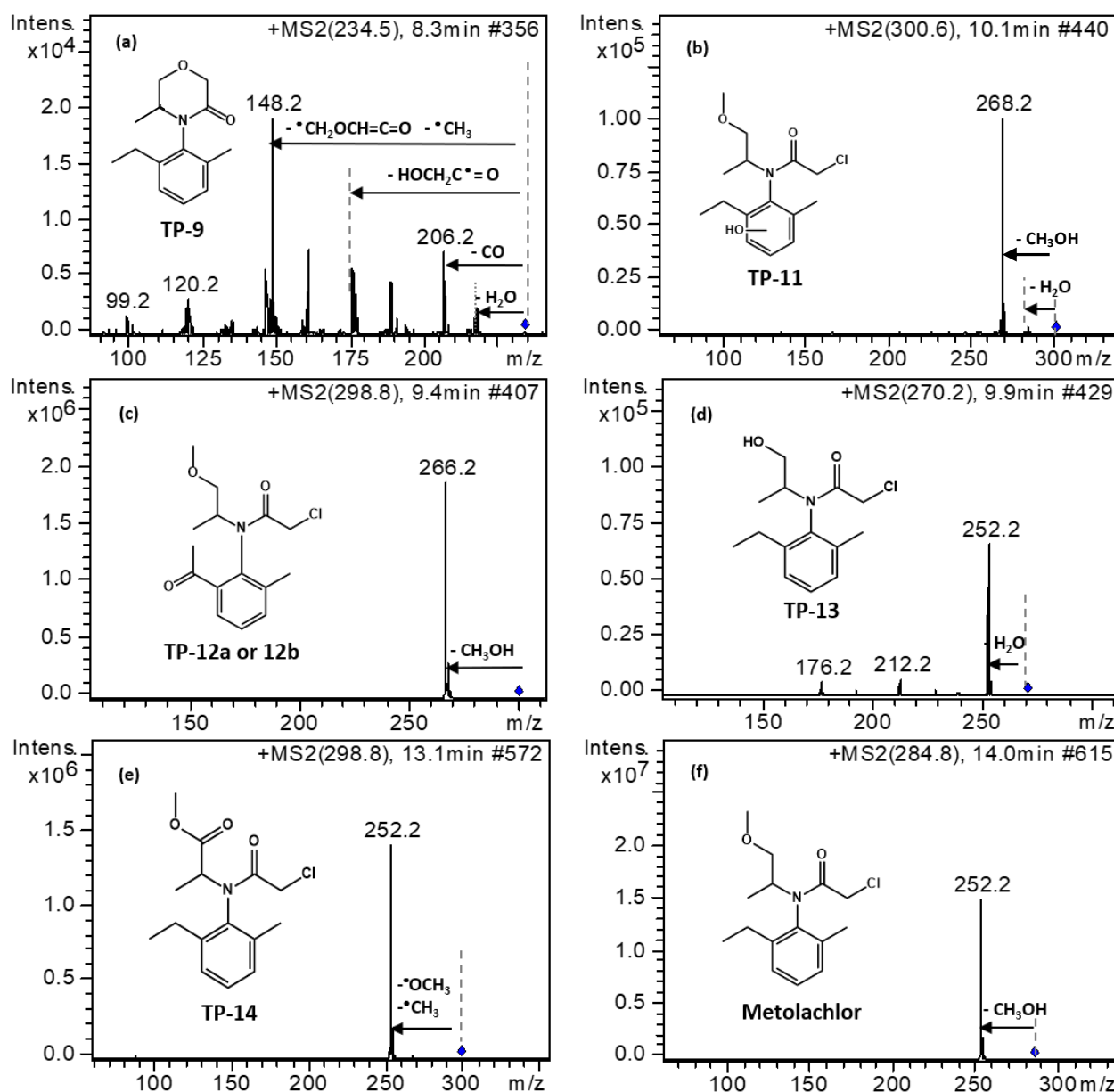


**Figure 5.** ESI(+)/MS<sup>2</sup> spectra of metolachlor (f) and its oxidation products: TP-9 (a), TP-11 (b), TP-12a or 12b (c), TP-13 (d) and TP-14(e)

The mineralization extent was also evaluated through Total Carbon Analysis. 53% of organic residues were measured after 4 h of plasma for the mixture with a total initial concentration of  $1 \cdot 10^{-4}$  M. Further experiments were performed at lower initial concentrations of the pollutants, namely  $5 \cdot 10^{-6}$  M, which is higher than that measured in real water samples. Complete conversion to CO<sub>2</sub> was observed after 5 h treatment with the mixture of metolachlor and mesotrione confirming an improvement of efficiency of plasma induced degradation as the initial concentrations of the

contaminants are decreased. Total mineralization extent is also coherent with 100% of conversion to CO<sub>2</sub> for both compounds treated at an initial concentration of 5 · 10<sup>-6</sup> M.

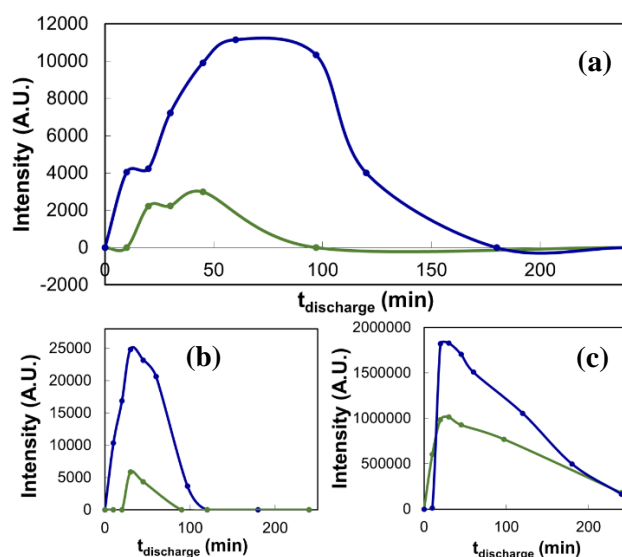


**Figure 6.** Time profile of compounds with m/z 300 and corresponding MS<sup>2</sup> spectrum (a) m/z 489 (b) and m/z 298 (c) as result of treatment of the herbicides alone, 1 · 10<sup>-4</sup> M (blue) and 5 · 10<sup>-5</sup> M in mixture (green)

#### 4.4 Conclusions

A novel advanced oxidation process was successfully tested in the degradation of mesotrione and metolachlor in water, treated individually and in mixture. In our reactor, dielectric barrier discharges in air at room temperature and atmospheric pressure are used to generate a strongly oxidizing cold plasma just above the water to be treated leading to oxidation of dissolved herbicides. Reaction probably occurs at the gas-liquid interface and within the bulk of the liquid. The results show that each herbicide reacts at a characteristic rate, which is significantly faster for mesotrione than for metolachlor, and appears to be unaffected by the presence of the other. These kinetic observations are matched by the results of product analyses: the same oxidation intermediates were detected for each herbicide regardless of whether it was treated as single component or in mixture. Based on previous experience with the same reactor [21] and on the consistency of the intermediate products identified in our experiments with those found in photodegradation, ozonation, and Fenton treatment of mesotrione and metolachlor [31, 34, 38, 39, 41], we can conclude that the major reactive species in our plasma induced advanced oxidation are the hydroxyl radical and ozone. In conclusion, both kinetic and product studies show that there is a negligible reciprocal influence in the degradation of mesotrione and metolachlor treated in a 1:1 mixture in our DBD reactor. This outcome is consistent with the considerable difference in reactivity of the two herbicides when treated in our reactor, which



is in line with data reported in the literature for other advanced oxidation processes. Finally, we have shown that if the treatment time is suitably extended beyond the time required for complete degradation of the herbicides, exhaustive mineralization can be achieved both when they are treated individually and in mixture.

## **Acknowledgement**

We thank University of Padova for financial support (grant CPDA147395/14 - Progetto di Ricerca di Ateneo 2014) and COST Action TD1208 for the stimulating environment provided

## **References**

1. Cabrera LY. Pesticides: A Case Domain for Environmental Neuroethics. *Camb Q Healthc Ethics*. 2017; 26(4) 602-615
2. Mitchell G, Bartlett DW, Fraser TE, Hawkes TR, Holt DC, Townson JK, Wichert RA. Mesotrione: a new selective herbicide for use in maize. *Pest Manag Sci*. 2001; 57:120
3. Bulletin OEPP/EPPO Bulletin. 2012; 42 (3): 353–35
4. Deneer JW. Toxicity of mixtures of pesticides in aquatic systems. *Pest Manag Sci*. 2000; 56(6): 516-520
5. Bethsass J, Colangelo A. European Union Bans Atrazine, While the United States Negotiates Continued Use. *Int J Occup Environ Health*. 2006; 12(3): 260
6. Pinna MV, Roggero PP, Seddaiu G, Pusino A. Soil sorption and leaching of active ingredients of Lumax® under mineral or organic fertilization. *Chemosphere*. 2014; 111:372-378
7. Tomlin C. British crop protection council. The e-pesticide manual: a world compendium. 11<sup>th</sup> Ed. Farnham : BPPC. 1999
8. Wauchope RD, Buttler TM, Hornsby AG, Augustijn-Beckers P, Burt JP. In: Ware GW (ed) *Reviews of Environmental Contamination and Toxicology: Continuation of Residue Reviews*, Springer New York, New York, NY; 1992. pp.1-155
9. Aga, DS. Analytical applications of immunoassays in environmental and agricultural chemistry--study of the fate and transport of herbicides: Lawrence, University of Kansas, Department of Chemistry, Ph.D. thesis. 1995; 220 p
10. Bonnet JL, Bonnemoy F, Dusser M, Bohatier J. Toxicity Assessment of the Herbicides Sulcotrione and Mesotrione Toward Two Reference Environmental Microorganisms: *Tetrahymena pyriformis* and *Vibrio fischeri*. *Arch Environ Contam Toxicol* 2008; 55(4):576-583
11. Joly P, Besse-Hoggan P, Bonnemoy F, Batisson I, Bohatier J, Mallet C. Impact of Maize Formulated Herbicides Mesotrione and S-Metolachlor, Applied Alone and in Mixture, on Soil Microbial Communities. *ISRN Ecology*. 2012; 2012: 9
12. Mendes KF, Reis MRd, Inoue MH, Pimpinato RF, Tornisielo VL. Sorption and desorption of mesotrione alone and mixed with S-metolachlor+terbuthylazine in Brazilian soils. *Geoderma*. 2016; 280:22-28
13. Oturan MA, Aaron J. *Advanced Oxidation Processes in Water/Wastewater Treatment: Principles and Applications. A Review*. *Crit Rev Environ Sci Technol* 2014; 44(23):2577-2641

14. Bruggeman PJ, Kushner MJ, Locke BR, Gardeniers JGE, Graham WG, Graves DB, Hofman-Caris RCHM, Maric D, Reid JP, Ceriani E, Fernandez Rivas D, Foster JE, Garrick SC, Gorbanev Y, Hamaguchi S, Iza F, Jablonowski H, Klimova E, Kolb J, Krcma F, Lukes P, Machala Z, Marinov I, Mariotti D, Mededovic Thagard S, Minakata D, Neyts EC, Pawlat J, Lj Petrovic Z, Pflieger R, Reuter S, Schram DC, Schröter S, Shiraiwa M, Tarabová B, Tsai PA, Verlet JRR, von Woedtke T, Wilson KR, Yasui K, Zvereva G. Plasma–liquid interactions: a review and roadmap. *Plasma Sources Sci Technol* 2016; 25(5) [053002]
15. Locke BR, Sato M, Sunka P, Hoffmann MR, Chang J. Electrohydraulic Discharge and Nonthermal Plasma for Water Treatment. *Ind Eng Chem Res* 2006; 45(3):882-905
16. Magureanu M, Mandache NB, Parvulescu VI. Degradation of pharmaceutical compounds in water by non-thermal plasma treatment. *Water Research* 2015; 81:124-136
17. Krishna S, Maslani A, Izdebski T, Horakova M, Klementova S, Spatenka P. Degradation of Verapamil hydrochloride in water by gliding arc discharge. *Chemosphere* 2016; 152:47-54
18. Cadorin BM, Tralli VD, Ceriani E, Benetoli, Luís Otávio de Brito, Marotta E, Ceretta C, Debacher NA, Paradisi C. Treatment of methyl orange by nitrogen non-thermal plasma in a corona reactor: The role of reactive nitrogen species. *Journal of Hazardous Materials* 2015; 300:754-764
19. Misra NN, Pankaj SK, Walsh T, O'Regan F, Bourke P, Cullen PJ. In-package nonthermal plasma degradation of pesticides on fresh produce. *Journal of Hazardous Materials* 2014; 271:33-40
20. Ballesteros Martín MM, Sánchez Pérez JA, Casas López JL, Oller I, Malato Rodríguez S. Degradation of a four-pesticide mixture by combined photo-Fenton and biological oxidation. *Water Research* 2009; 43:653-660
21. Marotta E, Schiorlin M, Ren X, Rea M, Paradisi C. Advanced oxidation process for degradation of aqueous phenol in a dielectric barrier discharge reactor. *Plasma Processes Polym.* 2011; 8:867-875
22. Marotta E, Ceriani E, Schiorlin M, Ceretta C, Paradisi C. Comparison of the rates of phenol advanced oxidation in deionized and tap water within a dielectric barrier discharge reactor. *Water Research* 2012; 46(19):6239-6246
23. Marotta E, Ceriani E, Shapoval V, Schiorlin M, Ceretta C, Rea M, Paradisi C. Characterization of plasma-induced phenol advanced oxidation process in a DBD reactor. *Eur Phys J Appl Phys.* 2012; 55(1):13811
24. Slater RC, Douglas-Hamilton DH. Electron-beam-initiated destruction of low concentrations of vinyl chloride in carrier gases. *J Appl Phys.* 1981; 52(9):5820
25. Madureira J, Ceriani E, Pinhão N, Marotta E, Melo R, Cabo Verde S, Paradisi C, Margaça FMA. Oxidation of clofibrac acid in aqueous solution using a non-thermal plasma discharge or gamma radiation. *Chemosphere* 2016; 187:395-403
26. Staehelin J, Hoigne J. Decomposition of ozone in water in the presence of organic solutes acting as promoters and inhibitors of radical chain reactions. *Environ Sci Technol.* 1985; 9(12) :1206-1213
27. Huang H, Liu G, Lv W, Yao K, Kang Y, Li F, Lin L. Ozone-Oxidation Products of Ibuprofen and Toxicity Analysis in Simulated Drinking Water. *J Drug Metab Toxicol.* 2015; 6:181
28. Hübner U, von Gunten U, Jekel M. Evaluation of the persistence of transformation products from ozonation of trace organic compounds – A critical review. *Water Research.* 2015; 68:150-170
29. Zazo JA, Casas JA, Mohedano AF, Gilarranz MA, Rodríguez JJ. Chemical Pathway and Kinetics of Phenol Oxidation by Fenton's Reagent. *Environ Sci Technol* 2005; 39(23) :9295-9302
30. Ter Halle A, Richard C. Simulated Solar Light Irradiation of Mesotrione in Natural Waters. *Environ Sci Technol.* 2006; 40:3842

31. Jović M, Manojlović D, Stanković D, Dojčinović B, Obradović B, Gašić U, Roglić G. Degradation of triketone herbicides, mesotrione and sulcotrione, using advanced oxidation processes. *J Hazard Mater.* 2013; 260:1092-1099
32. Ahmed MM, Brienza M, Goetz V, Chiron S. Solar photo-Fenton using peroxymonosulfate for organic micropollutants removal from domestic wastewater: Comparison with heterogeneous TiO<sub>2</sub> photocatalysis. *Chemosphere.* 2014; 117:256-261
33. Murati M, Oturan N, Aaron J, Dirany A, Tassin B, Zdravkovski Z, Oturan MA. Degradation and mineralization of sulcotrione and mesotrione in aqueous medium by the electro-Fenton process: a kinetic study. *Environ Sci Poll Res.* 2012; 19(5):1563-1573
34. Murati M, Oturan N, Zdravkovski Z, Petreska Stanoeva J, Efremova Aaron S, Aaron J, Oturan MA. Application of the electro-Fenton process to mesotrione aqueous solutions: Kinetics, degradation pathways, mineralization and evolution of the toxicity. *Maced J Chem Chem En.* 2014; 33(1): 121-137
35. Griesbaum K, Miclaus V, Jung C, Quinkert R. Gas-Phase Reactions of 1,2-Dimethylcyclopentene and of 2,6-Heptanedione with Ozone: Unprecedented Formation of an Ozonide by Ozone Treatment of a Diketone. *Eur J Org Chem.* 1998; 1998(4):627-629
36. Sun M, Dai W, Liu DQ. Fragmentation of aromatic sulfonamides in electrospray ionization mass spectrometry: elimination of SO<sub>2</sub> via rearrangement. *J Mass Spectrom.* 2008; 43(3):383-393
37. Laar J, Maouala-Makata P, Dore M. Rate constants for reactions of ozone and hydroxyl radicals with several phenylureas and acetamides. *Environ Technol.* 1996; 17(7): 707-716
38. Acero JL, Benitez FJ, Real FJ, Maya C. Oxidation of Acetamide Herbicides in Natural Waters by Ozone and by the Combination of Ozone/Hydrogen Peroxide: Kinetic Study and Process Modeling. *Ind Eng Chem Res.* 2003; 42(23):5762-5769
39. Pignatello JJ, Sun Y. Complete oxidation of metolachlor and methyl parathion in water by the photoassisted Fenton reaction. *Water Research.* 1995; 29(8):1837-1844
40. Mathew R, Khan SU. Photodegradation of Metolachlor in Water in the Presence of Soil Mineral and Organic Constituents. *J Agric Food Chem.* 1996; 44(12):3996-4000
41. Wu C, Shemer H, Linden KG. Photodegradation of Metolachlor Applying UV and UV/H<sub>2</sub>O<sub>2</sub>. *J Agric Food Chem.* 2007; 55(10):4059-4065
42. Liu S, Zheng Z, Zhang R, Bollag J. Sorption and Metabolism of Metolachlor by a Bacterial Community. *Appl Environ Microbiol.* 1989; 55(3):733-740



# Chapter 5 - Plasma treatment of other persistent organic contaminants: Triclosan and PFOA

## 5.1 Triclosan

### 5.1.1 Introduction

Triclosan (5-chloro-2-(2,4-dichlorophenoxy)phenol) is a common antimicrobial agent which inhibits bacteria growth by blocking the fatty acid biosynthetic pathway, which in turn disrupts lipid synthesis necessary for building cell membranes and reproduction [1,2].

Triclosan (TCS) was the active ingredient in personal care products (e.g. cosmetics, hand soaps) until recently. In September 2016 it was banned by the USA's Food and Drug Administration (FDA) due, in part, to a lack of evidence supporting the antibacterial claims. Moreover, it was reported that triclosan and its degradation products reduce testosterone levels and are potent endocrine disruptors [3,4]. Triclosan has been detected in fish, soil and sediments due to its hydrophobicity. *In vivo* studies showed that triclosan is toxic to fish, algae and other aquatic organisms [5,6]. However, the FDA only banned the chemical in consumer products. Triclosan remains one of the prevalent antibacterial agents in hospitals and other medical facilities. Conventional WWTPs have proven to be not an efficient barrier to the discharge of triclosan and its derivatives (forming during disinfection with chlorine) into surface water [7-9]. They are also known to react photochemically to form polychlorinated dioxins, harmful for the ecosystem [10]. Thus, a more effective oxidation treatment is necessary. To this purpose several advanced remediation technologies were tested recently as reported in literature, exploiting stronger oxidant species produced by e.g. photodegradation [11,12] or ozonation [7,13]. The use of plasma as advanced oxidation technology was also assessed, but only in combination with another technology: Kim et al. studied the removal of TCS by plasma in combination with activated nanofibers, reporting a synergistic effect [14].

The focus of this research was to evaluate the impact of the species produced by the DBD reactor implemented in our laboratory on triclosan in aqueous solution. Testing was performed with different initial concentrations and pH: mineralization extent and amount of inorganic ions produced after plasma treatment were evaluated. A few degradation products were also identified by LC/MS analysis.

## 5.1.2 Experimental section

### 5.1.2.1 Materials

Triclosan was purchased from Sigma-Aldrich while  $\text{KH}_2\text{PO}_4$  and  $\text{K}_2\text{HPO}_4 \cdot 3\text{H}_2\text{O}$  from Carlo Erba. Triclosan  $1 \cdot 10^{-4}$  M solutions were prepared by dissolving the solid compound in NaOH solution ( $1 \cdot 10^{-3}$  M) and successively readjusting pH to neutrality with a minimal volume of  $\text{H}_2\text{SO}_4$ . Ultrapure grade water (milliQ a Millipore system), obtained by filtration of distilled water with a Millipore system, was employed for all the experiments. Pure air used in the experiments was a synthetic mixture (80% nitrogen e 20% oxygen) from Air Liquid with specified impurities of  $\text{H}_2\text{O}$  (<3 ppm) and of  $\text{C}_n\text{H}_m$  (<0.5 ppm).

### 5.1.2.2 Plasma reactor

Experiments were performed with the DBD-like corona reactor, described previously [15]. It is made of a glass vessel (internal dimensions 95x75 mm and 60 mm height) closed by a Teflon cover. Four passing electrodes of stainless steel, hold to the cover, support two parallel wires (d. 0.15 mm) fixed upon their tips and placed at a distance of 38 mm one from the other, and of 15 mm from the aqueous solution. The outside surface of the reactor base is covered with silver film and connected to ground. The cover is constituted of two connectors for gas input and exhaust and a septum-provided port for sampling without altering the gas atmosphere inside the reactor. Synthetic air (flow 30 mL/min) flows through the reactor during plasma treatment. A bubbler, filled with milliQ water, is put along the feeding gas line in order to saturate dry air with humidity and prevent evaporation from the treated solution during the experiment. The discharge occurs in the gas phase above the liquid (70 mL). The reactor is energized with a high voltage power supply at 50 Hz operating in Dielectric Barrier Discharge (DBD) mode. During the experiments, power was kept constant (1.9 W): voltage and current profiles were monitored with a digital oscilloscope (TDS5032B) to assure the reproducibility of the electrical conditions.

### 5.1.2.3 Analysis of Triclosan and its degradation products

The decomposition of triclosan was monitored by measuring its conversion as a function of treatment time at constant applied voltage. At desired discharge times aliquots of the plasma treated solution were sampled. HPLC analysis was performed by a Thermo Scientific Products instrument with P2000 pump and UV6000LP Diode Array Detector operating at 270 nm, using a Phenomenex column, Kinetex® 5u C18 100Å 150x4.6 mm with the following eluents: A: 0.1% aqueous formic acid, and B: acetonitrile with 0.1% of formic acid. The flow rate was 1 mL/min, the column temperature was

maintained at 298 K. The gradient elution initial conditions were 20% B with linear gradient to 90% in 25 min, being maintained for 2 min, then followed by a return to the initial conditions within 5 min. The fraction of residual drug expressed as  $C/C_0$  was plotted against treatment time and the data were fitted by Equation (5.1)

$$C=C_0 \cdot e^{-kt} \quad (5.1)$$

to obtain  $k$ , the rate constant of the process. The half-life time of triclosan was thus calculated by Equation (5.2)

$$t_{1/2} = \ln 2/k \quad (5.2)$$

pH of the initial and final solutions was monitored during the experiments with a pH meter Seven Compact, S220 (Mettler Toledo).

LC/MS analysis were performed by using an HPLC instrument (Agilent Technologies 1100 series) connected to a diode array and a mass spectrometer detector (MSD Trap SL model G2245D). The ionization was performed by electrospray operating in negative polarity with the following parameters: nebulizer 50 psi, dry gas flow rate 8 L/min, dry gas temperature 350 °C. The oxidation products were tentatively attributed by comparison of their retention time, UV/Vis and MS spectra with those obtained from standard compounds, when available. Otherwise, peaks were tentatively identified on the basis of their mass spectra and information found in the literature.

The determination of ions produced by applying NTP was carried out by ion chromatography using a Dionex-ICS-900 instrument equipped with a Dionex IonPac AS22 IC Column after proper calibration with standard solutions of  $\text{NaNO}_3$  and  $\text{NaCl}$ . 4.5 mM sodium carbonate ( $\text{Na}_2\text{CO}_3$ ) and 1.4 mM sodium bicarbonate ( $\text{NaHCO}_3$ ) were used as the eluents at a flow rate of 1.2 mL/min for 15 min. The total carbon (TC) dissolved in the triclosan solutions, before and after plasma treatment, was determined by a TOC analyzer (Shimadzu TOC-VCSN instrument). It operates in the range of 50  $\mu\text{g/L}$ –25 g/L and is equipped with an autosampler and an automatic diluter. Calibration of the instrument was carried out by using solutions of standard potassium hydrogen phthalate automatically diluted in the range of interest. Two measurements were performed for each analysis, including the total carbon and the so-called "inorganic carbon" (IC), the latter representing the content of dissolved carbon dioxide and salts containing bicarbonate or carbonate anions. Subtracting the inorganic carbon from the TC the value of total organic carbon (TOC) is obtained. In this study only Total Carbon (TC) values are reported: this is due to negligible values of IC detected.

### 5.1.3 Results and discussion

#### 5.1.3.1 The effect of initial concentration and pH

The decay of triclosan upon treatment with non-thermal plasma in our DBD reactor follows to a good approximation an exponential function in time. Figure 1 shows examples of typical decay profiles for experiments run under identical conditions (full symbols) except for the initial concentration of TCS which changes from  $10^{-4}$  and  $5 \cdot 10^{-6}$  M. These experiments suggest that the rate of decomposition of TCS depends on its initial concentration,  $[TCS]_0$  (Table1).

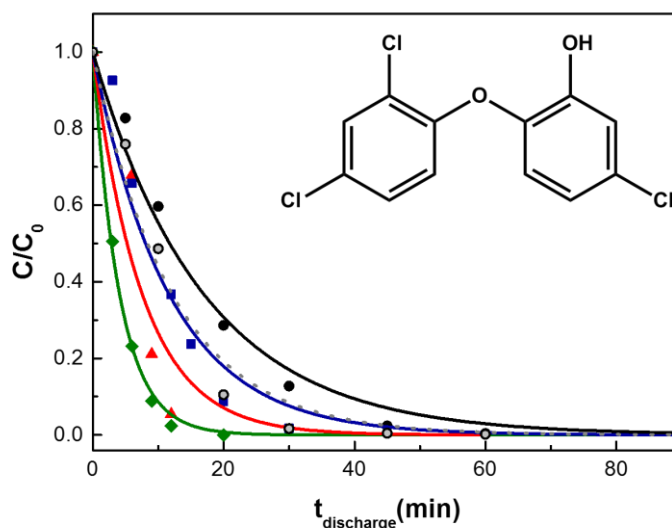


**Figure 1.** Degradation curves of TCS after plasma treatment at different initial concentrations (full symbols) in milliQ water:  $1 \cdot 10^{-4}$  M (●),  $1 \cdot 10^{-5}$  M (■),  $8 \cdot 10^{-6}$  M (▲),  $5 \cdot 10^{-6}$  M (◆). Decay of TCS  $1 \cdot 10^{-4}$  M at pH 7 (open symbols)

The influence of pH on triclosan degradation was also investigated. Plasma degradation curves of triclosan  $1 \cdot 10^{-4}$  M in milliQ water (full black symbols) and buffer solution at pH 7 (black open symbols) are shown in Figure 1. The degradation constants obtained from pseudo first-order exponential fittings are  $5.9 \cdot 10^{-2}$  and  $8.3 \cdot 10^{-2} \text{ min}^{-1}$ , respectively. This significant difference can be explained considering the speciation of triclosan in water and the species produced by atmospheric air plasma in the solution. Due to the presence of the phenolic function, triclosan can be present in water solution as neutral and anionic species ( $pK_a=8.1$ [16]), with only neutral triclosan at  $pH < 6$  and an excess of the neutral form at circumneutral pH compared to the anionic one [7]. In a previous work it was demonstrated that the major reactive species in our DBD reactor are ozone and OH radicals and that pH of a pure sample of milliQ water turns into acidic during plasma treatment ( $t_{\text{discharge}} \geq 30$  min), in the absence of a buffering system [17]. It is well known that this effect is caused by the production of nitric acid dissolved in solution, as result of reactions initiated by atmospheric plasma in air above the solution [17,18].

Taking into account triclosan reactivity towards  $\cdot\text{OH}$  and  $\text{O}_3$ , its degradation in our plasma reactor is presumably due to the reactivity of its phenol-like ring toward electrophilic attack by ozone and OH

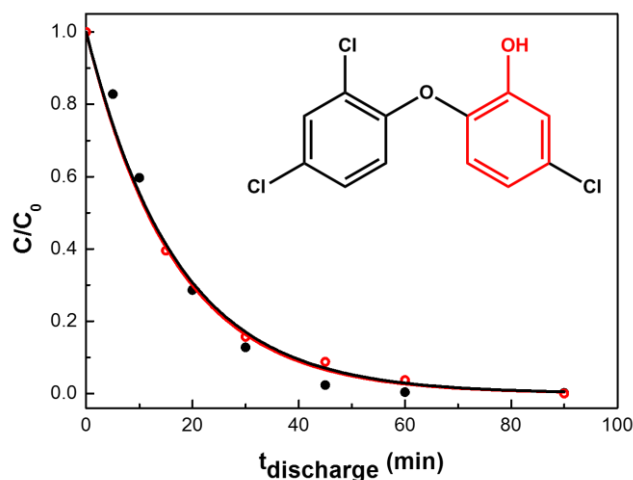


radicals. It is possible to make a comparison between triclosan and phenol, due essentially to similar reactive sites towards the major species formed upon application of the discharge in air.

**Table 1.** Initial concentrations ( $C_0$ ), decay constant ( $k_{degradation}$ ), solution conditions and half-life time ( $t_{1/2}$ ) achieved for phenol and triclosan in the DBD reactor.

Compound	$C_0 / M$	$k_{degradation} \cdot 10^2 / \text{min}^{-1}$	Solution	$t_{1/2} / \text{min}$
Triclosan	$1 \cdot 10^{-4}$	$8.3 \pm 0.8$	buffer pH 7	8
Triclosan	$1 \cdot 10^{-4}$	$5.9 \pm 0.4$	milliQ	12
Phenol	$1 \cdot 10^{-4}$	$6.0 \pm 0.1$	milliQ	12
Triclosan	$1 \cdot 10^{-5}$	$8.6 \pm 1.0$	milliQ	8
Triclosan	$8 \cdot 10^{-6}$	$13.0 \pm 0.4$	milliQ	5
Triclosan	$5 \cdot 10^{-6}$	$25.0 \pm 0.1$	milliQ	3

Considering phenol ring as the main reactive site of triclosan, significant effects of this equivalent reactivity can be observed empirically:



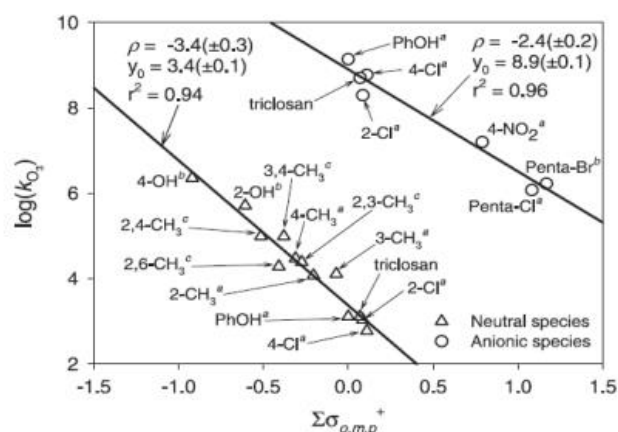
**Figure 2.** Comparison of decay curves of triclosan and phenol, at the same initial concentration,  $10^{-4}$  M, in milliQ water.

Figure 2 shows the exponential decays of both, triclosan and phenol, at the same initial concentration,  $1 \cdot 10^{-4}$  M, in milliQ water. The rate constants of the plasma process demonstrate a possible common degradation mechanism for both compounds.

A mechanistic hypothesis which can explain these experimental findings concerns the site of triclosan subjected to attack by the reactive species. Reactivity of triclosan in our plasma reactor is presumably due to its phenol-like ring and its activation toward electrophilic attack, mainly by hydroxyl radicals and ozone, with kinetics constants  $k_{OH} = 5.4 \cdot 10^9 \text{ M}^{-1} \text{ s}^{-1}$  [19];  $k_{O_3} = 1.3 \cdot 10^3 \text{ M}^{-1} \text{ s}^{-1}$  for the neutral

triclosan and  $k_{O_3} = 5.1 \cdot 10^8 \text{ M}^{-1} \text{ s}^{-1}$  for the deprotonated form [7]. In other words, ozone was found to be highly selective toward deprotonated triclosan. This is the result of electron-donating character of  $O^-$  relative to  $OH$  that improves electrophilic attack, initial step of triclosan decomposition, and explains the enhanced oxidation at circumneutral pH ( $k_{app_{O_3}} = 3.8 \cdot 10^7 \text{ M}^{-1} \text{ s}^{-1}$  at pH 7). As regards hydroxyl radical instead, as low selective species, it is expected to react not only with the phenol-like ring, but also with TCS' dichlorophenoxy ring. A similar behavior is found for phenol, considered as representative compound of TCS, which is characterized by a pKa (9.1) comparable to that of triclosan (pKa= 8.1); therefore the degree of dissociation varies alike as a function of pH. Phenol rate constants follow the same trends:  $k_{OH} = 1 \cdot 10^{10} \text{ M}^{-1} \text{ s}^{-1}$  and  $k_{O_3 \text{ phenol}} = 1.4 \cdot 10^9 \text{ M}^{-1} \text{ s}^{-1}$  and  $k_{O_3 \text{ phenoxide}} = 1 \cdot 10^{10} \text{ M}^{-1} \text{ s}^{-1}$ .

A further evidence of this claim is given by Brown–Okamoto correlations, which indicate dependence of  $k_{O_3}$  on phenol substituent effects [7]. The graph below supports the hypothesis of electrophilic mechanism by  $O_3$ ,



**Figure 3.** Brown- Okamoto correlations of  $k_{O_3}$  (Adaptation from Suarez et al.<sup>7</sup>)

$O_3$  electron-donating substituents activate the phenolic moiety towards  $O_3$  while electron withdrawing substituents deactivate the substrate, as predicted for an electrophilic attack.

### 5.1.3.2 Determination of Triclosan degradation products

Triclosan can be easily degraded by plasma, even at relatively high initial concentrations, as can be seen from  $t_{1/2}$  obtained by degradation curves in the range  $1 \cdot 10^{-4}$ - $5 \cdot 10^{-6} \text{ M}$  (Table 1). Nevertheless, it is known that more toxic compounds are generated as result of treatment with other advanced oxidation processes [13,20,21]. In particular, a byproduct of special concern is represented by 2,8-dichlorodibenzo-*p*-dioxin (2,8-DCDD), formed by triclosan ring closure in aqueous solution at

neutral and basic pH <sup>12</sup>. Thus, identification of byproducts was performed through negative ESI/MS and it was possible to appreciate four byproducts formed during DBD discharge. Figure 4A shows the MS<sup>2</sup> spectrum of the deprotonated ion, [M-H]<sup>-</sup>, of di-hydroxy-triclosan, (m/z 319 with the isotope <sup>35</sup>Cl for all chlorine atoms). Intermediates with the same mass but different fragmentation are reported for ozonation and photodegradation of the mother compound [12,13]. In this case, the identification was confirmed by the detection of the fragment ion peak at 177 corresponding to [C<sub>6</sub>H<sub>3</sub>O<sub>2</sub>Cl<sub>2</sub>]<sup>-</sup> and the fragment at 283 stemming from cleavage of HCl from [M-H]<sup>-</sup> peak. MS- spectrum of mono-hydroxy-triclosan was also identified at m/z 303, its formation is the result of the attack of OH on the phenolic ring (Fig. 4B). 1-chlorodibenzo-p-dioxin was identified through MS- analysis and fragmentation of [M-H]<sup>-</sup> signal: the isotopic pattern of the precursor ion is typical of compounds including one chlorine atom and loss of Cl<sup>-</sup> occurs during its fragmentation with consequent minor ion peak at m/z 192 (Fig. 4C). A second degradation pathway is initiated by ·OH acting on the ether bond of TCS <sup>21</sup>, resulting in the formation of 4-chlororesorcinol, with [M-H]<sup>-</sup> ion at m/z 143 (Fig. 4D).

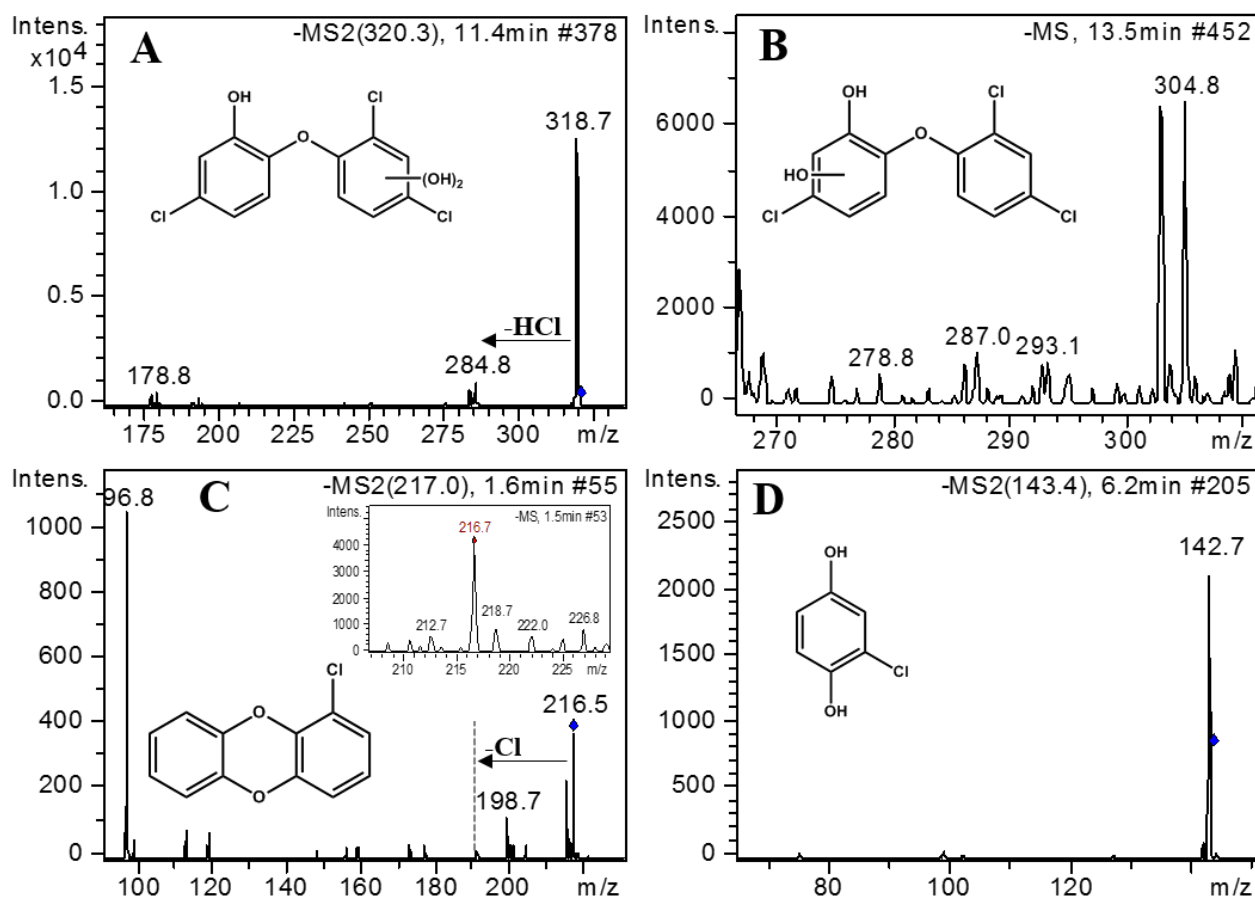


**Figure 4.** Negative ESI/MS or MS<sup>2</sup> spectra of triclosan byproducts of plasma treatment at m/z 319, MS<sup>2</sup> spectrum (A), m/z 303, MS spectrum (B), m/z 217, MS<sup>2</sup> spectrum (C) and m/z 243, MS<sup>2</sup> spectrum.

Thus, the degradation mechanism involves bond breaking, dechlorination and hydroxylation. As ultimate step of oxidation, ring-opening reaction occurs for aromatic intermediates, leading to the decomposition to CO<sub>2</sub>, H<sub>2</sub>O and Cl<sup>-</sup> at last. Ion chromatography was used to identify ionic species originated during plasma treatment. Figure 5 represents the chromatograms of a solution [TCS]<sub>0</sub>=1·10<sup>-5</sup> M, before and after plasma treatment. Three peaks were detected. The signal at 4.2 min is due to chloride ion. Quantification of free chloride was carried out obtaining 85% of Cl<sup>-</sup> after 360 min of treatment. It can be noted that the main peak is due to NO<sub>3</sub><sup>-</sup>, produced by air plasma interaction with the liquid phase, as previously mentioned. The other signal at 2.86 min (X) is expected to be an organic ion among formate, propionate and acetate, which have a similar retention time and were already detected in the case of phenol degradation [22].

**Table 1.** Half-life time ( $t_{1/2}$ ), decay constant ( $k_{degradation}$ ), plasma treatment time (total  $t_{discharge}$ ), % of chloride ions and degree of mineralization achieved for triclosan after plasma treatment

$C_0 / M$	$t_{1/2} / min$	total $t_{discharge} / min$	% Cl <sup>-</sup>	% Mineralization
1·10 <sup>-4</sup>	12	240	/	57
1·10 <sup>-5</sup>	8	360	65 ± 2	72
5·10 <sup>-6</sup>	3	360	85 ± 1	97

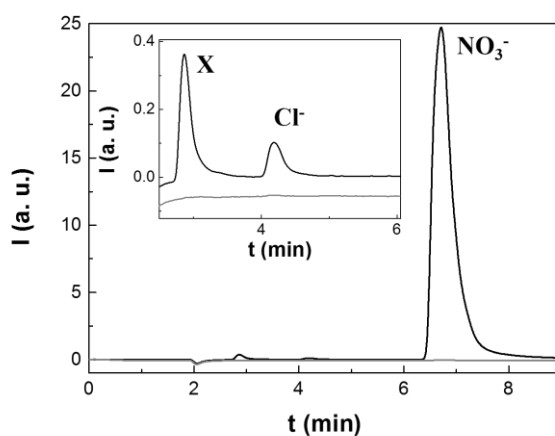


**Figure 5.** Ion Chromatogram of an aqueous solution of triclosan 1·10<sup>-5</sup> M before (grey line) and after (black line) plasma treatment,  $t_{discharge}$ =360 min. Three peaks were observed: X at 2.9 min, Cl<sup>-</sup> signal at 4.2 min and the signal corresponding to nitrate ions at 6.7 min.

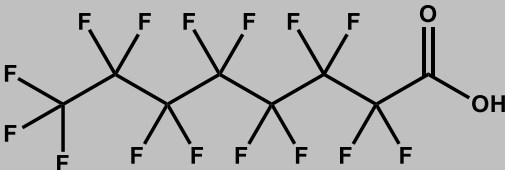
Extent of mineralization after plasma treatment was evaluated for three different TCS initial concentrations, 1·10<sup>-4</sup> M, 1·10<sup>-5</sup> M and 5·10<sup>-6</sup> M (Table 2). It is possible to observe that efficiency of TCS conversion increases as moving to lower initial concentrations of the pollutant: 97% of mineralization was achieved for TCS 5·10<sup>-6</sup> M, expressing efficient removal efficiency of plasma technology for TCS remediation.

## 5.2 Perfluorooctanoic acid (PFOA)

### 5.2.1 Introduction

Perfluorooctanoic acid (PFOA) is a representative fluorinated organic contaminant. This substance is widely used in various applications as surfactants, including stain removers, surface preparation agents, fire extinguishing foams, and semiconductor coating agents, due to its chemical stability and low volatility. Its physical properties stemming from its strong C–F bonds, in particular high water solubility and simultaneous hydrophobic/hydrophilic nature, contribute to its presence in all aquatic environments and even rain water [23]. PFOA has been classified as toxic to reproduction (category 1B) and carcinogenic (category 2) in Regulation (EC) 1272/2008 on the classification, labelling and packaging of substances and mixtures, the so-called ‘CLP Regulation and persistent, bioaccumulative and toxic (PBT). It has been on the Candidate List of Substances of Very High Concern (SVHCs) since June 2013. The EU has recently published measures to regulate PFOA, its salts and related substances in a wide range of products under Annex XVII of REACH and the new law, according to which PFOA and its salts will be prohibited, will be implemented in phases, starting July 4, 2020 [24,25]. Recent data regarding drinking water treatment plants indicate that PFASs, if present in raw water, are not substantially eliminated by most drinking water treatment processes including coagulation, flocculation, sedimentation, filtration, biofiltration, oxidation (chlorination, ozonation, AOPs), UV irradiation, and low pressure membranes. Activated carbon adsorption, ion exchange and high pressure membrane filtration have proven to be effective in controlling these contaminants [23]. It was recently found that non thermal plasma can easily decompose PFOA in solutions: Hayashi et al. reported high decomposition energy efficiency using dc plasmas generated within gas bubbles [26]. The aim of this work was the study of the removal of PFOA in our DBD reactor, the reaction products of this contaminant formed during plasma treatment and thus the mechanism beyond PFOA oxidation. Additionally, the efficiency of DBD in converting perfluorooctanoic acid to CO<sub>2</sub> was evaluated.

**Table 2.** Structure, molecular weight and pKa of PFOA.

Compound	Structure	Molecular Weight (g/mol)	pKa
Perfluorooctanoic acid (PFOA)		414.07	~0

## 5.2.2 Experimental setup

### 5.2.2.1 Materials and methods

Perfluorooctanoic acid (96%) was purchased by Aldrich Chemistry. Ultrapure grade water (milliQ, a Millipore system) was used for all the experiments. A synthetic air mixture (80% nitrogen and 20% oxygen) from Air Liquide with specified impurities of H<sub>2</sub>O (<3 ppm) and of C<sub>n</sub>H<sub>m</sub> (<0.5 ppm) was flown during plasma treatment.

Description of the dielectric barrier discharge was included in the previous paragraph (Section 5.1.2). PFOA solutions subjected to NTP were analyzed by LC/ESI-MS and LC/ESI-MS/MS in negative polarity with an Agilent Technologies system (1100 series) connected to a diode array and a MSD SL Trap. A Phenomenex Kinetex® column 5 μm EVO C18 100Å 150x4.6 mm was used for the analyses. The eluents (flow rate 1 mL/min) and the gradient were the following: A: H<sub>2</sub>O + MeOH 5% + NH<sub>4</sub>Ac 20 mM; B: MeOH, B: t=0 min 5%, t=22 min 100%, t=25 min 100%, t=30 min 5%. Degradation decays at different initial PFOA concentrations were plotted according to the kinetic model of Slater and Douglas-Hamilton<sup>27</sup>, found in previous studies of different contaminants removal by non thermal plasma<sup>15,28</sup>. Experimental results were fitted by Equation (1) to obtain k, the rate constant of the process. The total carbon (TC) residual in triclosan solutions, before and after plasma treatment, was determined by a TOC analyzer (Shimadzu TOC-VCSN instrument).

### 5.2.3 PFOA treatment by DBD discharge

Experiments were carried out using different initial concentrations of PFOA (11.6 and 5.80 μM) in MilliQ water and applying the discharge for long treatment times (5 h). The aim of this approach was to verify the positive effect on plasma removal efficiency due to the decrease of initial concentration of PFOA, as already demonstrated for other organic contaminants. LC-ESI-MS analysis of aliquots of the solution withdrawn at different treatment times provided normalized concentration of PFOA vs time profiles which in turn yielded conversion and kinetic constants. Extracted Ion Chromatograms (EICs) of the byproducts identified (Fig. 6) show that decay of the PFOA occurs by C-C bond cleavage yielding homologues of the precursor with shorter chain lengths, CF<sub>3</sub>(CF<sub>2</sub>)<sub>n</sub>COOH (n=2-6). The ESI(-)-MS spectra of all these products (M) comprise two signals, due to [M-H]<sup>-</sup> and [M-CO<sub>2</sub>H]<sup>-</sup>, respectively. The concentration profile for the first observed product (C7) shows a maximum (Fig. 6 b2), evidencing its presence as a reaction intermediate and suggesting the occurrence of a stepwise process:



As for the mechanism of these conversion steps, we propose the following sequence, which is consistent with that found in the literature for photooxidation [29]:



In which X is an unknown reactive species [30,31]. As one of the major reactive species in plasma,  $\bullet\text{OH}$  could in principle act as initiator but its reaction rate with PFOA resulted to be very low ( $3 \cdot 10^7 \text{ M}^{-1} \text{ S}^{-1}$ ) compared to that of the non fluorinated molecule ( $5.6 \cdot 10^9 \text{ M}^{-1} \text{ S}^{-1}$ ) [23]. X can induce the following reactions in water:



In the same manner, perfluorocarboxylic acids bearing shorter perfluoroalkyl groups are formed in a stepwise manner.

**Table 4.** Byproducts of degradation of PFOA by application of plasma.

Compound	Formula	t <sub>r</sub> (min)	m/z [M-H] <sup>-</sup> , [M-H-CO <sub>2</sub> ] <sup>-</sup>
PFOA	C <sub>7</sub> F <sub>15</sub> COOH	15.17	412.7, 368.8
PFHpA	C <sub>6</sub> F <sub>13</sub> COOH	14.08	362.8, 318.8
<u>PFHxA</u>	C <sub>5</sub> F <sub>11</sub> COOH	12.64	312.8, 268.7
PFPeA	C <sub>4</sub> F <sub>9</sub> COOH	10.43	262.8, 218.7
PFBA	C <sub>3</sub> F <sub>7</sub> COOH	6.18	213.0, 168.7
PFPrA	C <sub>2</sub> F <sub>5</sub> COOH	2.26	162.7, 118.8

A possible mechanism of PFOA degradation was hypothesized and described in 8 steps [32]. As it is possible to observe in Figure 7, the first step proceeds through the monoelectronic oxidation of carboxylate group by an oxidant species to produce a radical intermediate (Fig 7-species 2) [33]. The following steps include Kolbe decarboxylation, with formation of C<sub>n-1</sub> radical (species 3), and coupling reaction with formation of a peroxidic species (species 4). Disproportion of peroxyradicals leads to production of oxoradicals (species 5). Primary fluorinated alcohol (species 6) is then generated by reaction with water [34]. Primary perfluorinated alcohols are thermodynamically unstable <sup>35</sup> and thus can be easily oxidized to the acyclic fluoride (species 7). This implies the

elimination of HF, followed by hydrolysis and formation of perfluorinated C<sub>n-1</sub> carboxylic acid (species 8).

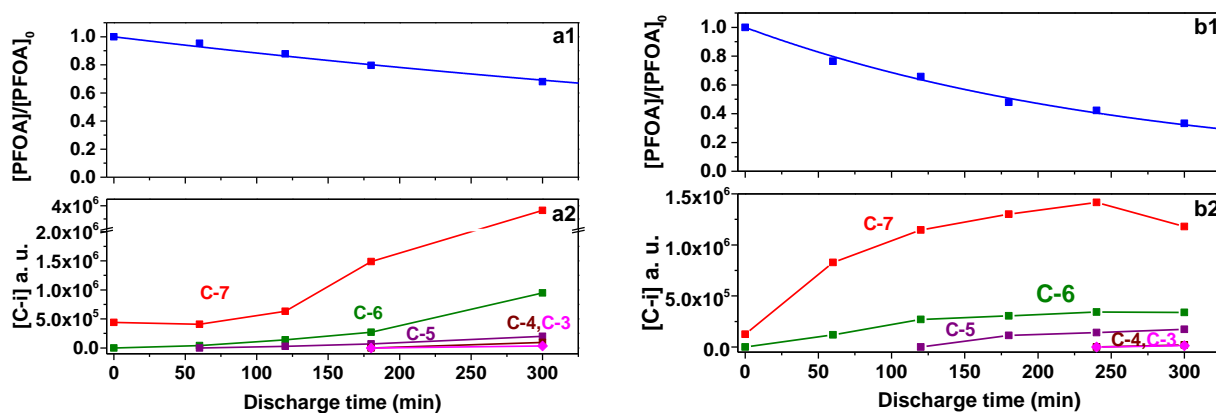


**Figure 6.** PFOA degradation curve and EIC areas of intermediates vs treatment time for [PFOA]=11.6  $\mu$ M (a1-2) and [PFOA]= 5.80  $\mu$ M (b1-2).

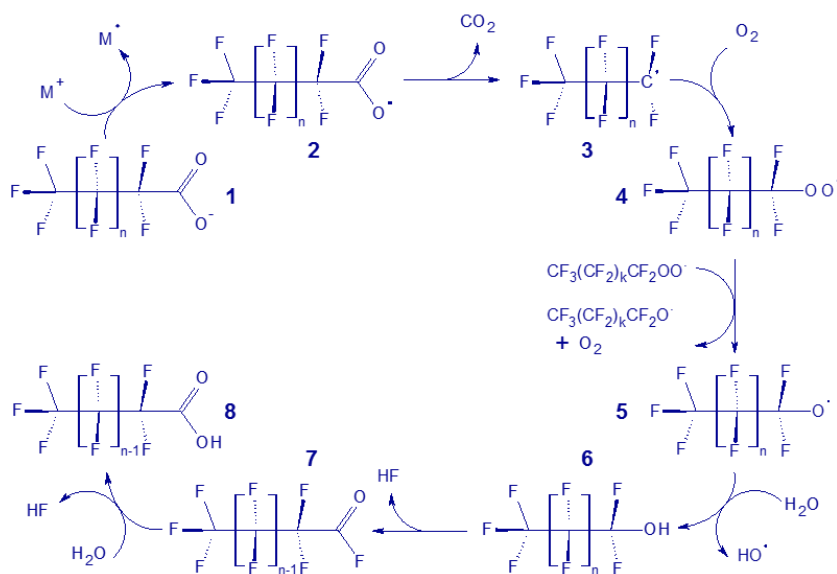


**Figure 7.** Scheme of PFOA degradation.

The acid may form C<sub>6</sub> according to the same mechanism. Considering the low percentage of mineralization of PFOA in our plasma system compared to that reported by Yasuoka et al. [33], it is possible to hypothesize that the rate determining step of PFOA oxidation is represented by the attack on carboxylate group.

The desired goal in treating organic pollutants is their exhaustive oxidation to CO<sub>2</sub>. To quantify the extent of mineralization, total carbon was measured before and after plasma treatment, for initial concentration of PFOA of 5.80  $\mu$ M. By extending the treatment time to 300 min, CO<sub>2</sub> produced



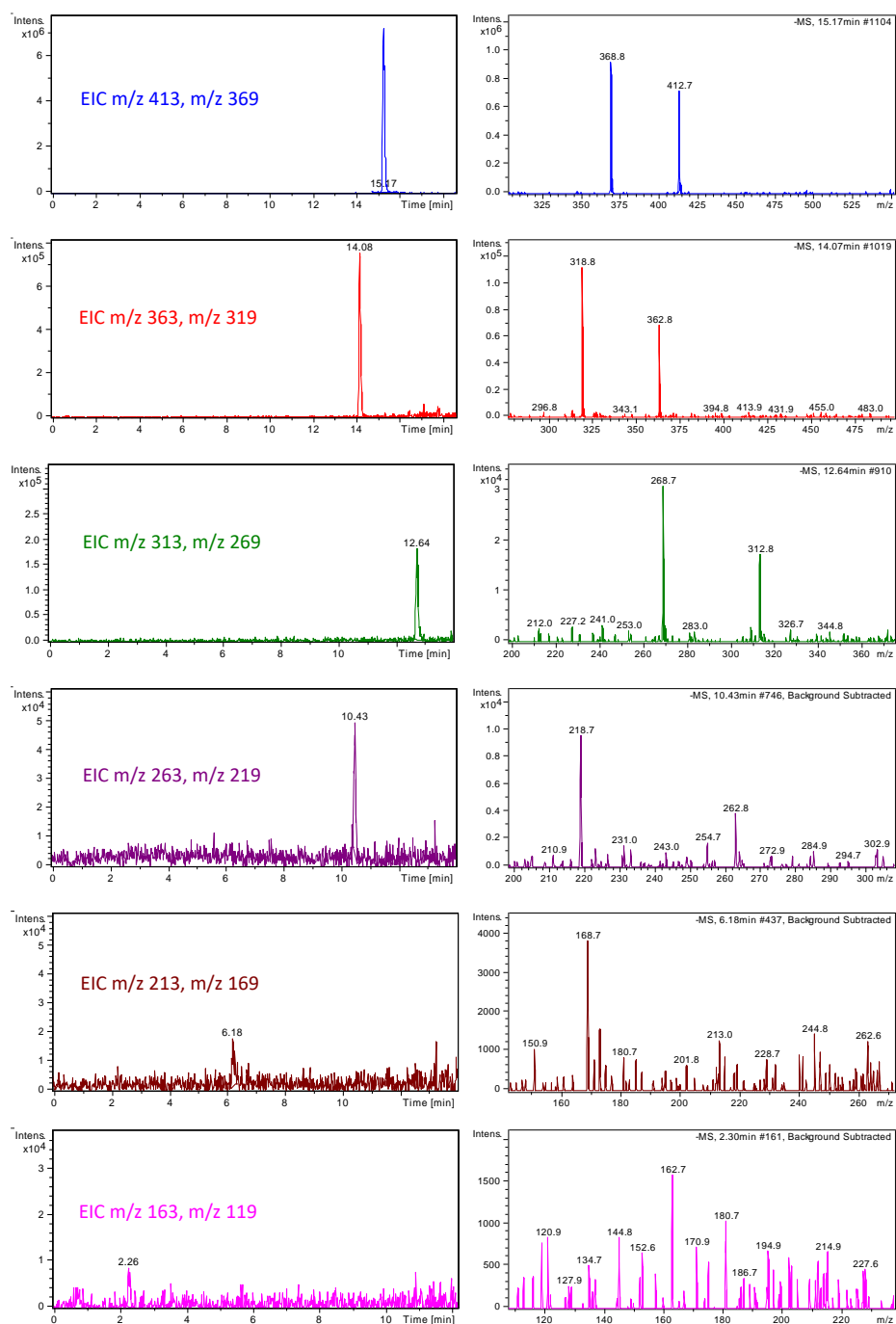


**Figure 7:** Extracted Ion Chromatograms (on the left) and MS spectra (on the right) of intermediates of PFOA plasma treatment.

corresponds to 42% of the total carbon subjected to the oxidation process. In other words, 58% of the total organic carbon originally present as PFOA remains dissolved in solution.

## 5.2.4 Conclusions

Considering that PFOA is chemically inert and is decomposed very slowly under conventional treatment, it was found an improvement in PFOA removal by plasma: within 5h, 67% of PFOA

(initial concentration 5.80  $\mu\text{M}$ ) was decomposed and mineralization ratio reached 42%. Degradation of PFOA was in good agreement with pseudo-first-order kinetics, with rate constants of  $1.23 \cdot 10^{-3} \text{ min}^{-1}$  and  $3.76 \cdot 10^{-3} \text{ min}^{-1}$  for higher and lower concentration under study, respectively. According to the intermediates identified, mechanism of degradation was hypothesized.

## References

1. Schweizer HP. Triclosan: A widely used biocide and its link to antibiotics. *FEMS Microbiol Lett.* 2001;202(1):1-7.
2. Levy CW, Roujeinikova A, Sedelnikova S, et al. Molecular basis of triclosan activity. *Nature.* 1999;398:383
3. Ishibashi H, Matsumura N, Hirano M, et al. Effects of triclosan on the early life stages and reproduction of medaka *oryzias latipes* and induction of hepatic vitellogenin. *Aquatic Toxicology.* 2004;67(2):167-179
4. Raut SA, Angus RA. Triclosan has endocrine-disrupting effects in male western mosquitofish, *gambusia affinis*. *Environmental Toxicology and Chemistry.* 2010;29(6):1287-1291.
5. Anton Lindström, Ignaz J Buerge, Thomas Poiger, Per-Anders Bergqvist, Markus D Müller, Hans-Rudolf Buser. Occurrence and environmental behavior of the bactericide triclosan and its methyl derivative in surface waters and in wastewater. *Environmental science & technology.* 2002;36(11):2322-2329
6. Orvos DR, Versteeg DJ, Inauen J, Capdevielle M, Rothenstein A, Cunningham V. Aquatic toxicity of triclosan. *Environmental Toxicology and Chemistry.* 2002;21(7):1338-1349
7. Suarez S, Dodd MC, Omil F, von Gunten U. Kinetics of triclosan oxidation by aqueous ozone and consequent loss of antibacterial activity: Relevance to municipal wastewater ozonation. *Water Res.* 2007;41(12):2481-2490.
8. Lee DG, Zhao F, Rezenom YH, Russell DH, Chu K. Biodegradation of triclosan by a wastewater microorganism. *Water Research.* 2012;46(13):4226-4234
9. Butler E, Whelan MJ, Sakrabani R, van Egmond R. Fate of triclosan in field soils receiving sewage sludge. *Environmental Pollution.* 2012;167:101-109
10. Anger CT, Sueper C, Blumentritt DJ, McNeill K, Engstrom DR, Arnold WA. Quantification of triclosan, chlorinated triclosan derivatives, and their dioxin photoproducts in lacustrine sediment cores. *Environmental science & technology.* 2013;47(4):1833-1843
11. Constantin LA, Nitoi I, Cristea NI, Constantin MA. Possible degradation pathways of triclosan from aqueous systems via  $\text{TiO}_2$  assisted photocatalysis. *Journal of Industrial and Engineering Chemistry.* 2018;58:155-162

12. Sanchez-Prado L, Llompарт M, Lores M, García-Jares C, Bayona JM, Cela R. Monitoring the photochemical degradation of triclosan in wastewater by UV light and sunlight using solid-phase microextraction. *Chemosphere*. 2006;65(8):1338-1347
13. Chen X, Richard J, Liu Y, Dopp E, Tuerk J, Bester K. Ozonation products of triclosan in advanced wastewater treatment. *Water Research*. 2012;46(7):2247-2256
14. Kim J, Yi B, Go R, Hwang K, Nam K, Choi K. Methoxychlor and triclosan stimulates ovarian cancer growth by regulating cell cycle-and apoptosis-related genes via an estrogen receptor-dependent pathway. *Environ Toxicol Pharmacol*. 2014;37(3):1264-1274
15. Marotta E, Ceriani E, Shapoval V, Schiorlin M, Ceretta C, Rea M, Paradisi C. Characterization of plasma-induced phenol advanced oxidation process in a DBD reactor. *Eur Phys J Appl Phys*. 2012;55(1):13811
16. Pillonel L. Diploma thesis; swiss federal institute of technology: Zürich. 1999.
17. Marotta E, Schiorlin M, Ren X, Rea M, Paradisi C. Advanced oxidation process for degradation of aqueous phenol in a dielectric barrier discharge reactor. *Plasma Processes Polym*. 2011;8(9):867-875.
18. Marotta E, Ceriani E, Schiorlin M, Ceretta C, Paradisi C. Comparison of the rates of phenol advanced oxidation in deionized and tap water within a dielectric barrier discharge reactor. *Water Res*. 2012;46(19):6239-6246.
19. Latch DE, Packer JL, Stender BL, VanOverbeke J, Arnold WA, McNeill K. Aqueous photochemistry of triclosan: Formation of 2, 4-dichlorophenol, 2, 8-dichlorodibenzo-p-dioxin, and oligomerization products. *Environmental Toxicology and Chemistry*. 2005;24(3):517-525.
20. Canosa P, Morales S, Rodriguez I, Rubi E, Cela R, Gomez M. Aquatic degradation of triclosan and formation of toxic chlorophenols in presence of low concentrations of free chlorine. *Analytical and bioanalytical chemistry*. 2005;383(7-8):1119-1126.
21. Xin L, Sun Y, Feng J, Wang J, He D. Degradation of triclosan in aqueous solution by dielectric barrier discharge plasma combined with activated carbon fibers. *Chemosphere*. 2016;144(Supplement C):855-863
22. Ceriani E, Marotta E, Shapoval V, Favaro G, Paradisi C. Complete mineralization of organic pollutants in water by treatment with air non-thermal plasma. *Chemical Engineering Journal*. 2017
23. Rahman MF, Peldszus S, Anderson WB. Behaviour and fate of perfluoroalkyl and polyfluoroalkyl substances (PFASs) in drinking water treatment: A review. *Water Res*. 2014;50:318-340.
24. Switzerland: EU regulates PFOA and related substances under REACH. *TendersInfo News*. Jun 27, 2017.

25. COMMISSION REGULATION (EU) 2017/1000 Registration, evaluation, authorisation and restriction of chemicals (REACH) as regards perfluorooctanoic acid (PFOA), its salts and PFOA-related substances . 2017.
26. Hayashi R, Obo H, Takeuchi N, Yasuoka K. Decomposition of perfluorinated compounds in water by DC plasma within oxygen bubbles. *Electrical Engineering in Japan*. 2015;190(3):9-16.
27. Slater RC, Douglas-Hamilton DH. Electron-beam-initiated destruction of low concentrations of vinyl chloride in carrier gases. - *Journal of Applied Physics*. 1981(- 9):5820
28. Bosi FJ, Tampieri F, Marotta E, Bertani R, Pavarin D, Paradisi C. Characterization and comparative evaluation of two atmospheric plasma sources for water treatment. *Plasma Processes and Polymers*. 2017. doi:10.1002/ppap.201700130
29. Von Gunten U. Ozonation of drinking water: Part I. oxidation kinetics and product formation. *Water Res*. 2003;37(7):1443-1467.
30. Takeuchi N, Oishi R, Kitagawa Y, Yasuoka K. Adsorption and efficient decomposition of perfluoro compounds at plasma–water interface. *IEEE Trans Plasma Sci*. 2011;39(12):3358-3363.
31. Sansotera M, Persico F, Rizzi V, et al. The effect of oxygen in the photocatalytic oxidation pathways of perfluorooctanoic acid. *J Fluorine Chem*. 2015;179:159-168.
32. Nani L. Caratterizzazione di un sistema al plasma per l'ossidazione avanzata di inquinanti organici nelle acque alimentato da diversi regimi di scarica. ; 2016.
33. Yasuoka K, Sasaki K, Hayashi R. An energy-efficient process for decomposing perfluorooctanoic and perfluorooctane sulfonic acids using dc plasmas generated within gas bubbles. *Plasma Sources Sci Technol*. 2011;20(3):034009.
34. Herron JT, Green DS. Chemical kinetics database and predictive schemes for nonthermal humid air plasma chemistry. part II. neutral species reactions. *Plasma Chemistry and Plasma Processing*. 2001.
35. Kogelschatz U. Dielectric-barrier discharges: Their history, discharge physics, and industrial applications. *Plasma Chem Plasma Process*. 2003;23(1):1-46

## Chapter 6-Removal of persistent organic pollutants from water using a newly developed atmospheric plasma reactor

Francesco Tampieri<sup>1</sup>, Agata Giardina<sup>1</sup>, Franco Javier Bosi<sup>2</sup>, Alice Pavanello<sup>1</sup>, Ester Marotta<sup>1</sup>, Barbara Zaniol<sup>3</sup>, Gabriele Neretti<sup>4</sup>, Cristina Paradisi<sup>1</sup>

<sup>1</sup>Department of Chemical Sciences, University of Padova, Via Marzolo 1, 35131 Padova, Italy

E-mail: ester.marotta@unipd.it

<sup>2</sup>Department of Industrial Engineering, University of Padova, Via Marzolo 9, 35131 Padova, Italy

<sup>3</sup>Consorzio RFX, corso Stati Uniti 4, 35127 Padova, Italy

<sup>4</sup>Department of Electrical, Electronic and Information Engineering, University of Bologna, Viale del Risorgimento 2, 40136 Bologna, Italy

A new bench-top reactor employing a streamer discharge in air was developed and tested for potential use in an advanced oxidation stage in water treatment processes. The complex heterogeneous system and the ensuing chemical processes were characterized using an integrated approach to map the morphology of the plasma/gas/liquid interface, identify the plasma short-lived excited species, determine the oxidants in solution and monitor the organic pollutants degradation. Three model pollutants were used in these experiments, Rhodamine B, phenol and Metolachlor. The first two are common standards used to evaluate the performance of advanced oxidation processes. Metolachlor is a widely used herbicide listed among the most important recalcitrant emerging organic pollutants. Energy efficiency, kinetics and products of our tests show a good performance of the reactor. Specifically, mineralization appears feasible also in the case of metolachlor.

### 6.1 Introduction

The search for novel and efficient technologies for advanced oxidation processes (AOPs) is warranted by the growing number of identified emerging organic contaminants (EOCs) found in waters and the concern for their ascertained or potential risks for the environment, in particular for the biosphere [1,2]. Non-thermalizing electric discharges have long been exploited to produce ozone *ex-situ*, which is then used, alone or in combination with other AOPs, in strong oxidation treatment steps to degrade recalcitrant organic pollutants [3]. More recent developments use electrical discharges to generate non-thermal plasma in air in near proximity, in contact or within the water to be treated [4,6] This approach benefits from the action of reactive species, present in the discharge zone or in its afterglow, which are much shorter lived and stronger oxidant than ozone. Different types of discharges, electrode

configurations and reactor designs have been developed and tested [7,8] in search for optimal performance in terms of efficiency of removal of the primary pollutant/s and of its/their transformation products (TPs). The strategic role of an air plasma based AOP is thus viewed in the context of an integrated water treatment process, as the stage to achieve the degradation of recalcitrant organic pollutants not necessarily all the way to carbon dioxide but to more easily oxidizable TPs. We have recently reported on the efficient AOP of phenol induced by a streamer discharge in air to form a plasma in contact with the phenol solution [9]. The good results obtained with that first prototype encouraged us to further pursue this approach. Thus, we built a new reactor and electrode assembly with improved design and using only inert materials to avoid possible contamination due to oxidative degradation of reactor parts. This is a stringent requirement in fundamental studies so as to avoid interferences in the quantitative chemical analyses necessary to characterize the new AOP, and besides, it is also necessary in the perspective of large scale developments. In addition, we used two interchangeable solution vessels: Pyrex glass for chemical and electrical measurements and quartz to characterize the plasma by optical emission spectroscopy (OES). This paper reports a description of the reactor and a characterization of the discharge and ensuing reactive species obtained by means of OES and by chemical methods. The reactor was then tested in the treatment of a few representative organic pollutants in water, rhodamine B, phenol and metolachlor. Rhodamine B ([9-(2-carboxyphenyl)-6-diethylamino-3-xanthenylidene]-diethylammonium chloride) is a dye, widely used in the textile, print, dye and food industry [10,12]. Harmful effects of dyes residual in wastewaters have been reported [13-15] so their removal, especially from industrial effluents, is very important for the environment. Since its oxidation is easily monitored by UV-Vis spectroscopy, it was used to optimize experimental conditions such as the air flow, the interelectrode gap and the thickness of the aqueous solution. Phenol was used because it is a widespread organic pollutant and, due to its well-known reactions (rate constants and products) with different reactive oxygen species, sort of a standard for testing and comparing AOPs [16-24]. Finally, we studied the degradation of metolachlor ((RS)-2-Chloro-N-(2-ethyl-6-methyl-phenyl)-N-(1-methoxypropan-2-yl) acetamide), an emerging organic contaminant, [25] also largely diffused in wastewaters [26] but, at best of our knowledge, not yet studied with plasma systems.

## **6.2 Experimental section**

### **6.2.1 Materials**

Rhodamine B (95%), phenol (99%), 2-nitrophenol (98%), 4-nitrophenol (98%), coumarin-3-carboxylic acid (97%), 7-hydroxycoumarin carboxylic acid (98%), potassium indigotrisulfonate, titanium (IV) oxysulfate sulfuric acid solution (27-31%), metolachlor, formic acid (98%) and

acetonitrile (99.9%) were purchased from Sigma Aldrich. Ultrapure grade water (milliQ water) was obtained by filtration of deionized water with a Millipore system. Pure air used in the experiment was a synthetic mixture (80% nitrogen and 20% oxygen) from Air Liquide with specified impurities of H<sub>2</sub>O (< 3 ppm) and of CnHm (< 0.5 ppm).

### 6.2.2 Experimental Apparatus

A schematic and a picture of the plasma reactor are reported in Figure 1. It is made of a Pyrex cylindrical vessel (ID = 4.1 cm, OD = 4.5 cm, h = 6 cm, volume 80 mL ca.) closed by a Teflon cover. A stainless steel tube (ID = 4.0 mm, OD = 6.0 mm), inserted in the reactor along its axis through the top cover, serves as active electrode and as gas input channel. The end part of the tube is flared, reaching an inner diameter of 0.5 mm at its tip, thus injecting gas with higher velocity. The gas outlet port is also placed in the Teflon cover.

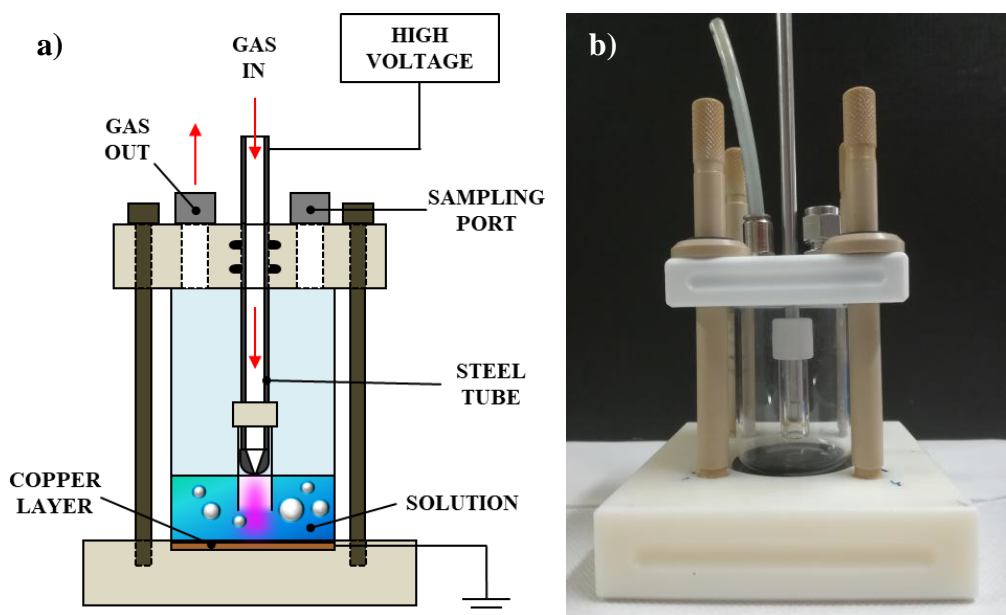


**Figure 1.** Reactor schematics (a) and picture (b).

The tip of the electrode touches the surface of the solution to be treated. The electrode lower part is embedded inside a Pyrex tube partially submerged in the solution (about 6 mm) with the purpose of forcing the gas to bubble within the liquid. As the gas flows in, an air pocket develops between the electrode tip and the liquid, which allows for the ignition of the discharge. The plasma is pushed against the liquid and penetrates it for 1-2 mm. The counter electrode is a thin copper layer in contact with the external surface of the vessel bottom and connected to the ground.

The whole set-up is gas-tight by means of Viton O-rings. The gas exiting from the reactor can be flowed through the cell of a FTIR spectrometer for gas analysis. In the top of the reactor there is also

a sampling port, closed by a Teflon lined septum, used to withdraw solution samples with a syringe without removing the cover. For the OES measurements (see later), the Pyrex vessel and tube were substituted with others with same shape and dimension, but made of quartz. All the materials used to build the reactor (Pyrex, quartz, Teflon, Viton, stainless steel) were selected because they are not attacked by ozone that is formed when the discharge is on.

The electrical excitation is provided by a high voltage electronic transformer (maximum peak voltage 16 kV) that produces a modulated output into the 12-18 kHz frequency range.

The average power consumption was determined by means of voltage-current measurements. The high voltage probe was a Tektronix P6015A (75 MHz bandwidth), whereas the current probe was based on a shunt compression circuit designed as indicated in the literature [27]. The voltage-current signal was recorded by a Tektronix-TDS5032B digital phosphor oscilloscope set at 2 MHz sampling frequency.

During the experiments, a flow of air of 100 mL/min entered the reactor through the high voltage electrode and was bubbled into the solution. To minimize evaporation from the solution, the air was saturated with humidity by passing it through a water bubbler placed before the reactor. The volume of liquid used in the plasma treatment experiments was 15 mL.

### **6.2.3 Schlieren Imaging**

Schlieren images were obtained by a Z-type configuration setup [28]. A tungsten halogen low voltage lamp equipped with a rear reflector was used as light source. The condenser of the optical system was a Schneider-Kreuznach Xenon 40 mm double-Gauss lens with a f/1.9 focal ratio. Two off-axis parabolic mirrors of a diameter of 138 mm and an f/3.5 focal ratio reflected the light beam. Images were detected by a PCO CCD camera, equipped with a super-video-graphics array (SVGA) resolution with a pixel size of  $6 \times 6 \mu\text{m}^2$ . The peak quantum efficiency was 55 % at a wavelength of 380 nm.

### **6.2.4 Emission Spectroscopy**

The spectroscopic system consisted of a PI-Acton spectrometer of 500 mm focal length equipped with a 1800 gr/mm grating and coupled to a PI-Pixis camera of 1340x400 square pixels of 13  $\mu\text{m}$ . With the entrance slit set at 50  $\mu\text{m}$ , the system had a resolution of about 50 pm at 500 nm. An optical head consisting of a fused silica lens of 50 mm focal length and 25 mm diameter focused the plasma light on a 1 mm core optical fibre. The fibre, also made of fused silica, was 5 m long and had the other end attached to the spectrometer entrance slit through an SMA connector. The spectral response of the system was measured from 350 nm to 700 nm using an integrating sphere. Only a relative



intensity calibration was possible, since the small dimensions of the plasma did not fill the entrance f-number. The instrument function was measured with a Cd lamp, and resulted fully Gaussian with a full width at half maximum (fwhm) of 3.5 pixels. The lack of matching on f-numbers led to an effectively smaller fwhm. Its true value of 2.9 pixels, was found analyzing the rotational transitions of N<sub>2</sub> spectra. The optical head was placed in front of the plasma source exit, looking directly on it. The weak plasma emission needed integration times ranging from 20 to 40 s.

### **6.2.5 Determination of Species produced by Plasma in Solution**

The pH of the solutions, after plasma treatment, was measured using a Mettler-Toledo S220 pH-meter equipped with an InLab Versatile Pro electrode.

The concentration of nitrate ions was measured by ion chromatography using a Dionex-ICS-900 instrument equipped with a Dionex IonPac AS22 IC Column after proper calibration with standard solution of NaNO<sub>3</sub>. 4.5 mM sodium carbonate (Na<sub>2</sub>CO<sub>3</sub>) and 1.4 mM sodium bicarbonate (NaHCO<sub>3</sub>) were used as the effluent at a flow rate of 1.2 mL/min for 15 min.

The concentration of ozone and hydrogen peroxide in solution were determined by the indigo [29] and titanium (IV) sulfate [30] methods, respectively. The rate of formation of hydroxyl radical was determined using coumarin-3-carboxylic acid as fluorescent probe [31]. All the procedures are described in detail in [9, 32].

### **6.2.6 Treatment of Organic Pollutants**

Solutions of the organic pollutant (rhodamine B, phenol, metolachlor) were prepared in milliQ water. We treated aliquots of 15 mL of solution for different times with a gas flow rate of 100 mL/min. Each point in the figures that have been reported in the Results and Discussion session corresponds to a single experiment. All the experiments were repeated at least twice, in order to verify the reproducibility.

The solutions of rhodamine B were analyzed with a Varian Cary 50 UV-Vis spectrophotometer running WinUV software. Absorbance data at 554 nm were collected and used to monitor the dye degradation profile.

The solutions of phenol were analyzed by HPLC/UV-Vis analysis (Shimadzu LC10AD pump with Shimadzu SPD-10A UV-Vis detector). An Agilent Zorbax Sb-Aq column (4.6 x 150 mm 3.5-Micron) was used with an eluent composed of 80% aqueous phosphate buffer (20 mM, pH = 2) and 20% acetonitrile. The elution was followed at 270 nm. The same analyses also allowed for the identification and determination of nitrophenols, which can form as undesired byproducts in air plasma treatment of phenol [9,33].

The solutions of metolachlor were analyzed by HPLC (Thermo Scientific Products instrument with P2000 pump and UV6000LP Diode array detector) at 270 nm. A Phenomenex Kinetex C18 column (5u C18 100A, 150x4.6 mm) was used and a mobile phase composed of water with 0.1% of formic acid (eluent A) and acetonitrile with 0.1% of formic acid (eluent B). The LC gradient for the separation was: from 0 to 25 min, a linear increase of B from 5 to 95. The initial conditions were re-established in 5 min.

Standard solutions of rhodamine B, phenol, nitrophenols and metolachlor prepared at known concentrations were used for calibration.

The efficiency of degradation of the pollutants in the plasma treatment was evaluated using two parameters: the decay constant  $k$ , obtained by interpolation of experimental data using equation 6.1, and  $G_{50}$  [7] (equation 6.2), the mass of pollutant converted divided by the energy required to reduce its quantity by one half,

$$C(t) = C_0 \cdot e^{-k \cdot t} \quad (6.1a)$$

$$C(E) = C_0 \cdot e^{-k \cdot E} \quad (6.1b)$$

$$G_{50}(g/kWh) = 1.8 \cdot 10^6 \frac{C_0(mol/L) \cdot V(L) \cdot MM(g/mol)}{P(W) \cdot t_{1/2}(s)} \quad (6.2)$$

where  $C_0$  and  $C$  are, respectively, the initial and residual pollutant concentration,  $t$  is the treatment time,  $E$  is the energy input,  $V$  is the volume of the treated solution,  $MM$  is the molar mass of the pollutant,  $P$  is the mean power of the reactor and  $t_{1/2}$  is the time required for the pollutant to achieve 50% conversion.

To measure the extent of mineralization achieved in the air plasma AOP, the solutions that were subjected to the longest treatment times were also analyzed for their total carbon content using a Shimadzu TOC -VCSN instrument, equipped with an autosampler and an automatic diluter. The instrument was calibrated using standard solutions of potassium hydrogen phthalate automatically diluted in the range of interest. Some constant carbon release was found and quantified in the reactor and was subtracted to the experimental measurements.

## 6.3 Results and discussion

### 6.3.1 Characterization of the reactor

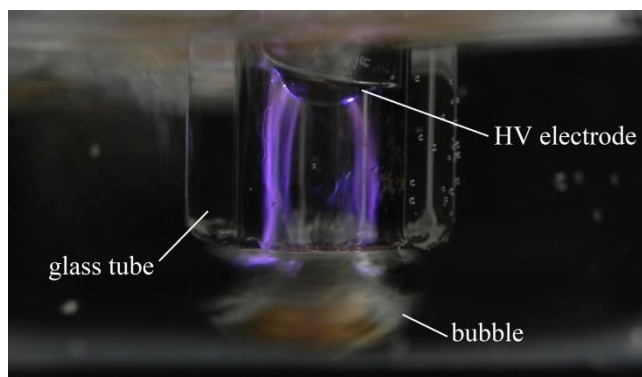


**Figure 2.** Photograph of the reactor during the generation of the discharge. Exposure time 125 ms.

Figure 2 reports a high resolution image of the reactor with the discharge on. The hemispheric tip of the HV electrode is seen inside the external protecting glass tube. An air bubble is coming out from the glass tube outlet immersed in the water. Several plasma streamers are clearly visible in the inner part of the tube. These filaments are produced on the HV electrode surface and then they propagate along the internal surface of the glass tube down to its edge. The approximate length of plasma streamers is about 6 mm.

We performed preliminary experiments using a solution of rhodamine  $1 \cdot 10^{-5}$  M in milliQ water in order to optimize the experimental conditions. Rhodamine B was chosen since its degradation can be easily monitored by means of UV-vis spectroscopy. The best conditions, i.e. those leading to the fastest degradation of the pollutant, were the following: solution volume 15 mL, gas flow rate 100 mL/min, distance between electrodes 13 mm. These conditions were then used in all experiments, unless otherwise stated. The data obtained in the degradation experiment with rhodamine B under these conditions are reported in Figure 3.

Under these conditions complete decomposition of the starting pollutant was achieved within 15 min of treatment. By fitting the data in figure 3 with a first order exponential decay function we obtained the decay constant of rhodamine as  $k_t = (4.6 \pm 0.8) \cdot 10^{-3} \text{ s}^{-1}$ , that, by taking into account for the average power of the reactor (see later), can be express also in terms of energy  $k_E = (7.9 \pm 1.3) \cdot 10^{-4} \text{ J}^{-1}$ . The efficiency parameters relative to this experiment (half life time, decay constant and energy efficiency) are reported in Table 2 (see later).

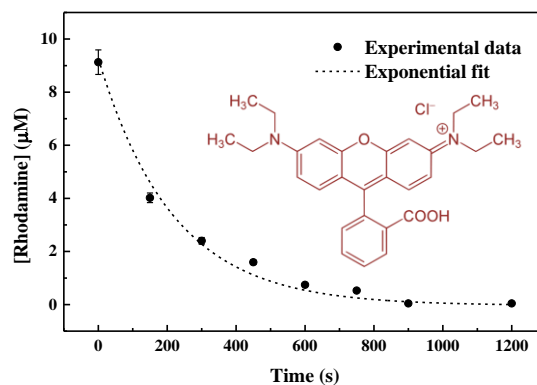


**Figure 3.** Rhodamine B conversion, as a function of treatment time in the plasma reactor. The black dashed lines are the best exponential fit of the experimental data to a first order exponential decay function.

An increase of the solution temperature has been measured, from room temperature up to 50 - 60 °C after 10 minutes of treatment. The measurements were performed after switching off the discharge and opening the reactor, so we expect the solution temperature to reach slightly higher values. This increase in the solution temperature could in principle affect the solubility of some species in solution and also the kinetics of some relevant processes.

Typical voltage and current profiles obtained with the reactor used are shown in Figure 4. The voltage signal is composed by the 50 Hz of the main grid modulated at high frequency (16 kHz) by the electric transformer. The average power of the reactor was estimated by integration of the voltage current signal. Average power was estimated by integration of the current voltage signal at different times during the tests. FFT analysis allowed us to estimate that the error caused by sampling the signal at 2MHz is less than 1%, while that due to the shunt is less than 0.1%. The non uniform - transient nature of the streamer discharge is the only issue to be addressed in order to have an “average power” parameter to characterize the reactor. These fluctuations were observed to be within  $\pm 12\%$  of the average value determined for the power. No larger fluctuations in power were recorded, partly because the number of streamers produced is high enough, partly because the high voltage transformer is equipped with an internal ballast resistor that helps stabilize the discharge. Statistical averages of the different acquisitions showed that the reactor consumes about  $5.9 \pm 0.7$  W. Since, to a first approximation, the power can be assumed constant during our experiments, in the following sections, all results are given as a function of energy rather than as function of time. The energy was obtained by multiplying the treatment time by the average power.

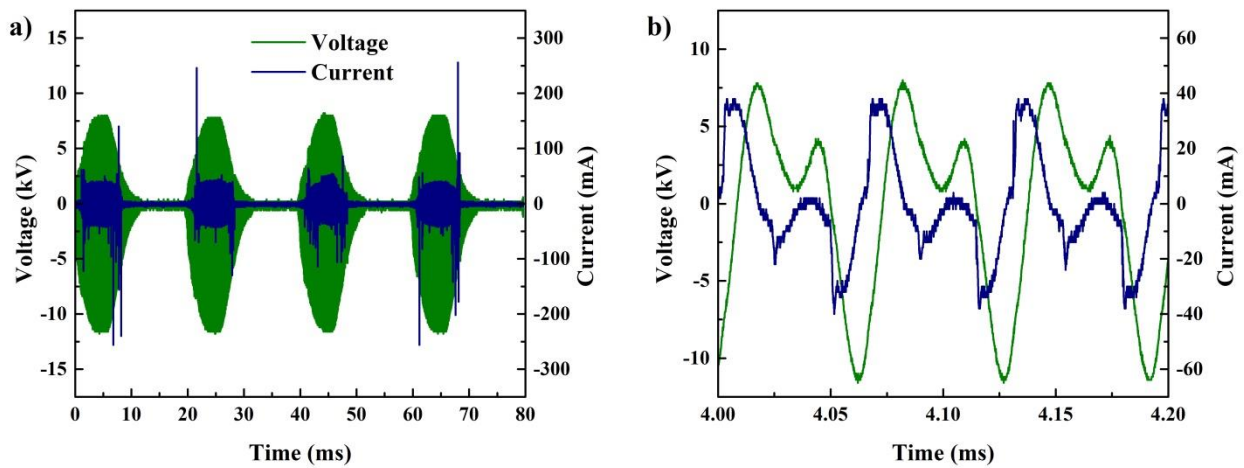


**Figure 4.** Voltage (—) and current (—) oscillograms with different timescales. a) modulation at 50 Hz; b) modulation at 16 kHz.

The influence of plasma generation on the air bubble structure/shape and consequently on the morphology of the air/water interface has been investigated by means of Schlieren imaging. This optical diagnostic is sensitive to refractive index gradients within a transparent medium. Figure 5 reports several images showing the evolution of a bubble without and with plasma. The exposure time was set at 1 ms, with a frame rate of 22 Hz. For clarity, in Figure 5a a reference scale of 1 mm and the outlet portion of the glass tube are depicted. When the discharge is off, the air bubble first increases both in height and width (a, b, c), subsequently it enlarges in the horizontal direction (d), and finally it begins to ascend toward the water surface moving along the outer surface of the glass tube (e).

When the discharge is on, the bubble morphology drastically changes. In Figure 5f, a protrusion is clearly visible on the bubble surface. This protrusion is associated with the formation of a streamer within the glass tube, a phenomenon that is able to locally deposit a considerable amount of thermal energy in very short times (streamers typically last for tens of nanoseconds). This fast deposition of thermal energy leads to the generation of strong thermal gradients propagating from the inner part of the air bubble into the water, following the plasma streamer propagation path. Figure 5g shows the air bubble expanding against the hot water region previously warmed up by the plasma filament. In Figure 5h a new plasma streamer is produced. The hot water region still expands in the vertical direction after several tens of milliseconds (Figure 5i). When the bubble is moving up toward the water surface, the hot water region generated by the second streamer is still clearly visible (Figure 5l). New protrusions due to the formation of new streamers are also seen.

The presence of plasma strongly modifies the bubble morphology and consequently the interface between air and water. The presence of hot protrusions is consistent with the relatively high translational temperatures associated with plasma filaments (see later).

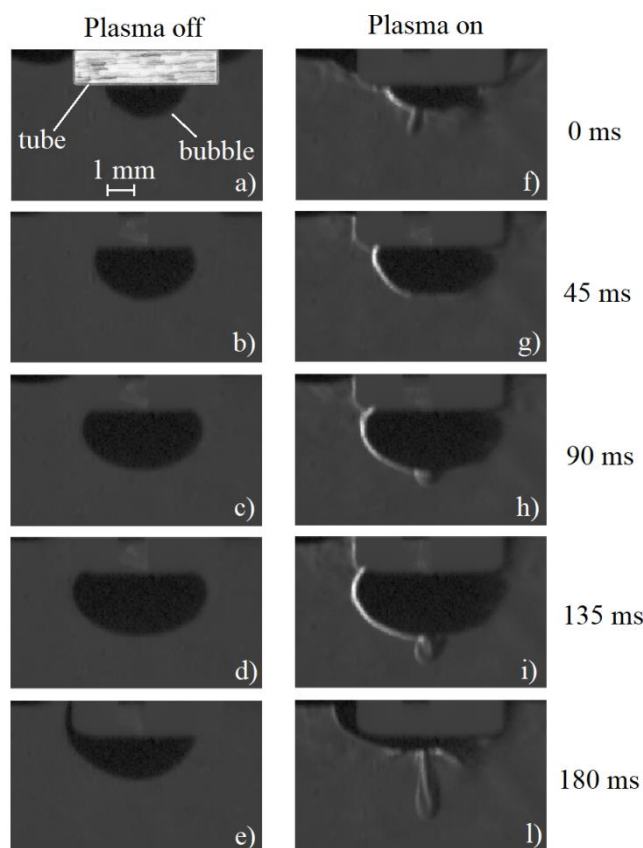


**Figure 5.** Time evolution of a bubble with the discharge off (a, b, c, d, e) and on (f, g, h, i, l).

The entire spectrum between 300 nm and 800 nm has been reconstructed by assembling together multiple acquisitions of different wavelength regions (see Figure 6a). The spectrum shows the  $N_2$  rovibrational lines of the Second Positive System (SPS), the  $N_2^+$  lines of the First Negative System (FNS), the OH band around 300 nm, then oxygen triplet at 777 nm, and the  $H_\alpha$  and  $H_\beta$  lines. No filter was used to prevent the second diffraction order to overlap to the first one above 600 nm. In this way it was possible to collect OH and  $N_2$  bands with a greater dispersion, which was most useful for determining the rotational temperatures of the two molecular species. The second order OH band at 306.357 nm ( $A^2\Sigma, v = 0 \rightarrow X^2\Pi, v = 0$ ) has been simulated for different rotational temperatures.<sup>[34]</sup> By minimizing the integral of the squared differences between the simulations and the experimental spectrum a rotational temperature of  $2660 \pm 250$  K was derived (Figure 6b).

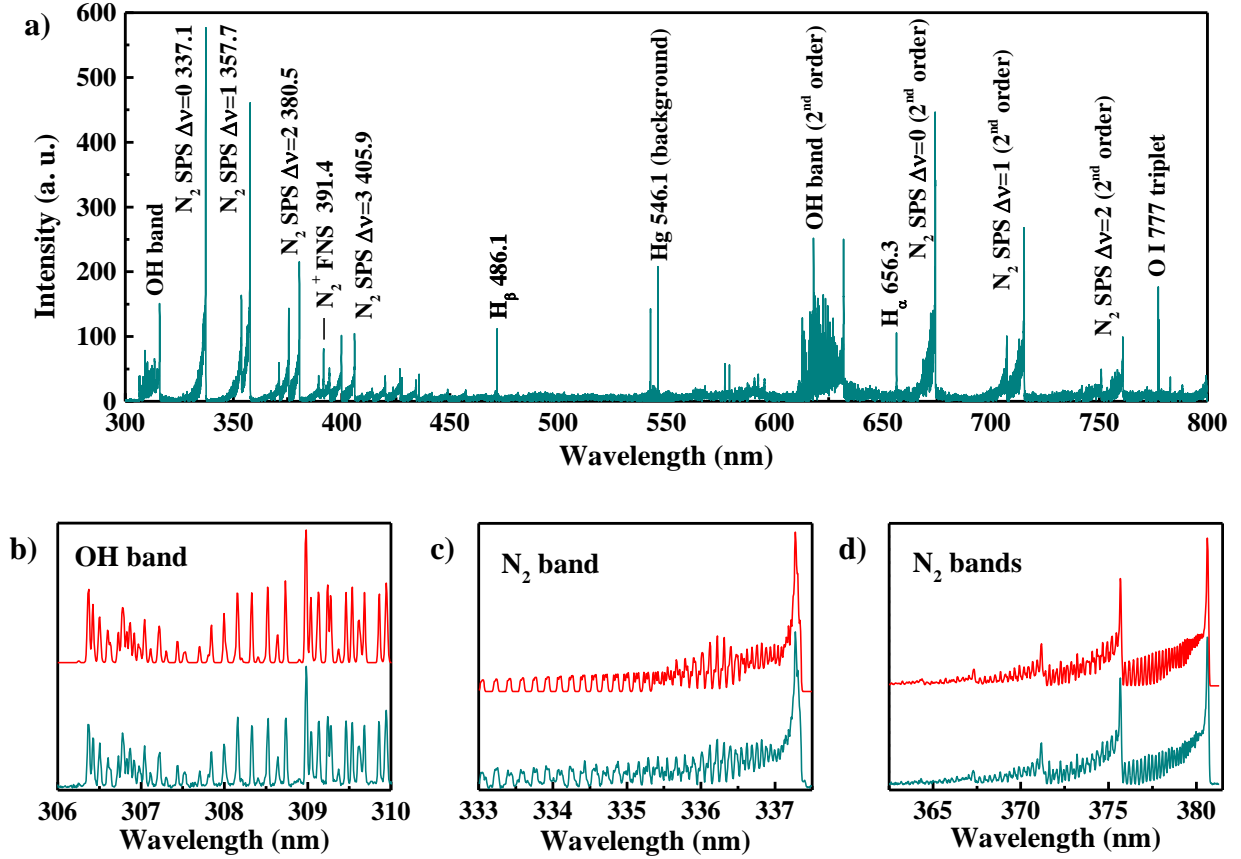


**Figure 6.** a) Typical raw spectrum acquired between 300 and 800 nm. The main emission lines have been identified. b) Second order OH band ( $A^2\Sigma, v = 0 \rightarrow X^2\Pi, v = 0$ ). c) Second order  $N_2$  band ( $C^3\Pi_u, v = 0 \rightarrow B^3\Pi_g$ ) with  $\Delta v = 0$ . d) Second order  $N_2$  band ( $C^3\Pi_u, v = 0 \rightarrow B^3\Pi_g$ ) with  $\Delta v = 2$ . The simulated spectra are also reported (red line).

The same procedure was applied to the second order  $N_2$  band at 337.1 nm ( $C^3\Pi_u, v = 0 \rightarrow B^3\Pi_g, v = 0$ ), using the atomic data reported in [35] for its simulation (Figure 6c). A rotational temperature of  $1700 \pm 150$  K was thus obtained. The rotational temperatures of the two molecular species are quite different. This difference has been observed already in literature for similar systems and in a 2014 review Bruggeman indicates the rotational temperature of  $N_2$  as a better estimation of the gas temperature, with respect to that obtained from OH radicals that can be substantially overestimated.<sup>[36]</sup> The vibrational temperature can be measured from the  $N_2$  emissions corresponding to  $C^3\Pi_u \rightarrow B^3\Pi_g$  transitions with  $\Delta v = 2$ , under the hypothesis that the vibrational states population follows a Boltzmann distribution (Figure 6d). Assuming a rotational temperature of 1700 K, the 5 rotational bands between 360 and 380 nm were simulated and their relative intensities found by comparison with the experimental data. This procedure yielded a vibrational temperature, rescaled to the ground state, of about  $1500 \pm 200$  K, so compatible with the rotational temperature of the same molecules. The electron temperature deduced by comparing the intensity ratio of first negative  $N_2^+$  band at 391.4 nm and second positive  $N_2$  band at 394.3 nm, in the hypothesis of being dominated by electron-impact

excitation [37] was of  $1.7 \pm 0.5$  eV. Finally, the method reported in [38] was applied to the width of  $H_\alpha$  line, finding an electron density value of about  $6 \cdot 10^{20} \text{ m}^{-3}$ . Table 1 collects the main results obtained in plasma characterization by OES.

**Table 1.** Main parameters obtained by OES analysis of the plasma.

Parameter	Value
Electron density ( $\text{m}^{-3}$ )	$(6 \pm 2)10^{20}$
Ionization degree	$10^{-5}$
$T_e$ (eV)	$1.7 \pm 0.5$
$T_{\text{rot\_OH}}$ (K)	$2660 \pm 250$
$T_{\text{rot\_N}_2}$ (K)	$1700 \pm 150$
$T_{\text{vib}}$ (K)	$1500 \pm 200$

The performance of a plasma reactor in the degradation of persistent organic pollutants is mainly due to its efficiency in the production of reactive oxygen and nitrogen species. Figure 7 collects the results of chemical determinations of the species generated by plasma treatment in solution. First we observed a lowering of the pH of the solution by increasing the treatment time (Figure 7a) and a corresponding increase of the concentration of the nitrate ion (Figure 7b). The lowering of the pH is due to the formation of nitrogen oxides that by further reactions form nitric acid that dissociates in solution.<sup>[39]</sup> The concentrations of  $\text{NO}_3^-$  and  $\text{H}_3\text{O}^+$  are in agreement (about 2-4 mM after 30 min of treatment), meaning that the production of nitric acid is the main source of the pH decrease in our experimental setup.

We measured the concentration of ozone and hydrogen peroxide in the liquid phase (Figures 7c and 7d) using the procedure reported by Bader and Eisenberg respectively [29,30]. Both species accumulate in water during the first part of the treatment, reach a maximum and are then consumed. These experimental data can be reproduced using a model typical of a transient species

$$C(E) = C_0 k_1 \frac{e^{-k_1 E} - e^{-k_2 E}}{k_2 - k_1} \quad (6.3)$$



where  $k_1$  and  $k_2$  are the formation and decomposition constant respectively, assuming simple unimolecular reactions. The maximum concentration of ozone in solution was about 14  $\mu\text{M}$ , after 300 s of treatment, corresponding to an energy input of 2 kJ. Hydrogen peroxide instead reached a maximum concentration of 0.5 mM after 800 s of treatment, corresponding to an energy of 4.5 kJ. The profiles of the two species are similar to those observed previously with a similar reactor [9]. Both species are produced and accumulate in solution during the first stages of treatment, then, other reactions, that consume them, prevail. Ozone is decomposed, in acidic solutions, by reacting with OH radicals and  $\text{NO}_2^-$  [40]; similarly, also the reaction of hydrogen peroxide with  $\text{NO}_2^-$  ions is favorite under acidic conditions [41].

The rate of formation of OH radicals in solution was measured following the procedure by Newton [31]. The assay uses coumarin-3-carboxylic acid (CCA), a chemical probe that reacts with OH radicals to give a fluorescent product 7-hydroxycoumarin carboxylic acid (7-CCA-OH). In Figure 7e the concentrations of 7-CCA-OH is reported as a function of the treatment energy. It grows linearly with energy in the first part of the graph and then reaches a plateau. This trend is due to two causes: CCA is decomposed significantly during plasma treatment, for the longest treatment times (Figure 7f), and correspondingly, 7-CCA-OH could become competitive in the reaction with OH radicals. By fitting linearly the first points, corresponding to a conversion of CCA of less than 20% (Figure 7f), it is possible to obtain the rate of formation of the hydroxylated product. With our reactor we obtained  $v_{7\text{-CCA-OH}} = (15.5 \pm 0.6) \mu\text{M kJ}^{-1}$ . Knowing that the yield of the reaction of formation of 7-CCA-OH is 4.7% [31] and assuming that 7-CCA-OH is not decomposed during the experiment (at least in the time/energy interval corresponding to the linear part of Figure 7e), we can calculate the rate of formation of OH radical. The hypothesis that the hydroxylated product is not significantly decomposed during the treatment is reasonable, since it is present in solution with a concentration at least 1000 times lower than that of its precursor (about  $10^{-3}$  M), so it cannot compete with it for the reaction with OH radicals. The value obtained for the rate of formation of OH radical is  $v_{\text{OH}} = (330 \pm 13) \mu\text{M kJ}^{-1}$ , a value quite high if compared with other reactors designed for water treatment [16].

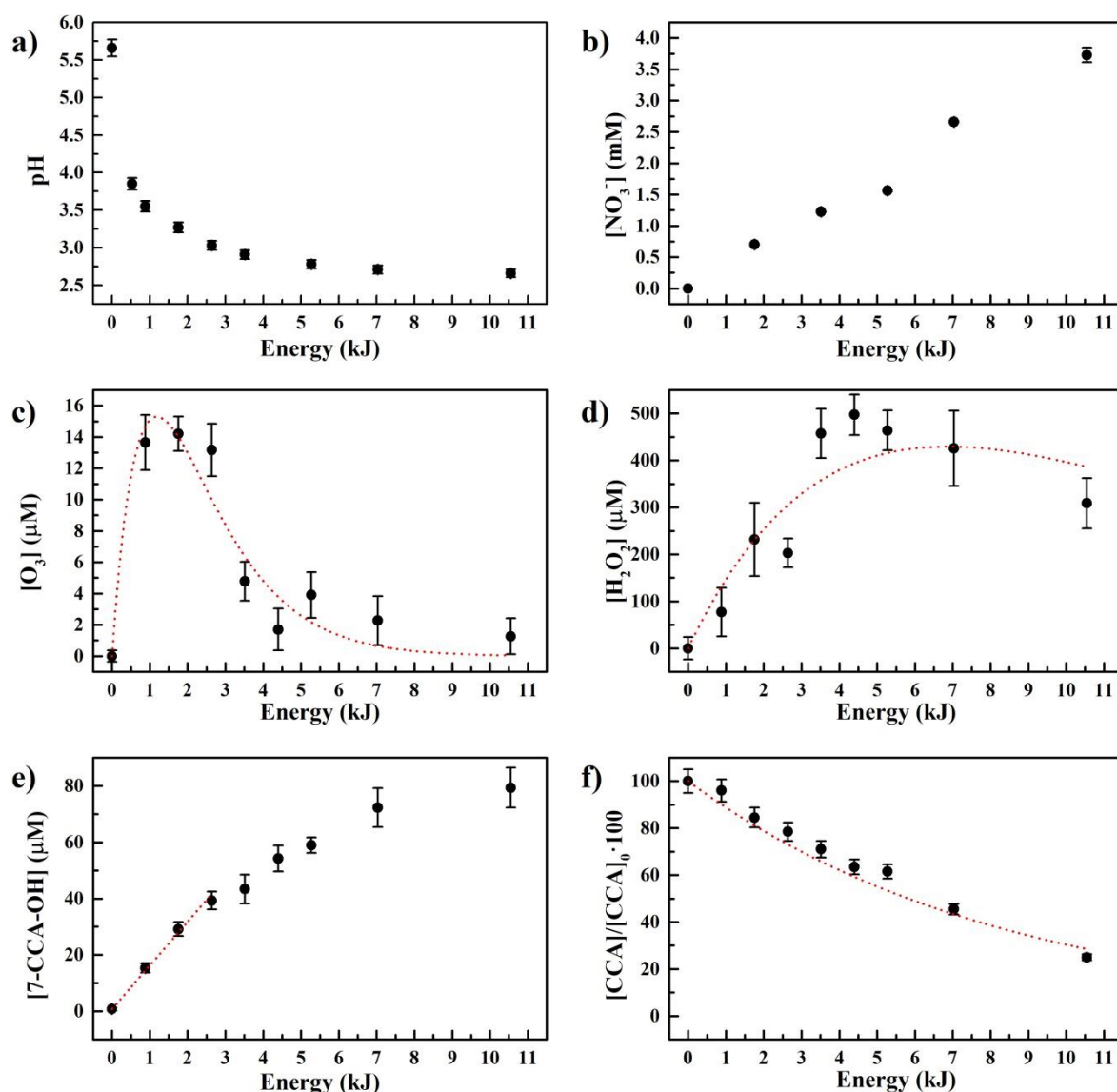


**Figure 7.** Species produced by plasma treatment as function of the energy of the process. a) pH; b) concentration of nitrate ions; c) concentration of ozone in solution; d) concentration of hydrogen peroxide; e) concentration of 7-CCA-OH; f) normalized concentration of CCA. The red dashed lines are the interpolations of the experimental data using eq 3 (c and d) a straight line (e) and eq 1b (f).

### 6.3.2 Removal of persistent organic pollutants

We tested the performance of our reactor by studying the oxidation of two representative persistent organic pollutants, phenol and metolachlor. Figure 8 summarizes the results of three experiments carried out with phenol at three different initial concentrations,  $1 \cdot 10^{-4}$ ,  $5 \cdot 10^{-4}$  and  $5 \cdot 10^{-5}$  M, respectively. The plots show the residual concentration of phenol as function of the energy. In the two more dilute solutions complete removal of phenol was achieved within 30 minutes of treatment; for the higher concentration, after 30 min, we observed less than 10% of phenol left in solution. By fitting the data with a first order exponential equation (eq. 1) we obtained the half life time and the

decay constant relative to each experiment. We also computed the energy efficiency of the process (eq. 6.2). These data are collected in Table 2. It is seen, from Figure 8 and from the data in the table, that the decay constant depends on the initial concentration of the pollutant, the half-life time being 470, 230 and 170 s for initial concentrations of  $5 \cdot 10^{-4}$ ,  $1 \cdot 10^{-4}$  and  $5 \cdot 10^{-5}$  M, respectively. Our data are consistent with previous results reporting an inverse dependence of the decay constant in plasma treatment on the pollutants initial concentration [17]. On the other hand,  $G_{50}$ , the energy efficiency increases, by increasing the pollutant initial concentration.

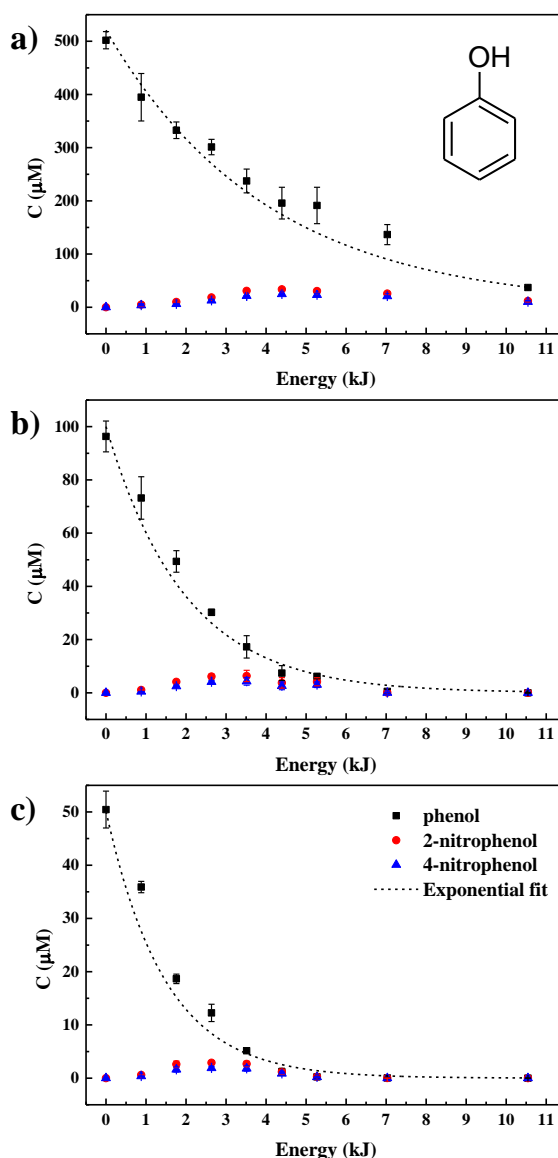


**Figure 8.** Concentration of phenol (■), 2-nitrophenol (●) and 4-nitrophenol (▲) as a function of energy in treatment of phenol in milliQ water with three initial concentrations: a)  $5 \cdot 10^{-4}$  M; b)  $1 \cdot 10^{-4}$  M; c)  $5 \cdot 10^{-5}$  M. The black dashed lines are the best fit of the experimental data to a first order exponential decay function.

This behavior is also consistent with results reported and discussed earlier [9,21,22,42]. The dependence of  $G_{50}$  on  $C_0$  is not easy to anticipate considering that also  $t_{1/2}$ , which appears in the denominator of eq. 2, depends on  $C_0$ .

It is known from the literature that plasma treatment of phenol in air generates 2- and 4-nitrophenol as byproducts due to side reactions of  $\text{NO}_x$  [9,33]. Nitrophenols are more toxic and persistent than phenol itself [33,43,44], so their formation is not desirable. We therefore searched for nitrophenols and monitored their formation and decay during the plasma treatment of phenol. Thus, for each experiment reported in Figure 8 we also show the concentration profiles of 2 and 4-nitrophenol. The total amount of nitrophenols and their rate of formation and decay observed in our experiments depend on the initial concentration of phenol. Specifically, in experiments with phenol at  $C_0$  equal to  $5 \cdot 10^{-4}$ ,  $1 \cdot 10^{-4}$  and  $5 \cdot 10^{-5}$  M maximum nitrophenols concentrations of, globally, 60, 10 and 5  $\mu\text{M}$  were reached in 600, 450 and 300 s of treatment, respectively. Almost complete removal of nitrophenols from the solution was however achieved in all cases within the first 30 min of treatment.

The extent of mineralization achieved during the plasma treatment was also determined, by measuring the total organic carbon (TOC) in phenol solutions before treatment and after 30 minutes of treatment. The data are collected in Table 2. For the most concentrated solution ( $5 \cdot 10^{-4}$  M) a mineralization yield of  $(31 \pm 2)\%$  was obtained. For the less concentrated phenol solutions higher mineralization yields were achieved, notably  $(50 \pm 5)\%$  for the  $1 \cdot 10^{-4}$  M solution and  $(59 \pm 10)\%$  for the  $5 \cdot 10^{-5}$  M one. The high experimental errors associated with the mineralization yield of the more dilute solutions are due to sensitivity limits of the TOC analyzer.

**Table 2.** Half-life time ( $t_{1/2}$ ), decay constant ( $k_E$ ), energy efficiency ( $G_{50}$ ) and degree of mineralization achieved in 30 min plasma treatment of pollutants solutions in milliQ water.

<b>Pollutant</b>	<b><math>t_{1/2}</math> (s)</b>	<b><math>k_E</math> (<math>\text{J}^{-1}</math>)</b>	<b><math>G_{50}</math> (g kWh<sup>-1</sup>)</b>	<b>%Mineralization</b>
Rhodamine B $1 \cdot 10^{-5}$ M	$150 \pm 20$	$(7.9 \pm 1.3) \cdot 10^{-4}$	$0.14 \pm 0.07$	n. d.
Phenol $5 \cdot 10^{-4}$ M	$471 \pm 9$	$(2.49 \pm 0.05) \cdot 10^{-4}$	$0.48 \pm 0.08$	$31 \pm 2$
Phenol $1 \cdot 10^{-4}$ M	$230 \pm 20$	$(5.2 \pm 0.4) \cdot 10^{-4}$	$0.19 \pm 0.06$	$50 \pm 5$
Phenol $5 \cdot 10^{-5}$ M	$170 \pm 10$	$(6.9 \pm 0.6) \cdot 10^{-4}$	$0.13 \pm 0.05$	$59 \pm 10$
Metolachlor $1 \cdot 10^{-4}$ M	$150 \pm 20$	$(7.7 \pm 1.2) \cdot 10^{-4}$	$0.9 \pm 0.3$	$20 \pm 3$

The results of plasma treatment of a solution of metolachlor with initial concentration  $1 \cdot 10^{-4}$  M are reported in Figure 9 and in Table 2. The rate of degradation of this pollutant is quite fast, with a half-life time of about 150 s, resulting in complete removal from the solution within 20 minutes of

treatment (Figure 9a). The energy efficiency of this experiment is quite high, especially if compared with those obtained with phenol and rhodamine in this work.

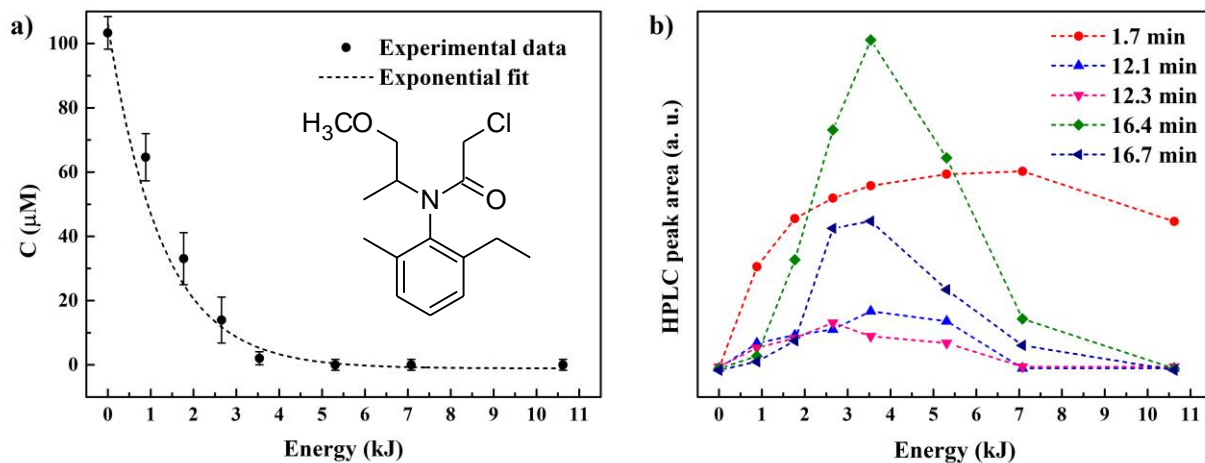


**Figure 9.** a) Decomposition of metolachlor (initial concentration:  $1 \cdot 10^{-4}$  M) in milliQ water. The black dashed line is the best exponential fit of the experimental data to a first order exponential decay function; b) evolution of metolachlor degradation products detected during the treatment. They are labelled according to their retention times. The dashed lines are just a guide for the eye.

From the HPLC-UV-Vis analysis at 270 nm of metolachlor treated samples we detected 5 oxidation products—(Figure 9b), which show the typical profile of reaction intermediates, forming during the first part of the treatment, reaching a maximum and then decomposing at longer treatment times. It is interesting to note that all these intermediates except one were completely removed after 30 minutes of treatment. In the HPLC chromatograms we also observed other unresolved peaks at short retention times, reasonably attributed to small and highly oxidized organic compounds, notably carboxylic acids.

TOC analysis of the metolachlor solution treated in the plasma reactor for 30 min indicated a mineralization yield of 20%. This is a good result, considering the high initial concentration used ( $1 \cdot 10^{-4}$  M), the molecular complexity of metolachlor and the short treatment time. By increasing the treatment time it is reasonable to expect higher oxidation degrees (as observed also by the analysis of the intermediates) and therefore higher mineralization extents.

## 6.4 Conclusions

Building on previous screening of the performance of different discharge systems to bring about advanced oxidation of organic pollutants in water, we have developed a small prototype reactor based on a streamer discharge in air, which had tested as the most promising option in previous work. The

reactor has features which make it suitable for fundamental kinetic and mechanistic studies on the advanced oxidation of emerging pollutants in water. It is built with inert materials to avoid contamination and interferences in the analysis of the advanced oxidation products and has a quartz vessel for optical emission spectroscopy characterization of the plasma. Thus, through a multidisciplinary approach and extensive complementary diagnostics the process was characterized in all of its major components: the plasma short-lived excited species and the ensuing reactive oxidizing species in solution, the morphology of the gas/plasma/liquid interface, the kinetics and efficiency of degradation of organic pollutants and the extent of mineralization achieved in their advanced oxidation.

Using phenol and Rhodamine B, common standards in the comparative evaluation of AOPs, the reactor performed quite satisfactorily with regard to the three major process parameters: duration and energy efficiency of the treatment and extent of mineralization achieved. It also tested positively in the treatment of metolachlor, a recalcitrant EOC (emerging organic contaminant), which was mineralized with a yield of 20% in 30 minutes. We found that in the present reactor the oxidation of metolachlor proceeds via several reaction steps and produces the same reaction intermediates observed when the treatment is carried out in the DBD reactor previously designed and fully investigated in our laboratory [17] The product analysis and the reaction scheme are thus described in detail in a parallel study dealing with that reactor (submitted) [45].

**Acknowledgments.** We thank Stefano Mercanzin and Mauro Meneghetti for the construction of the reactor, University of Padova for financial support (grant CPDA147395/14 - Progetto di Ricerca di Ateneo 2014 and grants CPDR151800 and CPDR152275 - Progetti per Assegni di Ricerca Junior 2015) and COST Action TD1208 for the stimulating environment provided.

**Keywords.** streamer discharge, metolachlor, phenol, reactive oxygen species, water treatment

## References

1. WWAP (United Nations World Water Assessment Programme), *The United Nations World Water Development Report 2017*.
2. L. P. Padhye, *Water Environ. Res.* **2016**, 88, 1619-1636.

3. C. Gottschalk, J. A. Libra, A. Saupe, *Ozonation of water and waste water: A practical guide to understanding ozone and its applications*, John Wiley & Sons, Weinheim, **2009**.
4. P. Bruggeman, M. Kushner, B. Locke, J. Gardeniers, W. Graham, D. Graves, R. Hofman-Caris, D. Maric, J. Reid, E. Ceriani, D. Fernandez Rivas, J. Foster, S. Garrick, Y. Gorbanev, S. Hamaguchi, F. Iza, H. Jablonowski, E. Klimova, J. Kolb, F. Krcma, P. Lukes, Z. Machala, I. Marinov, D. Mariotti, S. Mededovic Thagard, D. Minakata, E. Neyts, J. Pawlat, Z. Lj Petrovic, R. Pflieger, S. Reuter, D. Schram, S. Schröter, M. Shiraiwa, B. Tarabová, P. Tsai, J. Verlet, T. von Woedtke, K. Wilson, K. Yasui, G. Zvereva, *Plasma Sources Sci. Technol.* **2016**, 25, 053002.
5. B. Jiang, J. Zheng, S. Qiu, M. Wu, Q. Zhang, Z. Yan, Q. Xue, *Chem. Eng. J.* **2014**, 236, 348-368.
6. P. Vanraes, A. Y. Nikiforov, C. Leys. *Electrical discharge as water treatment technology for micropollutant decomposition in Plasma Science and Technology - Progress in Physical States and Chemical Reactions* (Ed: Mieno Tetsu) Intech, 2016 DOI: 10.5772/60692.
7. M. A. Malik, *Plasma Chem. Plasma Process.* **2010**, 30, 21-31.
8. G. R. Stratton, C. L. Bellona, F. Dai, T. M. Holsen, S. M. Thagard, *Chem. Eng. J.* **2015**, 273, 543-550.
9. F. J. Bosi, F. Tampieri, E. Marotta, R. Bertani, D. Pavarin, C. Paradisi, *Plasma Process. Polym.*, **2017**, DOI: 10.1002/ppap.201700130.
10. A. Cassano, R. Molinari, M. Romano, E. Drioli, *J. Membr. Sci.* **2001**, 181, 111-126.
11. D. Pokhrel, T. Viraraghavan, *Sci. Total Environ.* **2004**, 333, 37-58.
12. O. Tünay, I. Kabdasli, G. Eremektar, D. Orhon, *Water Sci. Technol.* **1996**, 34, 9-16.
13. R. D. Hood, C. L. Jones, S. Ranganathan, *Teratology* **1989**, 40, 143-150.
14. T. W. Sweatman, R. Seshadri, M. Israel, *Cancer Chemother. Pharmacol.* **1990**, 27, 205-210.
15. B. J. Y. Wuebbles, J. S. Felton, *Environ. Mutagen.* **1985**, 7, 511-522.
16. E. Marotta, M. Schiorlin, X. Ren, M. Rea, C. Paradisi, *Plasma Process. Polym.* **2011**, 8, 867-875.

17. E. Marotta, E. Ceriani, V. Shapoval, M. Schiorlin, C. Ceretta, M. Rea, C. Paradisi, *Eur. Phys. J. Appl. Phys.* **2011**, *55*, 13811.
18. E. Marotta, E. Ceriani, M. Schiorlin, C. Ceretta, C. Paradisi, *Water Res.* **2012**, *46*, 6239-6246.
19. E. Bobkova, E. Ivanova, R. Nevedomyi, A. Sungurova, *High Energy Chem.* **2014**, *48*, 346-349.
20. W. Hoeben, E. Van Veldhuizen, W. Rutgers, C. Cramers, G. Kroesen, *Plasma Sources Sci. Technol.* **2000**, *9*, 361.
21. N. Sano, T. Kawashima, J. Fujikawa, T. Fujimoto, T. Kitai, T. Kanki, A. Toyoda, *Ind. Eng. Chem. Res.* **2002**, *41*, 5906-5911.
22. N. Sano, Y. Yamane, Y. Hori, T. Akatsuka, H. Tamon, *Ind. Eng. Chem. Res.* **2011**, *50*, 9901-9909.
23. B. Sun, M. Sato, J. Clements, *Environ. Sci. Technol.* **2000**, *34*, 509-513.
24. L. Wang, X. Jiang, *J. Hazard. Mater.* **2009**, *161*, 926-932.
25. C. D. Tomlin, *The pesticide manual: a world compendium.*, British Crop Production Council **2009**.
26. M. Köck-Schulmeyer, M. Villagrasa, M. López de Alda, R. Céspedes-Sánchez, F. Ventura, D. Barceló, *Sci. Total Environ.* **2013**, *458-460*, 466-476.
27. D. Ashpis, M. Laun, E. Griebeler. *50th AIAA Aerospace Sciences Meeting Including the New Horizons Forum and Aerospace Exposition* **2012** 823.
28. G. Neretti, A. Cristofolini, C. A. Borghi, *J. Appl. Phys.* **2014**, *115*, 163304.
29. H. Bader, J. Hoigné, *Water. Res.* **1981**, *15*, 449-456.
30. G. Eisenberg, *Ind. Eng. Chem.* **1943**, *15*, 327-328.
31. G. L. Newton, J. R. Milligan, *Radiat. Phys. Chem.* **2006**, *75*, 473-478.
32. G. Neretti, F. Tampieri, C. A. Borghi, P. Brun, R. Cavazzana, L. Cordaro, C. Paradisi, E. Marotta, P. Seri, M. Taglioli, B. Zaniol, M. Zuin, E. Martines, submitted for publication.
33. E. Ceriani, E. Marotta, V. Shapoval, G. Favaro, C. Paradisi, submitted for publication.



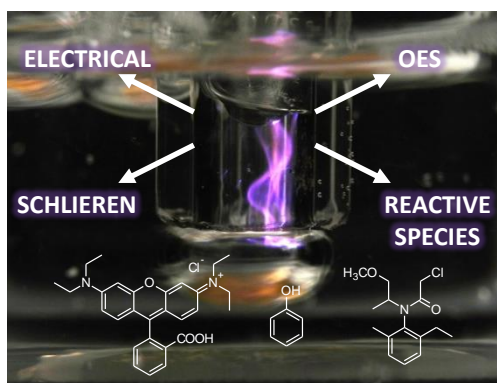
34. C. De Izarra, *J. Phys. D* **2000**, *33*, 1697-1704.
35. G. Hartmann, P. C. Johnson, *J. Phys. B: At. Mol. B* **1978**, *11*, 1597-1612.
36. P. J. Bruggeman, N. Sadeghi, D. C. Schram, V. Linss, *Plasma Sources Sci. Technol.* **2014**, *23*, 023001.
37. N. Britun, M. Gaillard, A. Richard, Y. M. Kim, K. S. Kim, J. G. Han, *J. Phys. D: Appl. Phys.* **2007**, *40*, 1022.
38. N. Konjević, M. Ivković, N. Sakan, *Spectrochim. Acta, Part B*, **2012**, *76*, 16-26.
39. S. N. Pandis, J. H. Seinfeld, *J. Geophys. Res.* **1989**, *94*, 1105-1126.
40. R. Flyunt, A. Leitzke, G. Mark, E. Mvula, E. Reisz, R. Schick, C. von Sonntag, *J. Phys. Chem. B* **2003**, *107*, 7242-7253.
41. B. R. Locke, K. Shih, *Plasma Sources Sci. Technol.* **2011**, *20*, 034006.
42. P. M. K. Reddy, B. R. Raju, J. Karuppiyah, E. L. Reddy, C. Subrahmanyam, *Chem. Eng. J.* **2013**, *217*, 41-47.
43. J. Kiwi, C. Pulgarin, P. Peringer, *Appl. Catal. B Environ.* **1994**, *3*, 335-350.
44. J. Michałowicz, W. Duda, *Polish J. Environ. Stud.* **2007**, *16*, 347-362.
45. A. Giardina, E. Marotta, C. Paradisi, submitted for publication.

## Graphical Abstract

### Removal of persistent organic pollutants from water using a newly developed atmospheric plasma reactor

Francesco Tampieri, Agata Giardina, Franco Javier Bosi, Alice Pavanello, Ester Marotta,\* Barbara Zaniol, Gabriele Neretti, Cristina Paradisi

**A new reactor employing a streamer discharge in air was developed and tested for potential use in water treatment processes.** The system was characterized using an integrated approach to: map the morphology of the plasma/gas/liquid interface, identify the short-lived excited species, determine the oxidants in solution and monitor the organic pollutants degradation. Three model pollutants were used in these experiments, Rhodamine B, phenol and Metolachlor.

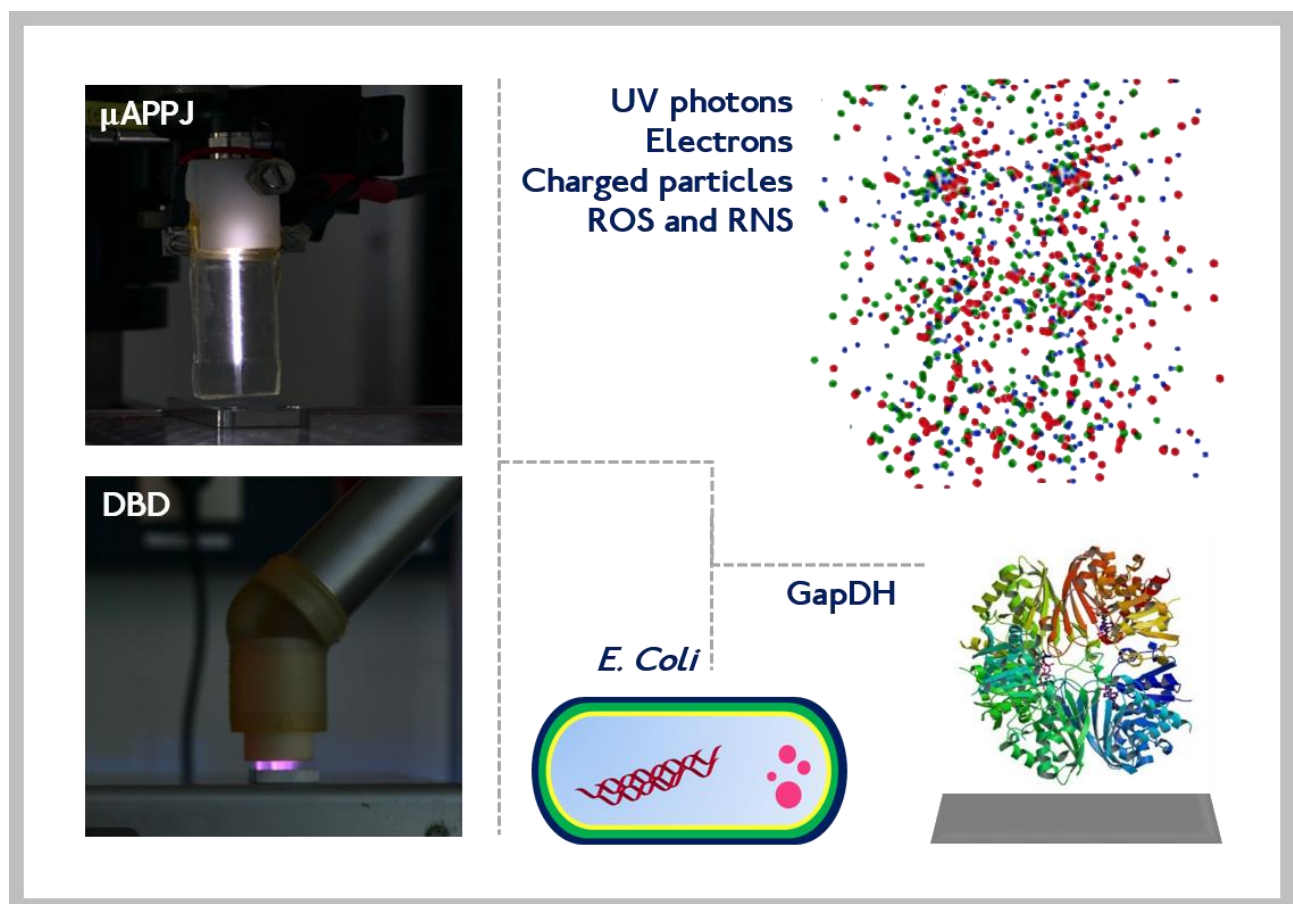


# Chapter 7.1 - Comparative study on the influence of two discharge sources on GapDH activity

Agata Giardina<sup>1</sup>, Marco Krewing<sup>2</sup>, Britta Shubert<sup>2</sup>, Ian Benedikt<sup>2</sup>, Cristina Paradisi<sup>1</sup>, Julia Bandow<sup>2</sup>

<sup>1</sup> Department of Chemical Science, University of Padova, Via Marzolo 1, 35131 Padova, Italy

<sup>2</sup> Ruhr Universität Bochum, Germany.



**Key words:** DBD,  $\mu$ -APPJ, GapDH, non-thermal plasma, *E. coli*.

## Abstract

Cold plasma has been attracting growing interest over the past decade due to its sterilizing properties. However, the study of inactivation mechanisms is challenging because of the diverse nature of both the plasma systems and the biological systems. An increasing number of certified devices are currently used for the treatment of patients. Literature on plasma interactions with biological systems is mainly focused on non-thermal plasmas (NTPs) produced by a single discharge source. Hence, the application of differently generated NTPs on the same target represents a step forward to improve the understanding of interaction mechanisms between plasmas and biological

substrates. The aim of the present study is the comparison of effects triggered by plasma originating from two fundamentally different discharges produced in two different well-characterized devices: a dielectric barrier discharge operated in ambient air and an RF plasma, or more precisely its effluent, generated by the microscale atmospheric pressure plasma jet ( $\mu$ -APPJ). The effects on live *E. coli* cells were assessed as well as the effects on the activity and structure of a key metabolic enzyme, glyceraldehyde-3-phosphate dehydrogenase (GapDH), which was exposed *in vitro*.

### 7.1.1 Introduction

Plasma represents a unique mixture of reactive radical and charged species, photons, electric fields and heat. Non thermal plasma (NTP), referred to also as “cold plasma”, is constituted of neutral particles and ions at a much lower temperature than electrons. The gas temperature is nearly at room temperature, making this technology suitable for applications where the absence of thermal damage and mild conditions are required. In particular, in biomedical research, NTP has gained growing interest due to its capability to affect prokaryotic and eukaryotic cells for sterilization, wound healing as well as cancer treatment [1-4]. Several studies have proved that cold plasma inactivates bacteria on the time range from seconds to few minutes [5,6]. Thus, the application of NTP is currently considered an perspective approach to antibiotics that could overcome the issue of the antibiotic resistance of microorganisms [7]. Huge advances in understanding principles of plasma phenomena have brought to a growing number of NTP sources. Recent devices, certified for patients treatment, produce plasma utilizing several methods, including dielectric barrier discharge (DBD), atmospheric pressure plasma jet and plasma pencil [8,9]. The gas employed are helium (He), argon (Ar), nitrogen ( $N_2$ ) or ambient air, pure or including an established amount of impurities, thus allowing to tune the chemical and physical characteristics of plasma. Hence, the impact on biological substrates is strictly correlated to the source applied and the gas composition originating a combination of charged particles (electrons, ions), electronically excited atoms and molecules, radicals and photons. Due to the complexity of the systems involved, mechanisms of microorganisms inactivation are not fully understood. Previous studies pointed out on the importance of the diverse composition of NTP as the effective peculiarity for biological treatment [10,11]. A key role is generally attributed to reactive oxygen (ROS) and nitrogen species (RNS), that includes  $H_2O_2$ ,  $O_3$ ,  $O$ ,  $\cdot OH$ ,  $NO\cdot$ ,  $O_2\cdot^-$ , that can accumulate in the cell inducing activation of death pathways [12,13]. The relevance of ions is a current debated topic [14,15]. The discrepancies in literature about the biological effect triggered by NTP suggested different mechanisms of inactivation of distinct plasmas. However, the knowledge concerning the comparison of NTP devices is basically lacking. Therefore, the aim of this study was the analysis of the impact of two plasma sources, a dielectric barrier discharge (DBD) and plasma jet,

$\mu$ -APPJ. Both the sources chosen were well characterized previously. DBD is a plasma source for biomedical application that can be applied directly on human skin without any damage.  $\mu$ -APPJ instead presents a remote character, with no direct contact of the plasma with the treated substrate: the reactive species produced in  $\mu$ -APPJ can reach over several centimeters distance in air without any electrical expedient. The differences in their mode of operation make a comparison among the two devices very appealing. For this purpose, interactions between plasma and simple biological substrates can be considered an useful starting point to shed light on modifications occurring at more complex levels. Glyceraldehyde-3-phosphate dehydrogenase (GapDH) was identified as a suitable model biomolecule. GapDH is an ubiquitous glycolytic enzyme, with a cysteine as active site. It is also implicated in several non-metabolic processes, including transcription activation and initiation of programmed cell death (PCD) in eukaryotes [16]. GapDH can undergo several oxidative modifications that may influence its structure and activity. Recent studies on GapDH demonstrated the over-oxidation of thiol groups of cysteines of the enzyme causing inactivation after plasma treatment [10,17]. The effect of the two plasma sources as a function of treatment time was evaluated by using *E. coli* bacteria. Then the enzyme was treated as dry sample to avoid the interference of the aqueous solution and simplify the system evaluated. Investigation and comparison of activity and chemical modifications of the protein were performed after treatment with DBD and  $\mu$ -APPJ to gain information on the potential targets of non-thermal plasma.

## 7.1.2 Experimental procedures

### 7.1.2.1 Plasma sources

The DBD source (Cinology Technologies, Duderstadt, Germany) was described in detail in previous papers [18-21]. Briefly, it is made up of a driven copper electrode (diameter= 10 mm) covered by aluminum oxide as dielectric (Fig. 1). The electrode is driven by a pulsed power supply with a trigger frequency of 300 Hz and a peak amplitude of  $-13.5$  kV, as the standard application mode. The distance between the dielectric and the counter electrode was kept constant at 1 mm producing a homogenous discharge. The amplitude and frequency are pre-selected to use the DBD source for direct application without causing damage to skin. The device operates in air and the gas temperature is 320 K. The generated species are photons, UV-A and UV-B ( $0.2 \text{ W}\cdot\text{m}^{-2}$  for both), electrons (density=  $10^{17} \text{ m}^{-3}$ ) and among reactive particles, NO and ozone, whose flux is about  $7\cdot 10^{18} \text{ m}^{-2}\cdot\text{s}^{-1}$  and  $6.6\cdot 10^{19} \text{ m}^{-2}\cdot\text{s}^{-1}$  [20,21]. Atomic oxygen density is  $2.98 \cdot 10^{16} \text{ cm}^{-3}$  [19].

The  $\mu$ APPJ is a capacitively coupled plasma jet, constituted by two stainless steel electrodes at a distance of 1 mm. The plasma volume that fills this gap is confined on two sides by glass plates and the operating gas is helium with 0.6% of  $\text{O}_2$  in the gas mixture. It was designed to expose the samples

to the plasma effluent, without direct contact with plasma, and in this study the total distance of the sample from the plasma is 12 mm, 8 mm inside the nozzle and 4 mm in ambient air. The plasma was generated by applying a sinusoidal voltage of 13.56 MHz at 230 V<sub>RMS</sub>. The produced species are particles, mainly atomic oxygen and ozone, and photons (emission lines of atomic oxygen around 99 nm, 102 nm, 115 nm and 130 nm) The highest O density obtained by molecular beam mass spectrometry (MBMS) is  $7.0 \cdot 10^{14} \text{ cm}^{-3}$  at a distance of 4 mm from the source and O<sub>3</sub> has a density of ca.  $4.50 \cdot 10^{14} \text{ cm}^{-3}$  at the same distance [22,23].

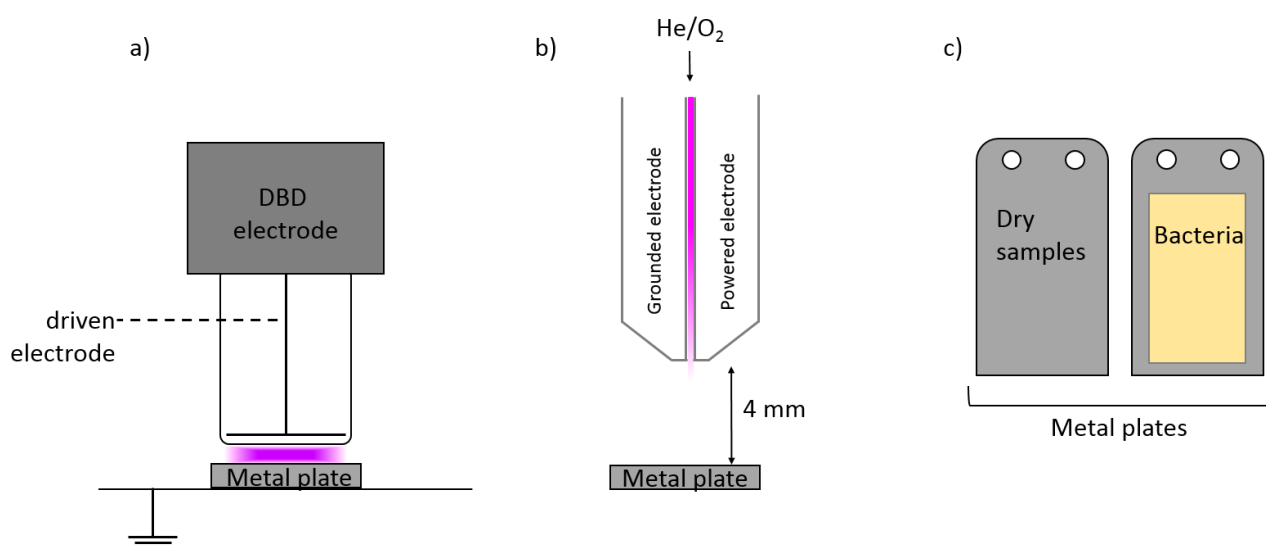


**Figure 1.** Schematic representation of the DBD source (a),  $\mu$ -APPJ (b) and metallic plate (c) used for dried GapDH (left) and *E. coli* (right)

### 7.1.2.2 GapDH activity assay

GapDH from rabbit muscle was used in all experiments (Sigma-Aldrich). 5  $\mu\text{L}$  of the enzyme, 1 mg/mL in *A. dest.*, were spotted on a metal plate (18x35x4 mm), dried and treated with the two sources. The enzyme was then washed from the support by using 50  $\mu\text{L}$  of  $\text{KH}_2\text{PO}_4$  50 mM. The amount of GapDH used for the activity assay was determined by measuring absorbance at 280 nm and applying Lambert Beer law. GapDH samples were mixed with 50  $\mu\text{L}$  of 10 mM glyceraldehyde 3-phosphate solution (GAP). The enzymatic reaction was initiated by adding 90  $\mu\text{L}$  of 10 mM  $\text{NAD}^+$  and monitored at 340 nm via UV/Vis spectroscopy, corresponding to NADH absorbance. The increase of absorbance intensity was plotted as function of time (range of 180 s) and enzyme activity was calculated considering the linear part of the plot. Enzyme activity is expressed relative to the activity of dry controls, obtained by drying GapDH spots on metal plate. When present, the gas

control was obtained by exposing the metal substrate with the enzyme to the gas flow of the source, for the maximum treatment time considered.

### **7.1.2.3 Inhibition zone tests**

*Escherichia coli* K12 cells were grown in LB medium supplemented with 1% glucose to an OD<sub>580</sub> of 0.35. Cells were thus diluted to OD<sub>580</sub> 0.1, sprayed onto LB agar plates to form a monolayer and treated by plasma.

### **7.1.2.4 Oxidative thiol modifications (Ellman's assay)**

Besides its active site (Cys 150), GapDH consists three thiols. Determination of non-oxidized thiols can be useful to evaluate oxidative stress levels in samples exposed to plasma. The relative amount of thiols was assessed through the Ellman's assay, based on reactions between thiols of GapDH samples and 5,5'-dithiobis-2-nitrobenzoic acid (DTNB). The 2-nitro-5-thiobenzoate produced is quantified spectrophotometrically by measuring the absorbance at 412 nm, in a 6 M guanidinium hydrochloride solution.

### **7.1.2.5 SDS-PAGE**

Plasma-treated GapDH solution (80  $\mu$ L) was mixed with 20  $\mu$ L of trichloroacetic acid 50%. Samples were stored at 4° C overnight to precipitate the protein, centrifuged at 4 °C and then washed twice with acetone. After discarding the solvent, 7  $\mu$ l of water were added onto the dried pellet and sonicated for 10 min. Each sample was boiled at 95 °C in protein loading buffer (0.1 M Tris/HCl pH 6.8, 2% SDS, 10 % glycerol, 0.01% bromophenol blue) for 10 min and loaded onto polyacrylamide gels. Gels were run at 200 V for 30 min and stained with Coomassie R-250.

## **7.1.3 Results**

### **7.1.3.1 Inhibition tests**

Preliminary experiments were performed to estimate the influence of DBD and  $\mu$ -APPJ as a function of time on the same biological substrate. To this purpose, *E. coli* monolayers on agar plates were treated in ambient air with both the sources. The amount of deposited bacteria before treatment was considered as control. A "gas control" was also performed with  $\mu$ -APPJ, flowing He/O<sub>2</sub> mixture for 300 s.

Figure 2 shows the pictures of the monolayer of *E. coli* for plasma treatment in the time range from 5 to 300 seconds. It can be observed a significant difference between the two sources for the shortest discharge times considered. In particular, treatments of 5 and 10 s leads to the formation of small

spots in the monolayer, when the  $\mu$ APPJ is employed. This corresponds to the inhibition of the growth of *E. coli* on agar, due to the effect of the jet. More extended zones of inhibition are measured for DBD, although they appear inhomogeneous and not clearly delimited. An increase in toxicity of the effluent is evident after 60 s treatment. It was verified that the  $\mu$ -APPJ can inactivate *E. coli* completely after 120 minutes with a more significant effect on the bacteria as the treatment time increases to 300 s. Remarkable zones of inhibition were observed after only 10 s for DBD treatment, with a complete inactivation of bacteria in the range of 120 s.

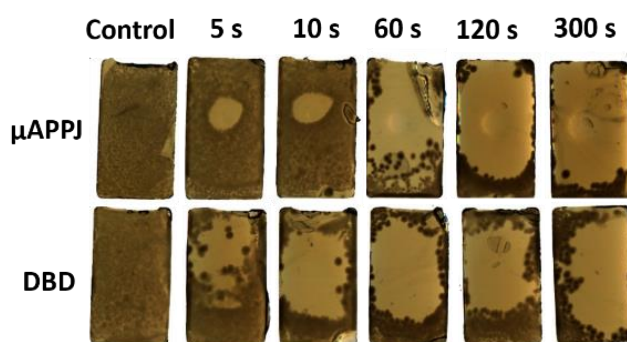


**Figure 2.** Photographs showing the size of the inhibition zone of *E. coli* K12 monolayer treated with  $\mu$ -APPJ and DBD.

In view of the above assessment, useful information was provided on discharge time needed to obtain a reproducible inhibition effect on prokaryotic cells. A maximum treatment time of 300 s was thus applied to study the influence of  $\mu$ -APPJ and DBD on a simpler biological substrate, the enzyme GapDH, for which the effect of the two sources are comparable. It was used as model protein to study the effect of plasma *in vitro*, because it is widespread enzyme, highly conserved from microorganisms to humans. GapDH was dried onto metallic supports and treated with  $\mu$ -APPJ for different exposure times.  $\mu$ -APPJ operated in ambient air with He/O<sub>2</sub> as gas effluent. Metal plates with dried samples were subjected to the plasma jet. GapDH activity was determined and plotted against the treatment time (Fig. 2 a). Compared to activity of the dry control, the enzyme activity is significantly decreased after exposing GapDH 1 min to  $\mu$ -APPJ, reaching a minimum of 53 ( $\pm$  8) % after 300 s of treatment.



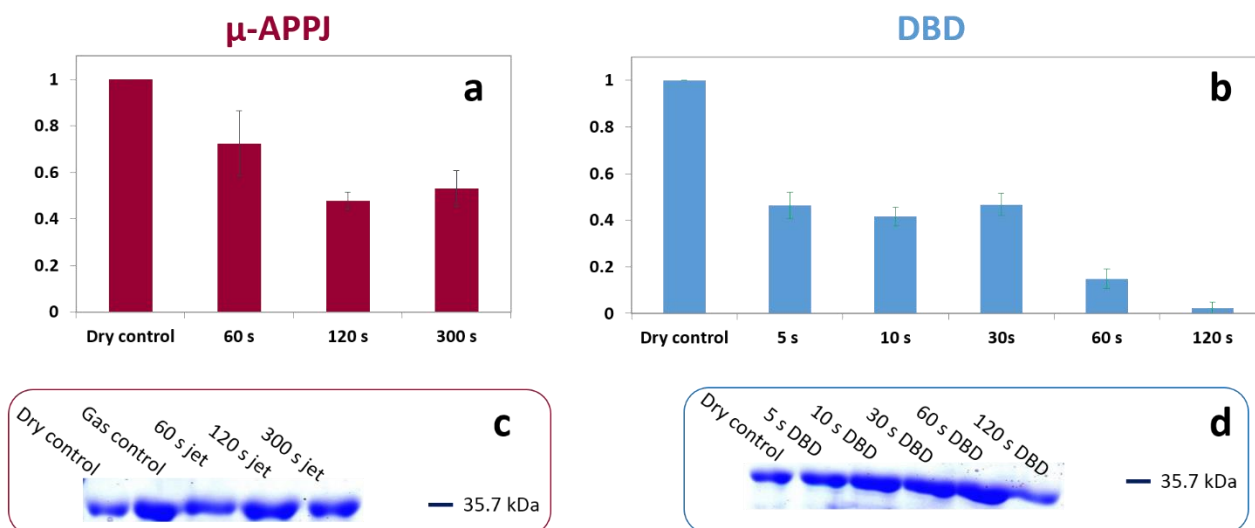


**Figure 3.** Impact of atmospheric plasma on dried glyceraldehyde 3-phosphate dehydrogenase. Activity of purified GapDH for jet (a) and DBD (b) exposures at different treatment times. All relative activities are normalized to the untreated dry sample (dry control). SDS-PAGE of GapDH samples exposed to  $\mu$ -APPJ(c) and DBD (d)

Next, GapDH inactivation was assessed by direct treatment in air with DBD. The plot of relative activity as a function of time highlights a prominent effect after 5 seconds with a 46 ( $\pm 6$ ) % decrease (Fig. 3 b). In this case the activity of GapDH subjected to DBD treatment was monitored for up to 120 s of treatment, corresponding to complete loss of the enzyme function.

The results show that DBD inactivates *E. coli* bacteria much more effectively and homogeneously than  $\mu$ -APPJ for the same treatment time, in line with experimental evidence found for the inhibition assays shorter time treatment. Possible loss or fragmentation of GapDH could occur as consequence of plasma treatment. Non-reducing gel electrophoresis was performed to investigate modification in protein size. SDS-PAGE separate the samples by their molecular weight. No backbone breaks were found by SDS-PAGE for DBD exposure (Fig 3d), indicating that inactivation is not due to etching or fragmentation. No molecular weight variation of the enzyme were observed also in the case of  $\mu$ -APPJ (Fig 2c).

Chemical modifications of the enzyme were also evaluated. GapDH contains four cysteines, among which C150 represents the active site. It is known from literature [10] that its oxidation is one of the mechanisms preventing the enzyme function (Fig. 4).

Free thiols were quantified through Ellman assay and compared to the dry control. It was observed for both the sources a decrease depending on plasma treatment time, indicating the irreversible oxidation of thiol group to sulfonic acid or nitrosylation (Fig. 5).

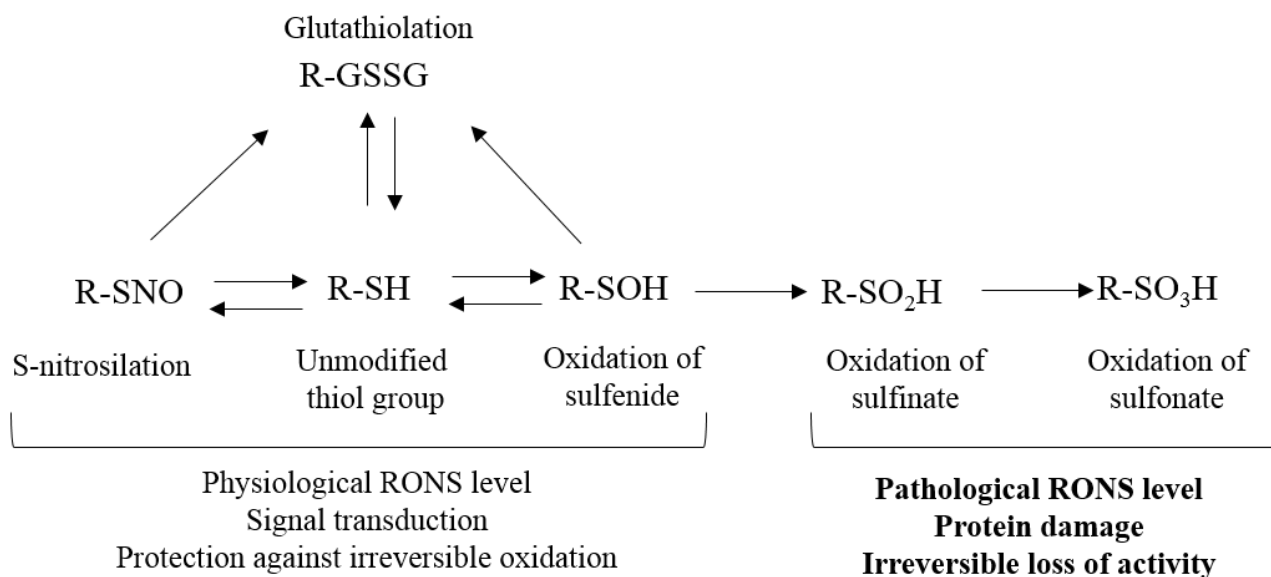


**Figure 4.** Reactive oxygen and nitrogen species-mediated modifications of thiol residues. Adaptation from Sharma *et al.*<sup>24</sup>

Relative amount of free thiols group reached a minimum of 55% after 10 min of exposure to the jet. This confirms also the trend observed for the variation of activity after  $\mu$ -APPJ treatment, with an enhanced effect for the DBD compared to the jet.

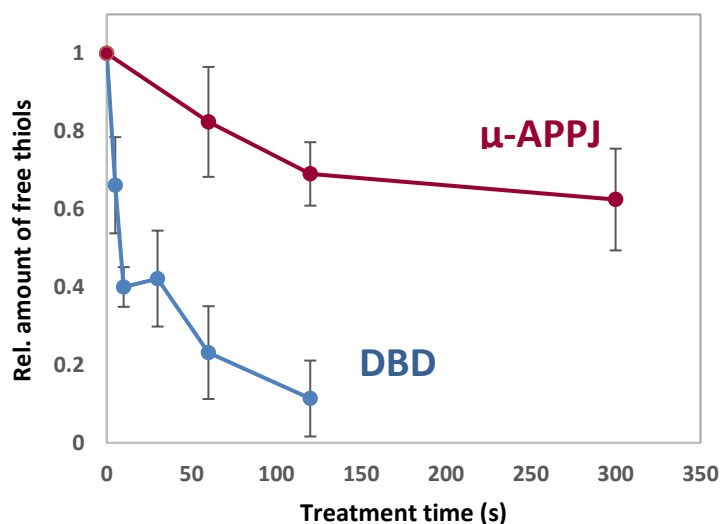


**Figure 5.** Decrease of free thiol groups in GapDH after DBD treatment. The amount of thiols in the dry control is set to 1 and other results are normalized to it

### 7.1.4 Discussion

It is known that non thermal plasma is a complex matrix producing positive and negative ions, UV radiation, and reactive radical species, which interact with the treated surface. The impact of different plasma-generated species on the treated systems are a topic of current scientific discussion. Reactive

oxygen species (ROS) as well as nitrogen reactive species (RNS) are considered key particles affecting the substrate directly or interacting with the liquid phase surrounding the biological systems. In this work the interaction of the aqueous solution was eliminated in order to simplify the system under study, minimizing secondary species in solution (e.g. H<sub>2</sub>O<sub>2</sub>) originated from the primary ones from air. We used two devices with distinct properties which are well-characterized [18-23] and that have demonstrated relevant effects in microorganisms inactivation [10,19]. As regards the jet, it is dominated by atomic oxygen that, at 4 mm from the source, results in the formation of the long-lived ozone. Douat *et al* studied generation of reactive nitrogen species NO and N<sub>2</sub>O as a function of the gas mixture in the source [25]. N<sub>2</sub>O is used in biomedical field as anesthetic and analgesic gas [26,27]; the nitrogen oxide (NO) is recognized as a fundamental molecule for cell signaling in inflammation processes and vascularization [28] and it can influence the cell death pathway and thus the antimicrobial effect due to oxidative stress [29]. In the jet in use, NO and N<sub>2</sub>O densities are strongly gas mixture dependent. In particular, they increase as a function of the N<sub>2</sub> admixture, while increasing oxygen, above a minimum value (710 ppm), reduces the densities of both NO and N<sub>2</sub>O. Thus, the above species are not significant for He/N<sub>2</sub>/O<sub>2</sub>=99.4%/0%/0.6% [25]. The impact of  $\mu$ -APPJ on GapDH *in vitro* could be rather ascribed to ozone and atomic oxygen, of which a significant density (around  $6 \cdot 10^{14} \text{ cm}^{-3}$ ) was measured at 4 mm from the source, for the same gas composition [22]. It was already proven in a previous study that the inactivation of GapDH by  $\mu$ -APPJ is due to the step-wise addition of oxygen to the thiol group of catalytic Cys150 to sulfonic acid [10]. The ratio of inactivated enzyme is in agreement with our tests on GapDH dried on metal plates, indicating no interference of the conductive substrate. Ellman's assay corroborated these results showing a reduction of free thiols in the same range.

*In vitro* test of GapDH were performed to compare two sources, a plasma jet and a dielectric barrier discharge. The species responsible for inactivation, also in the case of DBD, include ozone and atomic oxygen. The latter forms NO and NO<sub>x</sub> that can interact with the sample at a distance of 1 mm from the source [30]. The loss of activity, resulted from the interaction of the sample with the mentioned ROS and RNS, was complete after 120 s. Supports to activity assay information comes from Ellman test, in which 0.1% of free thiols are detected after 120 s. In this case the thiols of the cysteines were reasonably subjected to nitrosylation and oxidation to sulfonic acid and S-nitrosothiols. For both the sources no disulfide bond formation was observed: even though disulfide group intermediates are not excluded, this indicates the oxidation as the main pattern of inactivation. The different species inactivating GapDH can be explained considering that ozone is the ROS that affects more the enzyme during jet treatment and that amount of atomic oxygen densities in the case of DBD are about two orders of magnitude higher than that produced at 4 mm from the jet. This observation is also useful

to evaluate the importance of NO<sub>x</sub> species, especially of NO, in oxidative stress of the biological substrate.

When *E. coli* monolayers were treated by  $\mu$ -APPJ, the size of the zone of inactivation was not limited by the buoyancy force in ambient air. No etching was observed when the sample was at a distance of 4 mm from the device, even if it is known that the effluent can induce damage on model polymer substrates<sup>10</sup>. Inhomogeneous inhibition zones were observed in the range 60 s of jet treatment while for 300 s of exposure there was a maximum for the area of *E. coli* inactivation. This is due probably to different densities of reactive species in the gaseous phase or possible interaction of the species with the wet agar medium. During DBD treatment, at 1 mm of distance from the device, the cells were most probably inactivated by synergistic effects of ozone, NO<sub>x</sub> species, photons and charged particles. The inactivation analysis of monolayers of *E. coli* by applying the DBD device showed fast inactivation in 5 seconds, in agreement with the enzyme treatment results. As for the model protein, we have to take into account the role of atomic oxygen on the substrate and the species produced from its reactions in air. It is worth to note two different trends in inhibition zone as a function of treatment time: a significant gap between 5 (or 10 s) of the jet treatment and longer treatment times. The initial spots (5 s treatment) correspond to the distance of the long-living reactive species, responsible for bacterial inactivation. It was proven that ozone is one of the major ones and that the concentration produced by jet is lethal for *E. coli*. Ozone can diffuse at large distances from the jet and it is stable enough to survive the transport. Besides, an effects of UV and VUV radiation was observed as the treatment time increase [23]. On the other hand, DBD inhibition zones have similar diameter values, corresponding to the maximum distance the reactive species responsible for inactivation can reach.

The above experiments highlight the difference between inhibition assay and *in vitro* GapDH results, suggesting the importance of liquid presence in the sample during  $\mu$ -APPJ plasma treatment. Lackmann *et al* [10] reported a complete inactivation for *in vivo* GapDH after treatment with  $\mu$ -APPJ. In our experiments, to avoid the solvent interference, in all GapDH samples liquid was removed prior to plasma exposure. On the contrary, this effects seems to be negligible for DBD treatment. It was already proven that CT26 murine colon cancer cells are affected by different amount of liquid during plasma treatment [31]. This liquid may have the double role of scavenger and mediator of secondary reactive species produced in water, like nitrite, hydrogen peroxide, hydroxyl radicals and peroxyxynitrite that can be formed from short lived oxidant species. In particular, GapDH seems to be intrinsically more reactive toward H<sub>2</sub>O<sub>2</sub> than most other redox-regulated proteins, during the “oxidative stress” response [32]. Therefore, it is possible to conclude that the presence of aqueous medium represents a key parameter in determining the efficiency of  $\mu$ -APPJ in GapDH inactivation.

This effect is not prominent for DBD, for which short lived species could be the main responsible of inactivation. In contrast with results obtained for other DBD devices [31]. The results presented are preliminary but can be considered a first attempt to evaluate the effect of two different plasma sources on a simple biomolecule, in absence of the aqueous medium as oxidation mediator. This proof of principle still provide enough information to demonstrate how two sources can affect differently a biological sample and thus to hypothesize different targets for biomedical applications.

## References

1. Shi L, Ito F, Wang Y, et al. Non-thermal plasma induces a stress response in mesothelioma cells resulting in increased endocytosis, lysosome biogenesis and autophagy. *Free Radical Biology and Medicine*. 2017;108:904-917
2. Li Y, Ho Kang M, Sup Uhm H, Joon Lee G, Ha Choi E, Han I. Effects of atmospheric-pressure non-thermal bio-compatible plasma and plasma activated nitric oxide water on cervical cancer cells. *Scientific Reports*. 2017;7:45781
3. Xiong Z, Roe J, Grammer TC, Graves DB. Cover picture: Plasma process. polym. 62016. *Plasma Processes and Polymers*. 2016;13(6):579
4. Kubinova S, Zaviskova K, Uherkova L, et al. Non-thermal air plasma promotes the healing of acute skin wounds in rats. *Scientific Reports*. 2017;7:45183
5. J Jeon and T G Klaempfl and J L Zimmermann and G E Morfill and, T Shimizu. Sporicidal properties from surface micro-discharge plasma under different plasma conditions at different humidities. *New Journal of Physics*. 2014;16(10):103007
6. Kim J, Puligundla P, Mok C. Effect of corona discharge plasma jet on surface-borne microorganisms and sprouting of broccoli seeds. *J Sci Food Agric*. 2017;97(1):128-134.
7. Park JH, Kumar N, Park DH, et al. A comparative study for the inactivation of multidrug resistance bacteria using dielectric barrier discharge and nano-second pulsed plasma. *Scientific reports*. 2015;5(1):13849
8. Brehmer F, Haenssle HA, Daeschlein G, et al. Alleviation of chronic venous leg ulcers with a hand-held dielectric barrier discharge plasma generator (PlasmaDerm(®) VU-2010): Results of a monocentric, two-armed, open, prospective, randomized and controlled trial (NCT01415622). *Journal of the European Academy of Dermatology and Venereology : JEADV*. 2015;29(1):148

9. Mann MS, Tiede R, Gavenis K, et al. Introduction to DIN-specification 91315 based on the characterization of the plasma jet kINPen® MED. *Clinical Plasma Medicine*. 2016;4(2):35-45
10. Lackmann J, Schneider S, Edengeiser E, et al. Photons and particles emitted from cold atmospheric-pressure plasma inactivate bacteria and biomolecules independently and synergistically. *J R Soc Interface*. 2013;10(89)
11. Schneider S, Lackmann J, Ellerweg D, et al. Plasma process. polym. 6/2012. *Plasma Processes and Polymers*. 2012;9(6):n/a. doi: 10.1002/ppap.201290016.
12. Kang SU, Cho J, Chang JW, et al. Nonthermal plasma induces head and neck cancer cell death: The potential involvement of mitogen-activated protein kinase-dependent mitochondrial reactive oxygen species. *Cell Death and Disease*. 2014;5:e1056
13. Vandamme M, Robert E, Lerondel S, et al. ROS implication in a new antitumor strategy based on non-thermal plasma. *International Journal of Cancer*. 2012;130(9):2185-2194
14. Fridman G, Brooks AD, Balasubramanian M, et al. Comparison of direct and indirect effects of non-thermal atmospheric-pressure plasma on bacteria. *Plasma Processes and Polymers*. 2007;4(4):370-375
15. Lin A, Chernets N, Han J, et al. Non-Equilibrium dielectric barrier discharge treatment of mesenchymal stem cells: Charges and reactive oxygen species play the major role in cell death. *Plasma Processes and Polymers*. 2015;12(10):1117-1127
16. Seidler NW. *GAPDH: Biological properties and diversity*. Vol 985. Springer Netherlands; 2013
17. Stapelmann K., Lackmann J., Buerger I., Bandow J.E. and Awakowicz P. A H<sub>2</sub> very high frequency capacitively coupled plasma inactivates glyceraldehyde 3-phosphate dehydrogenase (GapDH) more efficiently than UV photons and heat. *J. Phys. D: Appl. Phys.* 2014;47:085402
18. Baldus S, Schröder D, Bibinov N, Schulz-von der Gathen V, Awakowicz P. Atomic oxygen dynamics in an air dielectric barrier discharge: A combined diagnostic and modeling approach. *J Phys D*. 2015;48(27):275203
19. Kartaschew, Baldus S, Mischo M, Bründermann E, Awakowicz P, Havenith M. Cold atmospheric-pressure plasma and bacteria: Understanding the mode of action using vibrational microspectroscopy. *J Phys D*. 2016;49(37):374003

20. Bibinov N., Rajasekaran P., Mertmann P., Wandke D., Viöl W. and Awakowicz P., *Biomedical engineering (trends in materials)*. New York: InTech, 2011):123–50.
21. Rajasekaran P, Mertmann P, Bibinov N, Wandke D, Viöl W, Awakowicz P. Filamentary and homogeneous modes of dielectric barrier discharge (DBD) in air: Investigation through plasma characterization and simulation of surface irradiation. *Plasma Processes and Polymers*. 2010;7(8):665-675
22. Ellerweg D, Benedikt J, von Keudell A, Knake N, Schulz-von der Gathen V. Characterization of the effluent of a he/O2 microscale atmospheric pressure plasma jet by quantitative molecular beam mass spectrometry. *New Journal of Physics*. 2010;12:013021
23. Schneider S, Lackmann J, Narberhaus F, Bandow JE, Denis B, Benedikt J. Separation of VUV/UV photons and reactive particles in the effluent of a he/O2 atmospheric pressure plasma jet. *Journal of Physics D: Applied Physics*. 2011;44(29):295201
24. Vijay Sharma John H McNeill. Parallel effects of  $\beta$ -adrenoceptor blockade on cardiac function and fatty acid oxidation in the diabetic heart: Confronting the maze. *World J Cardiol*. 2011;3(9):281-302
25. Douat CC, Hübner SS, Engeln RR, Benedikt JJ. Production of nitric/nitrous oxide by an atmospheric pressure plasma jet. *Plasma Sources Science and Technology*. 2016;25(2):025027.
26. Sher AM, Braude BM, Cleaton-Jones PE, Moyes DG, Mallett J. Nitrous oxide sedation in dentistry. A comparison between rotameter settings, pharyngeal concentrations and blood levels of nitrous oxide. *Anaesthesia*. 1984;39(3):236-239
27. Leelataweewud P, Vann J, W F, Dilley DC, Lucas WJ. The physiological effects of supplemental oxygen versus nitrous oxide/oxygen during conscious sedation of pediatric dental patients. *Pediatric dentistry*. 2000;22(2):125
28. Sharma J, Al-Omran A, Parvathy S. Role of nitric oxide in inflammatory diseases. *Inflammopharmacol*. 2007;15(6):252-259
29. Bernhard Brüne. Nitric oxide: NO apoptosis or turning it ON? *Cell Death and Differentiation*. 2003;10(8):864-869

30. Heuer K, Hoffmanns MA, Demir E, et al. The topical use of non-thermal dielectric barrier discharge (DBD): Nitric oxide related effects on human skin. *Nitric oxide : biology and chemistry / official journal of the Nitric Oxide Society*. 2015;44:52-60
31. Bekeschus S, Lin A, Fridman A, Wende K, Weltmann K, Miller V. A comparison of floating-electrode DBD and kINPen jet: Plasma parameters to achieve similar growth reduction in colon cancer cells under standardized conditions. *Plasma Chem Plasma Process*. 2018;38(1):1-12.
32. Peralta P, Bronowska A K, Morgan B, et al. A proton relay enhances H<sub>2</sub>O<sub>2</sub> sensitivity of GAPDH to facilitate metabolic adaptation. *Nature chemical biology*. 2015;11(2):156-163



## Chapter 7.2 - Effect of ions of cold atmospheric plasma on biological substrates

### 7.2.1 Introduction

As already mentioned, reactive molecules produced by plasma have demonstrated to be crucial regulators of cellular activity in health and disease. It is known that cold atmospheric plasma represents a unique mixture of neutral reactive species but also electric fields, photons and charged species, which make it appealing for biological applications, where the oxidative stress is essential for signaling pathways. Considering the effects on bacteria, the mechanisms underlying microorganisms inactivation are still unexplored, especially the role of ions in the treatment. For this purpose, a modified version of the  $\mu$ -APPJ, described in the previous section, was employed. The device was optimized for the generation of ions with the help of unfiltered (no window used) vacuum UV radiation of a pure helium plasma to assess the effects of charged and uncharged particles, respectively, and their combined effect on dried biological substrates, and possibly on living bacteria. Glyceraldehyde-3-phosphate dehydrogenase (GapDH) was identified as a suitable model enzyme, due to its ubiquitous presence in nearly all organisms. It is a redox-regulated protein with a cysteine as active site that can be inactivated by oxidative stress. The revised geometry of the  $\mu$ -APPJ, conveniently designed by Prof. Benedikt's group, was characterized and applied to GapDH in a cooperation laboratory. Two gas composition, He/O<sub>2</sub> and He/Ar mixtures, were employed to tune dominant species produced in the photoionization process. Lackmann *et al.* applied a similar approach, focusing on separation of reactive species and photons. They showed that GapDH can be inactivated to different extent by treatment with plasma generated particles compared to plasma emitted (vacuum) UV photons [1]. Here, for the first time, isolated and combined effect of ions and neutrals is studied using the same substrate. Experiments were performed also on *E. coli* bacteria, as model system that may guide to *in vivo* studies.

### 7.2.2 Experimental procedures

A detailed description of the experimental procedures relative to GapDH assay is reported in the previous section. The setup for the investigation of ions contribution is shown in Fig 1. Glass capillaries with a 0.4 x 4 mm<sup>2</sup> cross section are placed between a grounded electrode and powered electrode supplied with rf voltage at 13.56 MHz. The helium gas flowing through the capillaries flows at 1000 sccm through the flowmeter into a gas line out of the apparatus, through a vacuum pump. Plasma is ignited by applying root-mean-square RF voltage of 365 V. Three gas bottles are connected

to the source for helium, argon and oxygen respectively. Pure helium flows into the glass capillaries and through the cross-flow in front of the main chamber. Pure He gas in the plasma maximizes the vacuum UV emission of the He<sub>2</sub>\* excimer and hence the photoionization yield in the chamber. A second flow of He with small admixture of Ar or O<sub>2</sub> is realised through the second gas inlet. This gas mixture flows through the main chamber, where the sample is arranged. The chamber consists of a grounded cover and a rectangular cavity for a metallic plate (18 mmx 35 mmx 5 mm) that can be connected to a DC voltage. The DC voltage of -100 V was applied, and the resulting current was measured by a digital picoamperemeter. The metallic plates serve as substrate holders and, according to their shape, can be used for dry samples or bacteria on agar medium. The chamber is also connected to the gas outlet line with a glass window at an angle of 45 degrees, facing the plasma jet. The window has an its inner side a thin sodium salicylate layer, a fluorescent salt, to measure the relative VUV intensity of He<sub>2</sub> excimer radiation.

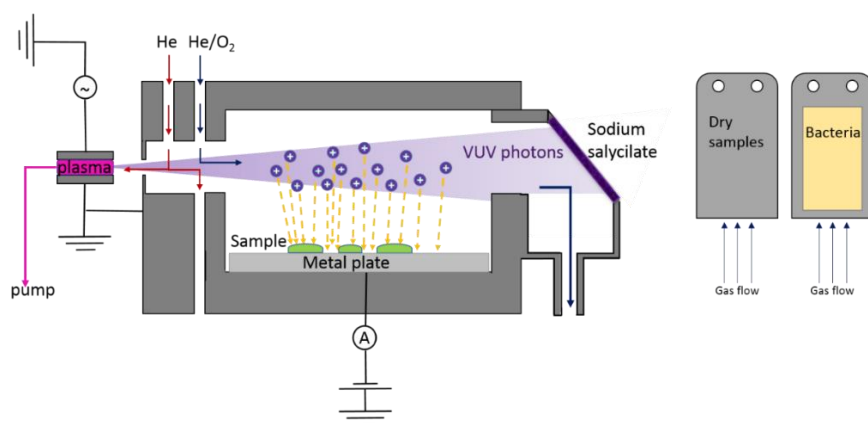


**Figure 1.** Scheme of the modified version of  $\mu$ -APPJ for charged and uncharged particles separation.

### 7.2.3 Characterization of the source

Optimization of the new device are discussed elsewhere [2,3]. Briefly, the vacuum UV photons in the wavelength range of 60-100 nm emitted by decay of He<sub>2</sub>\* excimers in the plasma ionizes O<sub>2</sub> or Ar species in the gas mixture. The emission intensity is further enhanced by operating the source in the contracted mode at higher applied power. Experimental tests of the setup were performed by evaluation of VUV intensity through the photoluminescence of the sodium salicylate and by measuring the ion current to the substrate.

Sodium salicylate is a fluorescent salt that absorbs VUV radiation and reemits photons in the visible spectrum in the 350-550 nm spectral region. In the spectral range of 30-340 nm, the quantum efficiency can be considered constant and the emission measured at the spectral range 350–550 nm with a maximum at 420 nm is proportional to the number of absorbed VUV and UV photons. Due to

interferences of several discrete lines above 450 nm, which are also generated by He plasma, the monitoring of the photoluminescence spectrum was performed in the range 350-450 nm only, see Figure 2.

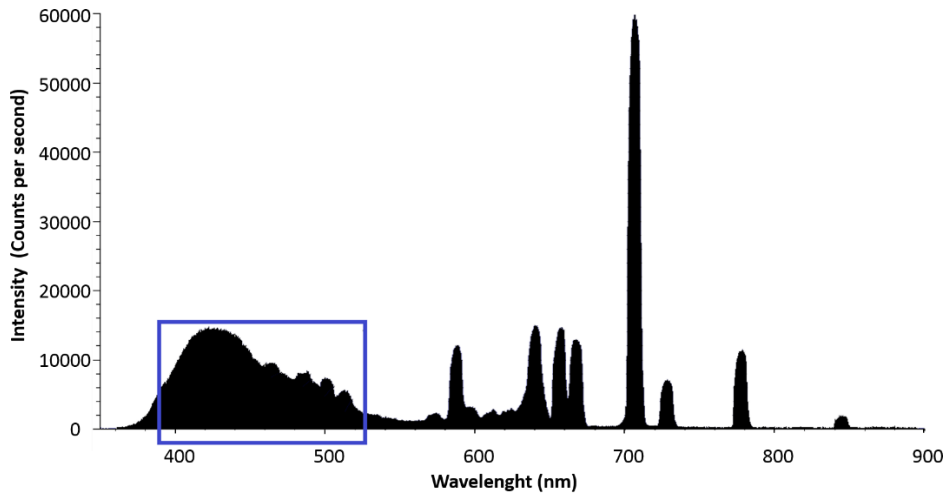


**Figure 2.** Emission spectrum of sodium salicylate.

Gaseous impurities can affect He<sub>2</sub> excimer photon yield, which is relatively proportional to the intensity of the emission band around 640 nm in the plasma emission spectrum as shown in Figure 3. The emission spectra were registered for each experiment to verify the purity of helium plasma and the correlation between the intensity of the above peak and the VUV radiation of He<sub>2</sub> excimers, which was also monitored during each experiment.

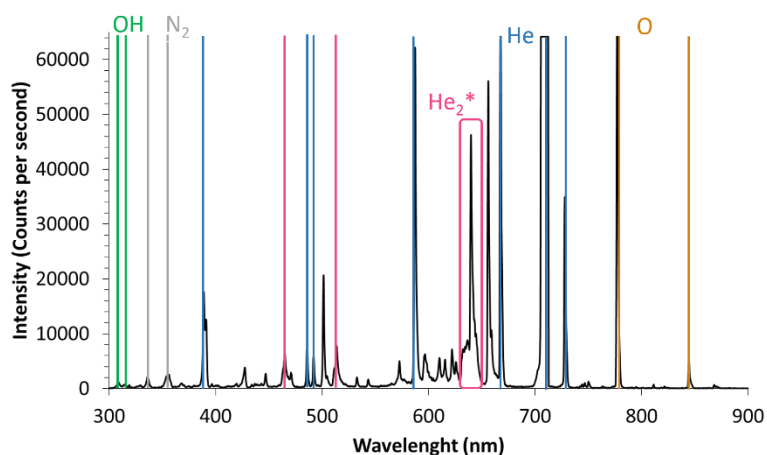


**Figure 3.** Emission spectrum of He/O<sub>2</sub> plasma. In the case of He/Ar plasma the spectral line at 763 nm is also present (Ar<sub>763</sub>).

The optimization of the gas flow was performed to minimize the back diffusion of admixed Ar or O<sub>2</sub> into the plasma. The gas flow of He line was set to 4000 sccm, for which the best performances were obtained. At the same time, the second He inlet, the flow of Ar/O<sub>2</sub> doped He was tested to maximize the ion current in the device, hence maximizing the ion dose per unit time.

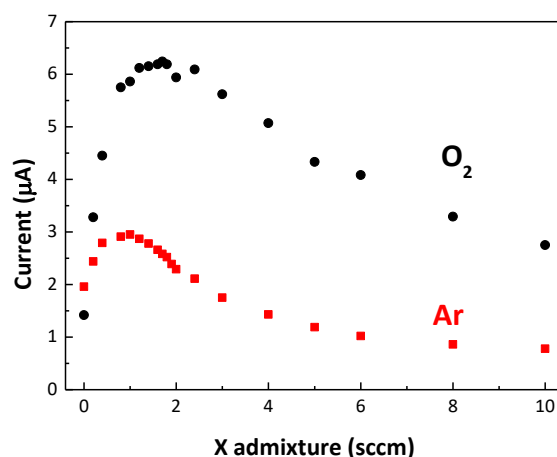


**Figure 4.** Measured ion current at the substrate for Ar admixture (■) and for O<sub>2</sub> admixture (■) to the second He line

Figure 4 shows the measured ion current at the substrate as a function of the admixture of O<sub>2</sub> or Ar (X) to the second helium inlet. The maximum values were observed at 1.7 sccm for oxygen, corresponding to -6.4 µA, and 0.8 sccm for argon, corresponding to -3.1 µA. It is worth to note that similar current profiles were observed for both admixed species showing that the same physical process is involved. In particular it is possible to identify an initial portion preceding the maximum values, at which the amount of VUV photons that can induce photoionization of X is too low. As the flow of X increases more ions are produced until reaching the saturation value. At low concentrations of O<sub>2</sub> or Ar only small amount of VUV photons is absorbed – the gas mixture is almost transparent. The VUV absorption and with it also the flux of generated ions increases ~linearly with the concentration. As the Ar/O<sub>2</sub> flow reaches 1-2 sccm, the VUV photons start to be significantly depleted (each photon generates one ion) and the current reaches the maximum. At even higher flows of oxygen or argon, the ion current decreases due to the strong absorption of VUV photons in and in front of the chamber at the flow crossing.

The ionization energy of argon is significantly higher than that of oxygen and a part of the VUV radiation is not absorbed by argon atoms. This is the main reason of the relatively smaller current values of argon compared to oxygen. Moreover, since argon particles are larger and heavier than oxygen molecules, they are accelerated more slowly by the electric field and probability of recombination with electrons is higher for argon.

For all the experiments presented in this work, argon and oxygen were added in the same amount (1.7 sccm of Argon or Oxygen and 2000 sccm of He) corresponding to the highest ion flow produced.

#### **7.2.4 GapDH activity assay**

In the ideal case, the plasma generated VUV photons generate ions in the chamber, which are then drifting along electric field lines towards the substrate. However, other possible effects have to be considered in the non-ideal system. First, some VUV photons can get scattered or reflected and can result into inactivation of the GapDH. Operating the chamber without applied voltage, with only plasma running, provides the estimation of this effect. Second, the VUV photons leads also to dissociation of O<sub>2</sub> molecules into two O atoms (photoionization yields of VUV photon absorption are typically between 50% to 90%). This neutral species should be carried away by the gas flow, but it can't be excluded that some of these neutral species can diffuse to the substrate and cause some inactivation as well, masking the effect of ions. Again, performing the control treatment without electric field (P treatment) compare to the treatment with plasma and applied substrate voltage (U+P) provides some estimation of the possible role of neutrals as well. For the sake of completeness, the treatment with the applied voltage only (100 V), without the plasma running (U treatment) have been performed as well.

Each experiment was performed for 30 min with a conditioning time of 10 min before treatment to flush the air out of the chamber and eliminate air impurities. Activities were compared to the dry control and the gas control was also carried out exposing GapDH to He/O<sub>2</sub> or He/Ar.

The first step consisted in establishing the appropriate treatment time for the experiments. The full treatment (ignited plasma and switched DC voltage) was applied for 10, 20 and 30 minutes to different dried enzyme samples. Activities of the three samples were thus evaluated and normalized to the "dry control".

It can be seen (Fig. 5a) that after 10 minutes still no significant activity loss can be observed. In the case of prolonged treatment, the activity decreases linearly with time: after 20 minutes the enzymes show 84% and after 30 minutes 64% of the original activity. Therefore, in the following experiments the treatment time of 30 minutes was applied.

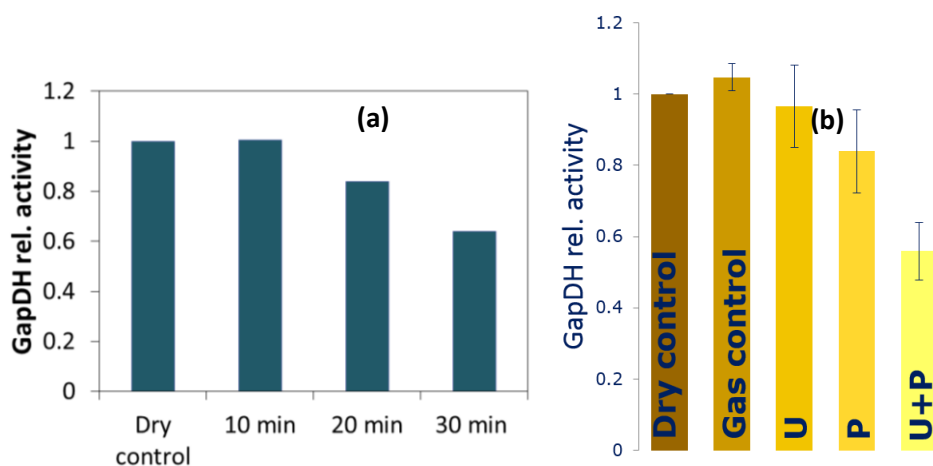


**Figure 5.** (a) Activity variation of GapDH as function of treatment time using He/O<sub>2</sub> gaseous mixture; (b) Impact of the electric field (U), plasma treatment (P) and plasma in the presence of an applied voltage (-100 V) on in vitro GapDH activity. The gas used is He/Ar.

The importance of ions as crucial species for the treatment of biological substrates has been suggested by several authors [4,5]. The peculiar feature of this study is that it represents the first attempt to evaluate the importance of ions on a biomolecule, the enzyme GapDH, treated by plasma. Through photoionization of Ar (or O<sub>2</sub>) in He gas, ions of argon or oxygen were put in contact with dried GapDH. Regarding the He/O<sub>2</sub> mixture, the ions generated in photo-ionization reactions have been measured previously for different concentrations of oxygen molecules in He [6] (Fig. 6). It is worth noting that the oxygen molecules are photo-ionized and their flux into the MS is roughly ten times higher than the flux of protonated water clusters, which are almost always present in the ion spectra due to water vapor impurity. Additional ions (O<sub>2</sub>(H<sub>2</sub>O)<sup>+</sup>, O<sub>4</sub><sup>+</sup>, O<sup>+</sup>) may be also observed, as result of ion-neutral reactions. Photoionization of argon produce Ar<sup>+</sup> as primary ions and larger water clusters as well (not shown).

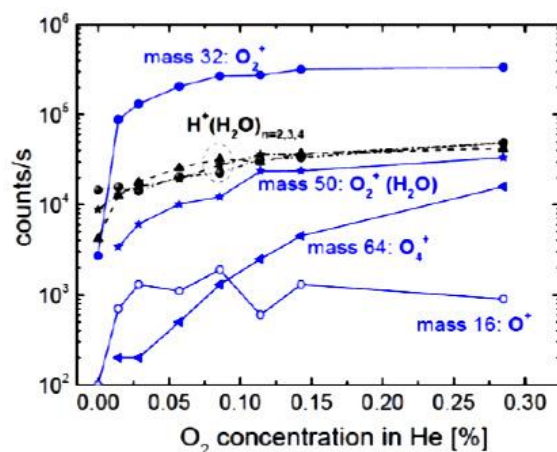


**Figure 6.** Ion densities as a function of O<sub>2</sub> concentration

Regarding He/Ar gas mixture (Fig. 5b), no significant decrease of GapDH activity was observed applying only -100 V to the metal plate. Plasma treatment of the enzyme on the grounded plate induced a slight inactivation that can be attributed to scattered photons in the chamber and impurities of the gaseous mixture, like H<sub>2</sub>O molecules. In this case for example, VUV photons can react with water producing OH radicals that can diffuse to the sample. The combination of plasma and electric field (P+U) led to the improvement of GapDH inactivation compared to plasma treatment (P). This effect can be attributed to positive ions drift in the electric field to the substrate.

He/O<sub>2</sub> source was also used to change reactive species produced (Fig 7). In this case no relevant difference was observed between plasma and plasma together with the electric field when negative voltage was applied to the metal plate. This was attributed to diffusion of O atoms or other impurities (e.g. OH radicals from water molecules) diffusion during plasma treatment.

On the contrary, for the application of positive voltage (+100 V) a distinct effect is evident when plasma treatment is associated with the application of the electric field due to the formation of negative ions such as O<sub>2</sub><sup>-</sup> or O<sup>-</sup> through (dissociative) electron attachment to O<sub>2</sub> molecules. Further MS experiments are needed to verify how many negative oxygen ions are produced in the chamber compared to positive oxygen ions.

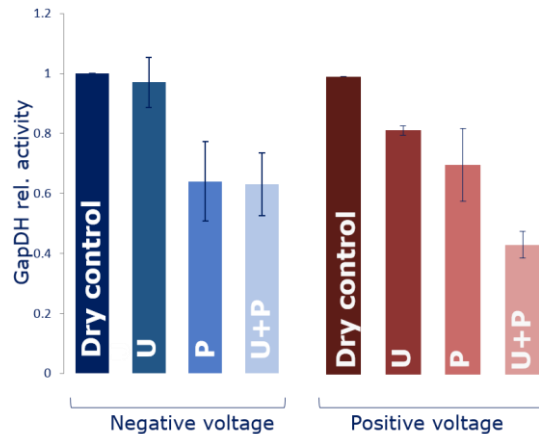


**Figure 7.** Effect of the electric field (U), plasma treatment (P) and plasma in the presence of an applied voltage on *in vitro* GapDH activity. The gas used is He/O<sub>2</sub> and both, negative (blue) and positive voltage (dark red) were applied to the substrate

### 7.2.5 *E. coli* test

Single layers of *E. coli* bacteria deposited on agar were treated in the modified version of  $\mu$ -APPJ (Fig. 8). The gas used for these experiments was He/O<sub>2</sub> mixture. Four tests were performed as in the case of the oxygen measurement series.

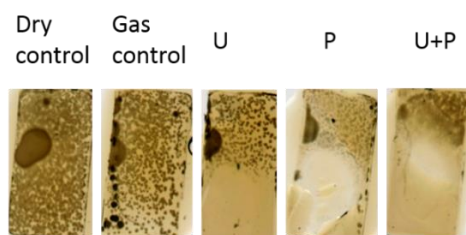


**Figure 8.** Effect of the ion separation-source on *E. coli*.

The sample gas control does not show significant differences compared to dry control, having a homogeneous bacterial growth. The *E. coli* distribution on agar, when a negative voltage of -100 V is applied to the substrate (U), shows a homogeneous half of the slide while the other half, near the electrode on the back of the metal plate, is severely affected by the treatment. In the sample of full treatment (U+P), the inhibition of bacteria growth is almost complete, with some etching effects on the center of the agar slide. An enhanced etching effect is visible in the sample exposed to plasma (P only), although in this case the inhibition zone is less extended than complete treatment. It is possible to note also the melting of the agar (white spot in Fig.8) for plasma and full treatment (U+P). This effect, greater for the complete treatment than plasma treatment, can be attributed to the increase of temperature, as result of the ion current. The results about the single layer of *E.coli* can be evaluated in light of an improvement of the setup. Further experiments have to be carried out to understand the interaction of atmospheric pressure plasmas with prokaryotic cells. Possible effects due to the presence of agar medium, influencing humidity and conductivity of the environment, could be evaluated.

## References

1. Lackmann JW, Baldus S, Steinborn E, et al. A dielectric barrier discharge terminally inactivates RNase A by oxidizing sulfur-containing amino acids and breaking structural disulfide bonds. *J Phys D*. 2015;48(49):494003.
2. Karczewski C. Bachelor thesis; 2017
3. Vogel P. Master thesis; 2017
4. Dobrynin D, Fridman G, Friedman G, Fridman A. Physical and biological mechanisms of direct plasma interaction with living tissue. *New Journal of Physics*. 2009;11(11):115020.
5. Fridman G, Brooks AD, Balasubramanian M, et al. Comparison of direct and indirect effects of non- thermal atmospheric- pressure plasma on bacteria. *Plasma Processes and Polymers*. 2007;4(4):370-375.
6. M.Hefny M, Große Kreul S. Private communication



## 8. Conclusions

This thesis addresses some important problems and questions related to environmental applications of air non-thermal plasma in water treatment processes. In chapter 2 a common antibiotic, sulfamethoxazole (SMZ), was treated in a DBD reactor. The effect of the pollutant initial concentration and of the aqueous solution pH on the decomposition kinetics was studied. Many oxidation products were identified by means of HPLC-MS/MS analysis and thus the oxidation scheme was proposed. Ecotoxicological tests were performed to verify the toxicity of SMZ solutions after plasma treatment, by using biological models belonging to various trophic levels: *Daphnia magna*, a crustacean, *Raphidocaelis subcapitata*, a microalga, and *Vibrio Fischeri*, a bioluminescent bacterium. It was found that the oxidation products of SMZ formed after 4 h of treatment of a solution  $5 \times 10^{-4}$  M are not toxic. This means that, in the case of water contaminated by SMZ, plasma treatment could be used as a preliminary step before biological treatment in the water treatment plants, shortening the time of application of this advanced oxidation step.

Chapter 3 concerned the investigation of air non thermal plasma treatment of a widespread algicide, Irgarol. The degradation kinetics due to plasma was compared to that observed by the combination of plasma and  $\text{TiO}_2$ , the most common photo-catalyst. In additional experiments, Irgarol was preliminarily deposited on  $\text{TiO}_2$  and different amounts of this mixture were treated in a DBD reactor and their degradation curves were compared. It was shown that the role of  $\text{TiO}_2$  is not significant for the photoinduced decomposition but it enhances pollutant solubility, by causing a decrease of the pH of the solution. An extent of mineralization near to 100% was reached and several oxidation products were identified.

In Chapters 2 and 3, the study of plasma induced AOP for water purification was limited to simple model solutions containing a single pollutant. In Chapter 4, the results are described and discussed of a more complex experiment concerned with the possible interactions of two pollutants in the same solution subjected to air plasma treatment. Metolachlor and mesotrione were chosen as model contaminants, since these two herbicides are present in mixture in common commercial formulations. The investigation involved the study of the degradation kinetics, oxidation products and extent of mineralization of the two compounds, first treated individually and then in mixture. It was found that the degradation rate is significantly faster for mesotrione than for metolachlor and that the AOP of each pollutant appears to be unaffected by the presence of the other. This result is corroborated by the data from product analyses, which for each herbicide are the same when it is treated as single component or in mixture. Finally, it was shown that complete mineralization can be achieved for both when they are treated individually and in mixture.

Chapter 5 describes the studies on the decomposition obtained by applying plasma on solutions of triclosan and perfluorooctanoic acid, respectively an antibacterial agent and a surfactant. The kinetics of degradation were studied at different initial concentrations of the contaminants and at different pH. The results reported in this chapter provide further evidence for the effectiveness of plasma in oxidizing also compounds of very persistent nature.

Chapter 6 is a recently published paper which reports work to which I contributed during my PhD program. In order to improve the interactions of the reactive species produced by plasma with the solution to be treated, a new plasma reactor was designed, developed and tested. It consists of a high frequency jet, allowing for the introduction of plasma effluent under the liquid surface. The plasma produced in air at atmospheric pressure was characterized by optical emission spectroscopy and visualized by Schlieren imaging. The reactive species were determined by specific chemical probes. The performance of this new reactor was tested on three compounds, rhodamine, phenol and metolachlor with regard to the three major process parameters: duration and energy efficiency of the treatment and extent of mineralization achieved. The oxidation pathway of metolachlor was studied and similarities were found between the results obtained with the new streamer reactor and the DBD reactor previously designed and fully investigated in our laboratory.

The final chapter, based on the research carried out during my stay at Ruhr University of Bochum, focuses on one of the hot topics related to applications of plasma, i.e. its sterilization properties. It includes two different parts: the first concerns the comparison between a microjet plasma and a DBD source in affecting *E. coli* and the enzyme glyceraldehyde-3-phosphate (GapDH); the second reports on the comparison of effects achieved by using the whole plasma and only its ionic component in GapDH inactivation. Best inactivation results were obtained with DBD, achieving complete loss of GapDH function in 120 s. To investigate the contribution of ions in plasma GapDH interactions, a modified version of  $\mu$ -APPJ was used, in which, for the first time, charged and uncharged particles of plasma can be separated. Two gaseous mixtures were used, He/Ar and He/O<sub>2</sub>. The study of inactivation of the enzyme via plasma, with and without ions, showed a synergic effect between radicals and ions. Further analysis will be necessary to better evaluate the species produced in this new source.

## Appendix A

### Application of Slater and Douglas-Hamilton kinetic model

The linear dependence of the degradation constant on the reciprocal of concentration is consistent with a simple inhibitor kinetic model proposed by Slater and Douglas-Hamilton and found to fit many experimental data thereafter. According to this model A, that is the pollutant removal agent formed from the host gas G (synthetic air in this case), reacts with the pollutant P, at a constant rate, S, producing a product I which competes with the examined EOC for A, as shown in the following scheme:



I, therefore, acts as an inhibitor. The rate equations corresponding to this kinetic scheme are given by:

$$d[A]/dt = S - k_1[A][P] - k_2[A][I] \quad (4)$$

$$d[\text{VOC}]/dt = -k_1[A][P] \quad (5)$$

Assuming:

- A in steady-state conditions;
- $k_1 \approx k_2$ ;
- $[Z] \ll [I]$  and consequently  $[P]_0 = [P] + [I]$

for low concentration of pollutants, it is possible to integrate the rate equations obtaining:

$$[P] = [P]_0 \cdot e^{-\left(\frac{S}{[EOC]_0} t\right)} = [P]_0 \cdot e^{-(k \cdot t)} = [P]_0 \cdot e^{-(k_E \cdot Energy)} \quad (6)$$

In these equations the dependence of  $k$  on initial concentration of the EOC in exam is expressed. Since decomposition of most organic compounds can be described through this kinetic model, NTP processing is particularly suitable for the removal of pollutants in low concentration from large gaseous masses.